CELL TYPE-SPECIFIC DOUBLE STRAND BREAK REPAIR: AN INTER-CHROMOSOMAL HOMOLOGOUS RECOMBINATION STUDY USING THE RAINBOW MOUSE MODEL

by

Kiran Lalwani

A dissertation submitted to the faculty of
The University of North Carolina at Charlotte
in partial fulfillment of the requirements
for the degree of Doctor of Philosophy in
Biology

Charlotte

2023

Approved by:

_____
Dr. Christine Richardson

_____
Dr. Andrew Truman

_____
Dr. Chandra Williams

_____
Dr. Dider Dréau

_____
Dr. Yvette Huet

ABSTRACT

KIRAN LALWANI. Cell Type-Specific Double Strand Break Repair: An Inter-Chromosomal Homologous Recombination Study Using the Rainbow Mouse Model. (Under the direction of DR. CHRISTINE RICHARDSON)

Faithful repair of DNA lesions is central to maintaining genomic integrity. Illegitimate repair of chromosomal DNA damage, especially double-strand breaks (DSBs), can lead to mutations and genome rearrangements. Homologous recombination (HR) is a highly conserved molecular process that plays an important role in the repair of DSBs and the maintenance of genome stability. However, it is not fully understood which cell populations at which developmental stages *in vivo* have the potential to use this "error-free" repair mechanism. Further, although HR is considered to be "error-free", illegitimate inter-chromosomal HR has been linked to the formation of chromosomal translocations that are a hallmark of leukemias, lymphomas, and sarcomas. For my studies, I engineered a transgenic mouse "Rainbow Mouse" model to induce specific chromosomal DSBs *in vivo* and score for inter-chromosomal HR repair in multiple tissues and cell types. I used the Rainbow Mouse to address critical biological questions- *What is the relative frequency of inter-chromosomal HR repair among different tissue subpopulations? Which cell types are more likely to utilize this mechanism? Can DSBs induced in utero be repaired by inter-chromosomal HR repair*? I hypothesized a significant difference in inter-chromosomal HR observed in different cell types based on their cellular differentiation state.

Overall, my research demonstrates a function reporter model to evaluate inter-chromosomal HR in vivo. My research identified specific cell types, such as pancreatic duct cells and hematopoietic stem cell enriched LIN-/CD34+ populations that undergo DSB-induced inter-chromosomal HR leading to mutation. The findings from my research highlight developmental and cell type-specific differences in the potential for inter-chromosomal HR to be used in the repair of DSBs. The Rainbow mouse model utilized in this study has the potential for long-term application in assessing

the mutagenic effects of various environmental and dietary compounds, as well as understanding the role of specific proteins involved in repairing DNA damage induced by these compounds.

ACKNOWLEDGEMENTS

I am immensely grateful to Dr. Christine Richardson for her constant support and guidance throughout my graduate experience. I deeply admire your dedication towards your students and her love for science. You have been a fantastic mentor and helped me become a scientist and a better person. Learning essential laboratory techniques and life skills under your tutelage has been an esteemed privilege, and I aspire to honor your teachings by applying them diligently.

To my committee members, Drs. Andrew Truman, Chandra Williams, Didier Dréau, and Yvette Huet, thank you for all your guidance and feedback throughout my research. Dr. Truman, thank you for being such an enthusiastic scientist; your love for science has always been an inspiration. I enjoyed taking your classes; they helped me design my experiments. To Dr. Williams, thank you for taking the time to train me in mice handling. I appreciate all the insights you shared regarding mice behavior, which have helped me immensely throughout my research. To Dr. Dréau, thank you for helping me with the tissue staining protocol and statistical analysis. Without your mentorship, I would have struggled to get good-quality images. To Dr. Huet, thank you for your knowledgeable insights into my research project.

I want to thank my lab members and dear friends Dr. Donna Goodenow, Caroline French, and Lori Ungur. Donna, I am so grateful to have you as a friend and even more grateful that you decided to return to UNC Charlotte. Caroline, you have been a fantastic friend and lab partner, and I will always cherish our endless conversations and wish you the best for the future. Lori, thank you for constantly shadowing me; I know you will do well in your future endeavors. To other lab mates, present and past, thank you for your companionship and support.

Thank you to my friends and fellow graduate students in the biological sciences department. Thank you to, Dr. Farida Yasmin. I am grateful for our friendship. Please remember I am so proud of you and wish you all the best for the future.

Thank you to my friends, Darshita Parikh, Rasik Sarup, Harshal Gandhi, Shivani Sheth, Anuja Khairnar, Atul Goel, and Aarush Sood, for becoming my family here in the United States. I am fortunate to have many dependable people who have stood by me throughout my journey. Seeing every one of you thrive in any aspect of life brings me immense joy, and I am incredibly proud of your achievements.

DEDICATION

I dedicate my doctoral thesis work to my parents, Mr. Prakash Lalwani and Mrs. Jyoti Lalwani, and my sibling Aarti Lalwani. Without their constant love and support I would not have been the person I am today.

TABLE OF CONTENTS

LIST OF TABLES

LIST OF FIGURES

LIST OF ABBREVIATIONS

DNA: Deoxyribonucleic Acid

DSBs: Double-Strand Breaks

ROS Reactive Oxygen Species

SSBs: Single-Strand Breaks

BER: Base Excision Repair

DDR: DNA Damage Response

IR: Ionizing radiation

ATM: Ataxia-Telangiectasia-Mutated Kinase

c-NHEJ: classical Non-Homologous End Joining

HR: Homologous Recombination

MRN: MRE11-RAD50-NBS1

GC: Gene Conversion

SDSA: Synthesis-Dependent Strand-Annealing

dHJ: double Holliday Junction

NCO: no crossover

CO: Crossover

LOH: LOSS OF HETEROZYGOSITY

GFP: Green Fluorescent Protein

FACS: Fluorescence-Activated Cell Sorting

AML: Acute Myeloid Leukemia

mES: Mouse Embryonic Stem Cells

MEFS: Mouse Embryonic Fibroblasts

OGY cell line: Orange-Green Yellow cell line

IRES: Internal Ribosome Entry Site

ISCE1: Intron-Encoded Endonuclease I

FL: Fetal liver

BM: Bone Marrow

HSC: Hematopoietic Stem Cells

MPP: Multipotent Progenitor

CMP: Common Myeloid Progenitor

CLP: Common Lymphoid Progenitors

PCR: Polymerase Chain Reaction

Rt-PCR: Reverse Transcription Polymerase Chain Reaction

IHC: Immunohistochemistry

CHAPTER 1: INTRODUCTION

1.1 DNA Double-Strand Breaks

The faithful repair of deoxyribonucleic acid (DNA) lesions is central to maintaining genome integrity (Hoeijmakers, 2009). Illegitimate repair of chromosomal DNA breaks, including double-strand breaks (DSBs), can lead to mutations and genome rearrangements, which are a well-known hallmark of multiple cancers, aging, and disease (Ciccia & Elledge, 2010; Elliott & Jasin, 2002; Hoeijmakers, 2009). It has been estimated that 10-50 DSBs occur per cell per day. It underscores the importance of their correct repair (Lindahl & Barnes, 2000; Tubbs & Nussenzweig, 2017). DSBs can occur in a programmed manner during a metabolic process such as DNA replication, meiosis, the development of the immune system during V(D)J recombination, and immunoglobulin class switch recombination, or from endogenous production of reactive oxygen species (ROS) (Mehta & Haber, 2014). DSBs also occur as a result of exposure to exogenous agents such as ionizing radiation, UV radiation, alkylating agents, topoisomerase inhibitors, and chemotherapeutic drugs, which induce DSBs more broadly across the genome and in physiologically relevant contexts (Lindahl & Barnes, 2000; Tubbs & Nussenzweig, 2017). Evidence shows that a growing list of natural compounds in the human diet or the environment also cause DNA breaks.

1.1.1 Endogenous causes of DNA DSBs

Endogenous processes such as replication and transcription require DNA substrates during the S phase of the cell cycle, however mis-coordination between the two types of machinery leads to genome instability and disease (Zeman & Cimprich, 2014). Replication errors in human cells lead to 1 spontaneous DSB per 10^8 bp (Coïc et al., 2008; Mehta & Haber, 2014; Vilenchik & Knudson, 2003). This implies that at least one out of eight cells will give rise to a mutant daughter cell. Replication stress is any event causing changes to the replication rate, which can include halting replication. The replication machinery encounters structural barriers to replication fork progression, such as G quadruplexes, common fragile sites, or difficult-to-replicate sites in

centromeric regions, heterochromatic telomeric regions. In addition, DNA adducts, and unrepaired lesions contribute to replication stress by acting as a physical block to the replication fork and its motion (Zeman & Cimprich, 2014). Single-strand breaks (SSBs) generated by replication stress can further generate DSBs by nucleases, deamination, or spontaneous hydrolysis (Lalwani et al., 2022). Stalled replication fork can cause replisome disruption and fork collapse, ultimately resulting in DSB formation (Mehta & Haber, 2014; Nickoloff et al., 2021). DNA: RNA intermediates formed during transcription by annealing of nascent RNA to the DNA strand to develop a three-strand structure known as R-loops (Rinaldi et al., 2021; Zeman & Cimprich, 2014). A growing body of evidence implicates that R-loops not only stall the replication fork but are also the leading cause of DSBs and associated genome instability (Rinaldi et al., 2021).

The accumulation of reactive oxygen species (ROS) and ROS-induced oxidative stress leads to DSBs. ROS are often linked to neurological diseases and cancer, although they result from endogenous cellular metabolism. Some examples of endogenous ROS include the superoxide radical anion ($O_2^{\cdot -}$), hydroxyl radical ($OH^{\cdot}$), peroxynitrite ($ONOO^-$), and hypochlorous acid (HOCl). ROS cause DNA damage through their ability to alter the overall reduction-oxidation (redox) cell conditions to cause oxidative stress. By changing the redox conditions of the cell, important cellular processes, including signal transduction and proliferation, may not be able to occur. The failure of these processes can be lethal for the cell or promote mutagenesis through GC - TA changes. Guanine lesions that lead to a miscoding error change the structural integrity of the DNA by weakening hydrogen bonding between bases. These guanine mutations are associated with ROS-related oxidative stress and can promote cancer development. 8-Oxo-7,8-hydroxyguanine (8-oxoG) is an expected output of guanine oxidation. It is an important compound because of its susceptibility to further oxidation and overall genotoxicity. The base excision repair (BER) pathway is a mechanism deployed to resolve DNA lesions, in the presence of 8-oxoG, and has three major steps: (1) recognition of the lesion by DNA glycosylases; (2) base excision; (3)

resynthesizing and replacement of the removed base. Defects in the BER pathway's mechanism can lead to the accumulation of BER intermediates, unrepaired lesions, point mutations, and DNA DSBs. DNA polymerase β (Pol β) is one of the most active DNA polymerases involved in BER. A single nucleotide polymorphism (SNP) on the gene coding for Pol β results in proline residue 242 becoming arginine (P242R). This mutation is suggested to cause chromosomal aberrations, and therefore, genome instability. P242R was associated with an increase in single-strand breaks (SSBs) and DSBs compared to wild-type cells, and cellular transformation in mouse and human cells (Lalwani et al., 2022).

1.1.2 Exogenous agents that generate DNA DSBs

(Information from 2020 and 2022 book chapters, cited remaining text)

Exposure of mice to nonspecific agents such as IR, Top2 inhibitors, and chemotherapeutic drugs induces DSBs more broadly across the genome and in physiologically relevant contexts. Ionizing radiation such as X-rays and gamma rays can cause direct damage by depositing energy or indirectly by ionizing water molecules to produce free radicals that influence SSBs or DSBs (Vignard et al., 2013). The complexities of the damage vary according to the linear energy transfer of the radiation. Alpha particles are high radiation and directly cause breaks, while non-ionizing radiations such as UVA and UVB create indirect DSBs and SSBs. The base excision repair (BER) and SSB repair pathways repair the DNA damage from radiation. When two SSBs occur approximately 10–20 bp apart on opposing DNA strands, DSBs are created. (Mori et al., 2018). Furthermore, additional DNA damage could exist in the DNA next to the DSB, leading to complex or clustered lesions that may cause cell death if not corrected.

DSBs can potentially cause chromosomal translocations and genomic instability if improperly repaired. Several DSB response and repair pathway-specific proteins have been examined based on IR sensitivity, such as a network of pathways, avoiding the proliferation of cells

bearing DNA damage or genetic Ataxia-telangiectasia-mutated kinase (ATM) (Blackford & Jackson, 2017), MRE1 resection protein, BRCA1, and Pol θ (Lalwani et al., 2020).

Commonly used chemotherapeutic drugs are categorized into five types based on their chemical composition and mode of action. Widely used anti-cancer drugs for DNA damage include alkylating agents such as temozolomide (TMZ), melphalan, and cyclophosphamide. These agents attach the alkyl groups to the DNA and interfere with the cell cycle and transcription process. They can also crosslink two double-strand DNA molecules, creating inter-strand crosslinks (ICLs). Alkylating agents can add mismatched nucleotides, which can cause genome instability. Studies targeting DDR and DSB repair proteins that can alter the sensitivity of chemotherapeutic drugs are used for cancer treatment modalities. ICL-inducing agents, such as mitomycin C (MMC), nitrogen mustards, and platinum, can create crosslinks that hinder DNA replication, thus preferentially targeting highly proliferative cells. Thus, these agents are widely used to treat cancers and several skin conditions. The repair of ICLs involves both translesion break repair and homologous recombination (HR) proteins, and mutation of HR genes leads to sensitivity to ICL agents. Brca1 mutant mice ear fibroblasts (MEFs) treated with MMC showed significantly reduced HR frequency and increased sensitivity to MMC. Interestingly, ATM mutant mice did not significantly change HR frequency even with higher MMC doses, suggesting that ATM is dispensable for HR (Lalwani et al., 2020).

Molecular studies indicate the necessity of Top2 in the maintenance of genome integrity. The ability to halt Top2 function and generate enzyme-mediated DNA damage is a crucial reason why it is used in secondary cancer chemotherapy, such as therapy-related acute myeloid leukemia (t-AML).Top2 enzyme acts by catalyzing the interconversion of topological DNA isomers through the generation of a transient DSB on one DNA helix ("gate" strand) while remaining covalently linked to the five ′ ends of the DNA, followed by passage of a second DNA helix ("transfer" strand) through the DSB, and then relegation, failure to do so results into genomic rearrangements.

Mammals have two isoforms of Top2—α and β. Chemotherapeutic drugs doxorubicin and etoposide inhibit the catalytic activity of Top2 after generating the DSB, resulting in high levels of trapped Top2: DNA complexes and unrepaired DSBs. Such agents are referred to as Top2 "poisons". A novel insight into secondary malignancies induced by these Top2 targeting drugs has come from studies using a transgenic mouse model with a skin-specific ablation of Top2β (Bandele & Osheroff, 2007; Goodenow et al., 2021).

Chemical compounds, including air and water pollutants, pesticides, and some dietary compounds, are genotoxic and linked to carcinogenesis. The combustion of fossil fuels releases air pollutants such as benzene and sulfur dioxide, which are linked with leukemias. Bisphenol A (BPA) is a hormonally active environmental xenoestrogen widely found in food products. It is an epigenetic toxicant that can alter the DNA by generating ROS. Bioflavonoids are polyphenolic compounds in various dietary products such as soy, coffee, fruits, and vegetables. These compounds are mechanistically and biochemically similar to the Top2 inhibitor and chemotherapeutic drug etoposide (Bandele & Osheroff, 2007; Goodenow et al., 2021). In addition, bioflavonoids have been shown to cross the placental barrier and can induce *MLL* gene locus breakpoint cluster region cleavage, suggesting an association with the initiation of infant leukemia (Goodenow et al., 2021; Strick et al., 2000) (Lalwani et al., 2022).

1.2 Programmed DSBs

Several developmental and physiological processes require site-specific DSBs to generate genetic diversity. These programmed DSBs include the V(D)J recombination, mating-type switching, and meiotic recombination processes.

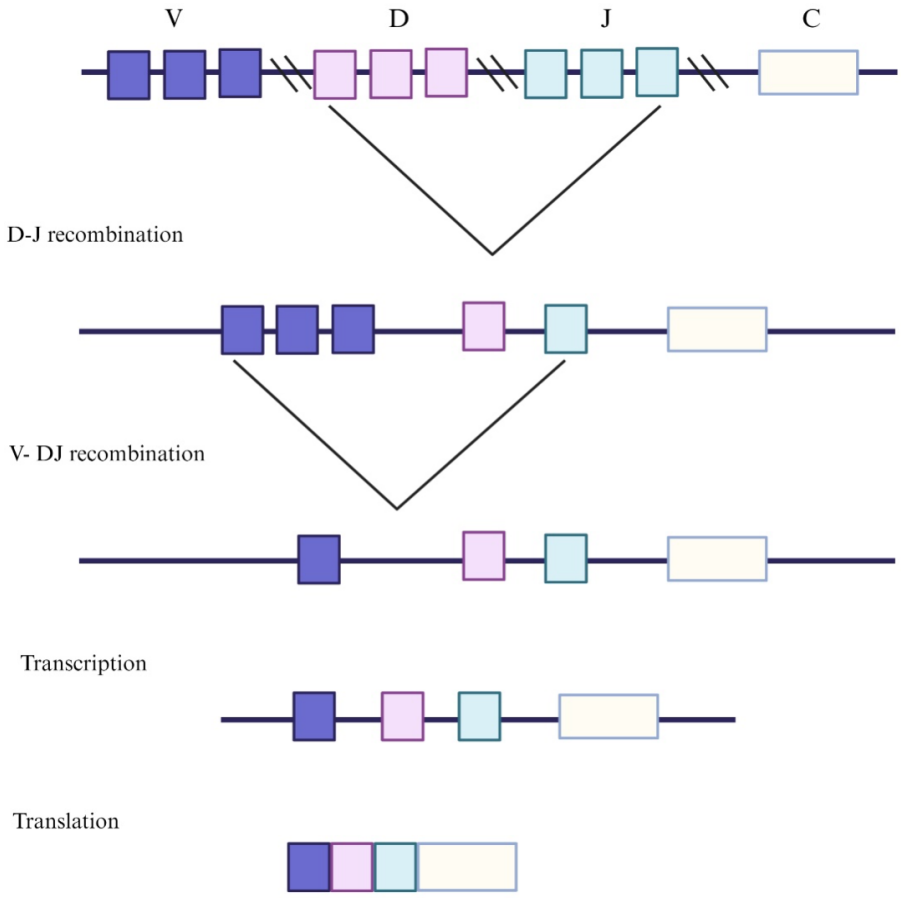

Figure1: Schematic showing VDJ recombination. The antigen binding domains for immunoglobulin and T-cell receptor- encoding genes are arranged as variable (V), diversity (D), and joining (J) gene segments. The recombination begins with DSBs at the recombination signal sequence (RSS) flanking VDJ segments by the RAG complex (RAG1 and 2) which is only expressed in early lymphocytes.

Expressing a diverse repertoire of antigen receptors by immunoglobulins and T-cell receptors (TCR) is critical for an adaptive immune response. The antigen-binding domains for immunoglobulin and T-cell receptor-encoding genes are arranged as variable (V), diversity (D),

and joining (J) gene segments (Roth, 2014). VDJ recombination generates antigen receptor diversity and the development of new lymphocytes. The recombination begins with very specific DSBs at the recombination signal sequence (RSS) flanking VDJ segments by the RAG complex (RAG1 and 2), which is only expressed in early lymphocytes (Helmink & Sleckman, 2012; Roth, 2014). These homologous ends join (c-NHEJ) and several others. These recombination events result in several deletions, insertions, and inversions of several base pairs (Schatz & Ji, 2011).

Meiotic recombination requires the generation of specific DSBs by a topoisomerase-like enzyme called Spo11 (Lam & Keeney, 2015). The DSBs initiate repair by HR and are necessary for segregating homologous chromosomes during the first meiotic nuclear division (Coopera et al., 2016). Research shows that generating meiotic DSBs across the genome is not random but rather under several levels of regulation (Khil et al., 2012; Lam & Keeney, 2015). These non-random and distinctive regions are called DSB hotspots. S. cerevisiae has roughly 3600 across the genome, while mammals have between 10,000 and 40,000 (Khil et al., 2012). Recent research has demonstrated that a wide range of variables, including the recruitment of Spo11 and the facilitation of cleavage susceptibility, can affect the identification of a hotspot. Additionally, there is spatial regulation that not only quantitatively limits the number of DSBs developing per cell but also ensures that those DSBs that do occur are spread more uniformly among all chromatids (Coopera et al., 2016; Khil et al., 2012; Lam & Keeney, 2015).

Spo11 initiates meiotic-specific DSBs with the assistance of at least eight other proteins (Keeney et al., 1997). The relationship between Spo11 and meiotic recombination initiation has been recognized in species of asexually reproducing organisms where genes orthologous to SPO11 take part in the meiotic cell cycle. A study conducted on Spo11 mutant mice suggested that the SPO11 gene is required for normal homologous synapses in females and males and for forming axis-associated DMC1 complexes. The association of SPO11 with the MRX/MRN complex is observed in many organisms (Barlow et al., 1996). In mammals, errors in meiotic recombination

can lead to cell cycle arrest or apoptosis, leading to loss of function. Many of the RAD52 epistasis group homologs are expressed in multiple tissue types, with higher levels seen in the testis and proliferating cells, indicating their involvement in both meiotic and mitotic recombination, respectively. The ATM gene is essential for mitotic cell cycle progression, and the initiation of DSB repair by HR is significant during meiosis progression as well. ATM-deficient mice have disrupted spermatogenesis and are entirely infertile, suggesting that it is required for regulation and progression in meiosis, similar to its role in the mitotic cell (Lukaszewicz et al., 2018).

1.3 DSB sensing, signaling, and repair.

Eukaryotic cells have evolved sophisticated mechanisms to ensure appropriate detection orchestrated by the DNA damage response (DDR) and DNA damage repair.

1.3.1 DNA damage response

DDR promotes genome stability by precisely coordinating a network of pathways, avoiding the proliferation of cells bearing DNA damage or genetic rearrangements (Jackson & Bartek, 2009). Defects in this cellular response result in genetic instability, which can confer a selective advantage to mutated cells. Syndromes defective in DDR and DNA repair are associated with high genetic instability, cancer predisposition, and premature aging (Jackson & Bartek, 2009; Maréchal & Zou, 2013).

The initial study of DDR was performed in fission yeast in 1994. DDR involves a series of biochemical reactions that trigger the response cascade, starting with sensors, followed by transducers and effectors. Over the years, many comparative studies have shown that DDR is a highly conserved pathway within mammals and yeast. Based on the type of damage, there are three phosphatidylinositol-3 kinases, the ATM, ATM- Rad3 related (ATR) kinase, and DNA-Pkcs, which play a significant role in the response cascade by phosphorylating other proteins (Blackford & Jackson, 2017). The ATM kinase is involved in DSB response and corresponding repair pathway initiation, while the ATR is more prominent during single-strand break response and repair;

however, several reports suggest interlaced involvement of the two proteins (Blackford & Jackson, 2017; Lavin et al., 2006; Maréchal & Zou, 2013)

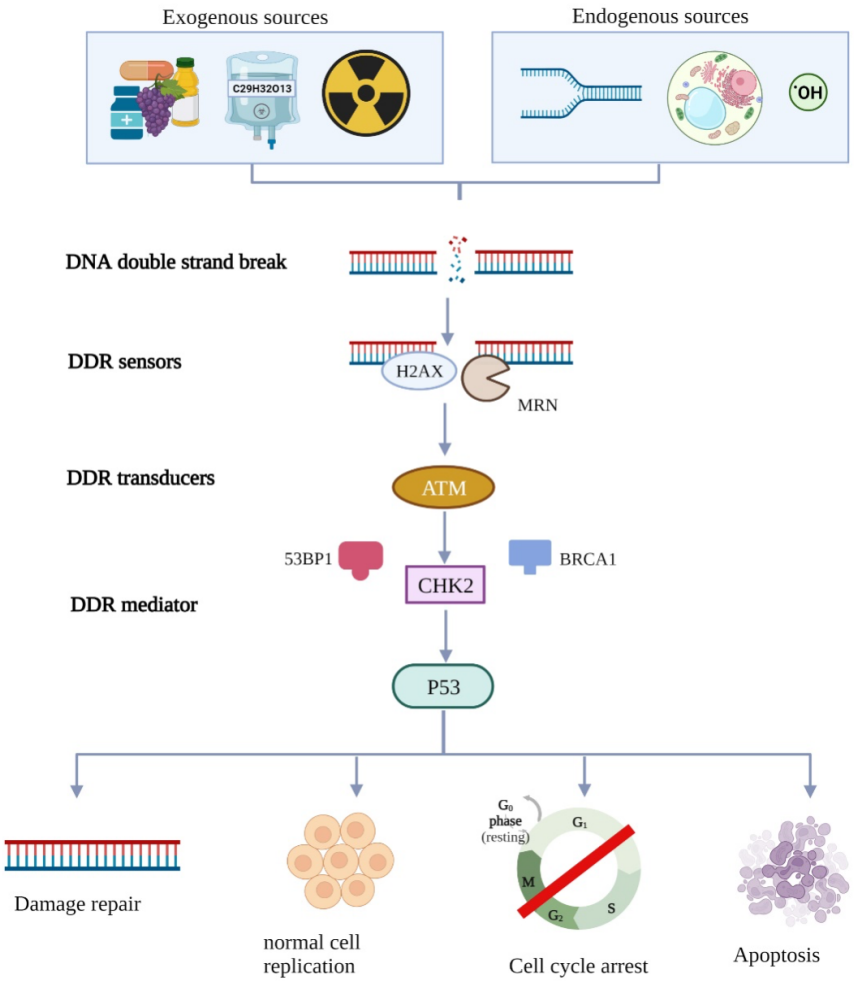

Figure 2: Schematic flowchart depicting dna damage response pathway. The dsb induced by exogenous and endogenous sources begins a sensory response cascade that consists of number signals, sensors transducer and effector proteins which ultimately initiate either dna repair or cell death or cell cycle arrest.

The MRE11-RAD50-NBS1 (MRN) complex is involved in the initial detection and processing of DSBs due to its nuclease activity (Lavin et al., 2006; Stracker & Petrini, 2011). The MRN complex recruits an ATM kinase at the site of DNA damage, which in turn activates by autophosphorylation and phosphorylates several proteins (Uziel et al., 2003). One of the proteins to be phosphorylated by ATM is histone protein H2A at the S139 site, forming H2A foci.

(Blackford & Jackson, 2017; Maréchal & Zou, 2013) Phosphorylated H2AX (gH2AX) promotes histone remodeling by acting as a scaffold for other proteins, such as MDC1 (Coster & Goldberg, 2010). MDC1 phosphorylation recruits ubiquitin ligases: E3 ligase, RNF8, and RNF168 (Kolas et al., 2007; Mailand et al., 2007) that add ubiquitin to the histones and allow the recruitment of activator proteins, 53BP1 and BRCA1. 53BP1 is essential for inhibiting MRN complex resection, so it promotes repair via NHEJ (Daley & Sung, 2014; Georgieva, 2019; Lei et al., 2022). Contrary to this, BRCA1 inhibits NHEJ and promotes HR (Daley & Sung, 2014; Lei et al., 2022).

1.3.2. DSB repair pathways

DSB repair pathways are cell-cycle specific and differ based on their requirement for a donor DNA template with significant homology (Bishop, 2000). Studies suggest NHEJ is most prevalent in non-cycling somatic cells during the G1 stage, while HR is particularly active during the S, G2, and M stages due to its requirement for a homologous sequence as a donor template. In the NHEJ pathway, the broken ends are processed and ligated together without requiring any homology (Hustedt & Durocher, 2017; Rothkamm et al., 2003). By contrast, HR uses an undamaged homologous sequence from a sister chromatid, an allelic locus, or an ectopically located sequence from a heterologous chromosome as a template to initiate homologous recombination or replication repair at the broken site.

The analysis of mating type switch (MAT) from *Saccharomyces cerevisiae* revealed homologous recombination as a major DSB repair pathway (Jasin, 1996; Sukup-Jackson et al., 2014). Demonstration of HR as a major DSB repair pathway in mammalian cells originally came from direct examination of repair of a chromosomal DSB in the hamster genome in which a single DSB was introduced into a plasmid direct repeat recombination substrate by the I-*Sce*I endonuclease. (Haber, 2018). Clones grown under nonselective growth conditions demonstrated that 41% of repair events were the result of HR and the remaining were NHEJ events (Richardson & Jasin, 2000). Sequence analysis of NHEJ products showed rejoining of ends with either minimal

sequence loss or small insertions from a variety of sources, including single copy DNA, repetitive elements and the transfected expression plasmid (Richardson & Jasin, 2000).

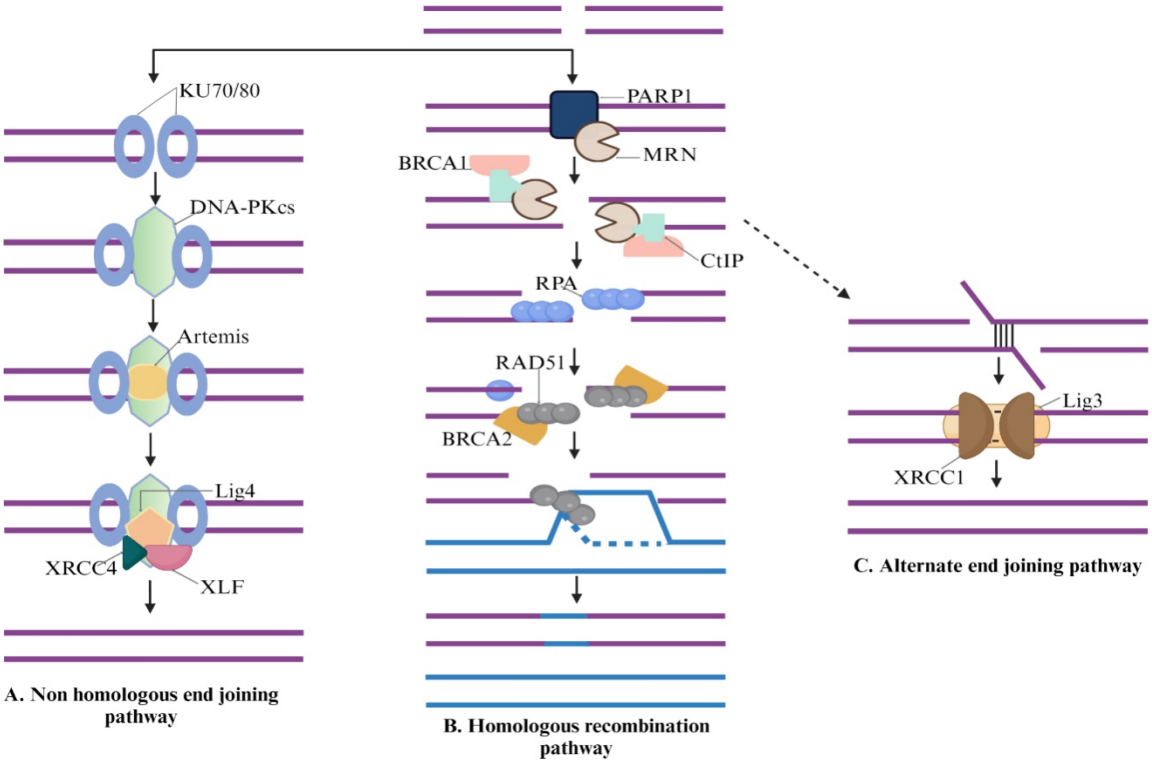

Figure 3: Overview of the three major DSB repairs. Left is the NHEJ pathway that uses several proteins to process and ligate the broken DNA without homology. Middle is the HR pathway which involves resection to form ssDNA. Rad51 protein facilitate homology search. The homologous sequence serves as a template strand to repair the break. Right is the Alt-EJ pathway which uses small homologous sequence close to the resected DNA and ligates the ends together.

NHEJ

In the NHEJ (Lalwani et al., 2020) pathway, the broken ends are processed and ligated together without requiring any homology (Hustedt & Durocher, 2017; Rothkamm et al., 2003). Similar to C-NHEJ, alternative end-joining (Alt-EJ) results in the deletion or insertion of nucleotides. The Alt-EJ pathway was initially identified in *saccharomyces cerevisiae* in cells deficient in HR and C-NHEJ pathways (Decottignies, 2013; Kuzminov, 2011). Unlike C-NHEJ,

Alt-EJ utilizes end resection by CTBP-interacting protein CtIP and additional HR proteins and requires microhomology of 2–20 nucleotides for SSA-type ligation (Sallmyr & Tomkinson, 2018). The exposed resected single DNA strands are coated with RPA protein, which is later displaced by a DNA polymerase, Pol ɵ (Seol et al., 2018). Pol ɵ is essential for the Alt-EJ pathway as it inhibits HR proteins and aids in the search and alignment of the microhomologies (Seol et al., 2018). Alt-EJ is highly mutagenic and may be an alternative to other repair pathways. For example, in immune cells with a deficiency of C-NHEJ proteins, Alt-EJ is utilized for immune cell receptor recombination.

The assembly of Ku dimers on the two DSB ends initiates the NHEJ pathway (Mahaney et al., 2009). Ku70/80 forms a ring dimer that serves as a scaffold for the assembly of the NHEJ components such as DNA-PKcs, X-ray cross-complementing protein 4 (XRCC4), DNA Ligase IV, XRCC4-like factor (XLF), and Artemis (Mahaney et al., 2009; Mani et al., 2020). Ku proteins' N- and C- domains have distinct regions that facilitate binding to the broken ends and anchoring them together (Walker et al., 2001; Yoo & Dynan, 1999). Structural analysis of DNA-PKcs kinase reveals a distinctive C and N terminal arrangement, creating a holoenzyme that enhances dsDNA binding (Davis et al., 2014). The KU-DNA complex directly recruits DNA-PKcs, allowing the serine/threonine kinase function of DNA-PKcs to bring the broken DNA ends together to repair the break and protect against nuclease attack. This complex also translocates KU dimers towards the inner dsDNA (Yoo & Dynan, 1999). Phosphorylation by DNA-Pkcs and ATM enables the 5’-3' endonuclease activity of Artemis to process the broken ends, although the specific role of phosphorylation on Artemis is unclear (Goodarzi et al., 2006; Mahaney et al., 2009). Other components like Pol mu, Polynucleotide kinase protein (PNKP), APRATAXIN, WRN, and APLF have a potential role in processing the DSB ends since they are not always compatible and are deemed as 'dirty'; therefore, they have been processed accordingly before relegation. The PNKP produces a religable 5′-phosphate/3′-hydroxyl termini group (Weinfeld et al., 2011), while

Aprataxin removes the aldehyde group from 5' ends, the parataxis-PNKP-like factor (APLF) has 3' exonuclease and endonuclease activity, Pol mu removes five deoxyribose phosphate groups. Werner's syndrome protein (WRN) is a 3'-5' DNA helicase protein that DNA-PKcs phosphorylates to enhance its exonuclease activity. WRN and Artemis are stipulated to process the ends in a way that results in compatible DNA ends. XRCC4 and XLF proteins bind to the DNA-PK complex and assist in the stabilization of the broken strand while promoting the recruitment of the additional NHEJ proteins (Chiruvella et al., 2013; D. B. Francis et al., 2014; Gu et al., 2007). XRCC4 binds to Ligase IV, forming the X4-L4 complex, essential for ligation to repair the DSB. XLF protein is stipulated to enhance the X4-L4 complex and, therefore, enhances the ligation of the ends (D. B. Francis et al., 2014; Gu et al., 2007). Excessive processing of the DSB results in gaps filled by DNA polymerases, Pol μ and ʎ. After the DSB is repaired, the assembly proteins are removed; however, the removal of Ku requires using a unique complex called SCF, which breaks the dimer, or ubiquitin, adding protein RNF8 (Mailand et al., 2007).

Homologous recombination

Investigation of the genetic control of recombination pathways (Lalwani et al., 2020) in Saccharomyces cerevisiae initially developed from isolating mutants characterized by sensitivity to IR, which were later found deficient in recombination. The genes defective in these mutants are collectively known as the RAD52 epistasis group (RAD50, RAD51, RAD52, RAD54, RAD55, RAD57, MRE11, and XRS2), which is central to DSB repair and recombination. Homologs of many of these genes have been identified in mammals based on sequence similarity, facilitating understanding of their functions and mechanism of action in mammals. Early genetic analysis indicated the involvement of at least three pathways during DSB-induced mitotic recombination between direct repeats of S. cerevisiae. These are a conservative pathway dependent on the RAD52 epistasis group of genes, a nonconservative SSA pathway dependent on RAD52, RAD1, and RAD10, and a less characterized one-sided recombination deletion pathway.

The protein–protein interactions among various members of the RAD52 epistasis group comprise two different complexes involved in DSB-induced recombination, the first involved in presynaptic functions, including the processing of the DSB ends, and the second involved in synaptic functions for invasion, creation of repair intermediates and resolution. The MRX/MRN complex is involved in the first stage of DSB-induced recombination, including processing of the broken DNA ends. Yeast MRX complex consists of Rad50, Mre11, and Xrs2 and cofactor Sae2 helicase. The homologous MRN complex in mammals consists of Rad50, Mre11, and NBS1, along with the cofactor CtIP endonuclease that interacts with Mre11 (Wright et al., 2018). As a complex, these proteins influence the 5′ to 3′ resection rate of DSB ends—rad50 dimers tether DNA molecules together through interactions at their metal ion hook domains. Mre11 has DNA unwinding ability and exo- and endonuclease activity, resulting in 5′ overhangs on either side of the DSB. Xrs2 and NBS1 do not have enzymatic activity but are responsible for the interaction of the complex with other proteins. The long-end procession of resection is accomplished by helicase Sgs1 in yeast and by mammalian EXO1 exonuclease in conjunction with Dna2 helicase/nuclease to generate 3′ overhangs. Helicases BLM and WRN unwind double-stranded deoxyribonucleic acid (dsDNA) in mammalian cells to facilitate long-end resection (Nimrat Chatterjee* and Graham C. Walker, 2017), Replication protein-A RPA complex (RPA1, RPA2 and RPA3) binds to the single-stranded deoxyribonucleic acid (ssDNA) exposed by resection to protect from nuclease activity and forms a barrier for Rad51 binding. The second stage of DSB-induced HR repair requires synaptic invasion, the creation of repair intermediates, and resolution. Rad52 removes RPA in yeast and BRCA2 and DSS1 in mammals. Rad51 is assembled on the ssDNA strand by forming a nucleoprotein filament with either Rad52 or BRCA2 and, like its homolog, the bacterial strand transferase RecA, Rad51 can catalyze a strand exchange reaction. Rad51-coated DNA 3′ end invades a homologous template and initiates base pairing on one strand and D-loop formation. Epigenetic analysis suggests a critical role of BRCA2 in the recruitment of Rad51, and depletion of BRCA2 can skew repair pathway choice towards SSA or NHEJ (Jasin & Rothstein, 2013).

Strand invasion and subsequent recombination are promoted by BRCA2 and partner and localizer of BRCA2 PALB along with multiple Rad51 paralogs (Xrcc2, Xrcc3, Rad51L2, Rad51L3) (Chun et al., 2013). Rad54B then removes the Rad51, and the ssDNA acts as a primer to synthesize the strand. DNA polymerase Ɛ or Pol δ uses intact sequence as a template for synthesizing the broken ends and restoring any lost information. The other end of the broken DNA is also captured and repaired.

HR contains various interlinked sub-pathways that use the DNA strand invasion and template-directed DNA repair synthesis to achieve accurate repair. Two significant outcomes of HR repair are gene conversion (GC) and break-induced repair (BIR) based on the extent of homology available between the broken and donor sequences (Jasin & Rothstein, 2013; Mehta & Haber, 2014). GC occurs when the broken ends have homology with the donor, such as at a broken replication fork.

GC is associated with both the formation of double Holliday junction (dHJ) or synthesis-dependent strand annealing (SDSA) (Szostak et al., 1983; Thompson, 2012). dHJ can lead to non-crossovers (NCO) or crossovers (CO), while SDSA produces NCO (Thompson, 2012). dHJ model was first proposed by Renick in 1976 using yeast as model organisms. In this model, after resection and strand invasion into template DNA, the Rad51-coated ssDNA forms a displacement loop (D-loop) that contains displaced ssDNA and heteroduplex DNA. This D-loop can be further extended by DNA synthesis at the 3' end of the invading strand and annealing the ssDNA from the opposite side, forming dHJ intermediates. Alternatively, two independent strands could invade from both ends, followed by simultaneous DNA syntheses and annealing. These intermediates can be resolved, resulting in either crossover outcomes (CO) or non-crossover outcomes (NCO). Alternatively, these intermediates can be dissolved, resulting exclusively in NCOs. The resolution of intermediates requires processing by BLM helicase along with TOPO II alpha-RM1-RM4. The BLM facilitates the movement of junctions towards each other, forming a hemi-catenane structure.

In case of dissolution, the GEN1 nuclease creates two nicks at the end of each junction, which are then ligated by ligase IV. Conversely, 1-4 from 3' and Mus8- EME1 at 5' can also create the two nicks at the junctions. The relegation results in CO or NCO products.

The SDSA was initially studied in T4 phage and *Saccharomyces cerevisiae* as a prominent HR process. The SDSA-mediated recombination involves the formation of the D-loop. Unlike the dHJ pathway, SDSA proceeds without the formation of junctions. The DNA synthesis in SDSA is initiated at the 3'end of invading single-strand DNA end without forming junctions and continues the synthesis of new DNA. The newly synthesized strands are annealed after being separated from the template strand. The d-loop aids in the alignment and joining of strands, repairing the broken DNA without creating a Holliday junction. Following the synthesis, the D loop is reversed and dissolved by the RTEL enzyme. This dissolution results in the formation of NCO products.

BIR pathway occurs when only one broken end is present for repair, for example, if damage occurs in the telomeric region of the chromosome or at a collapsed replication fork (Malkova, 2018; Sakofsky & Malkova, 2017). In such cases, the synthesis continues to the end of the chromosome, where it stops abruptly and cannot proceed further, creating a non-crossing over product. As the second arm is never utilized, this type of repair causes a loss of heterozygosity. Even so, BIR is considered an alternative pathway for telomere elongation, underlying its importance as a repair pathway. The repair mechanism is similar to replication fork repair, including resection and homology search (Malkova, 2018).

In the single-strand annealing (SSA) pathway, exonucleolytic digestion of the DNA ends may reveal homologies within the 3′ single-strand DNA near the ends, as in the case of direct repeat elements within the same locus. The two single strands may then base pair within the homologous region and extrude 3′ ends cleaved away by endonucleolytic cleavage. This microhomology-directed repair results in a deletion of the intervening sequence between the repeat elements.

Mechanism of repair is similar to replication fork repair including resection and homology search (Malkova, 2018).

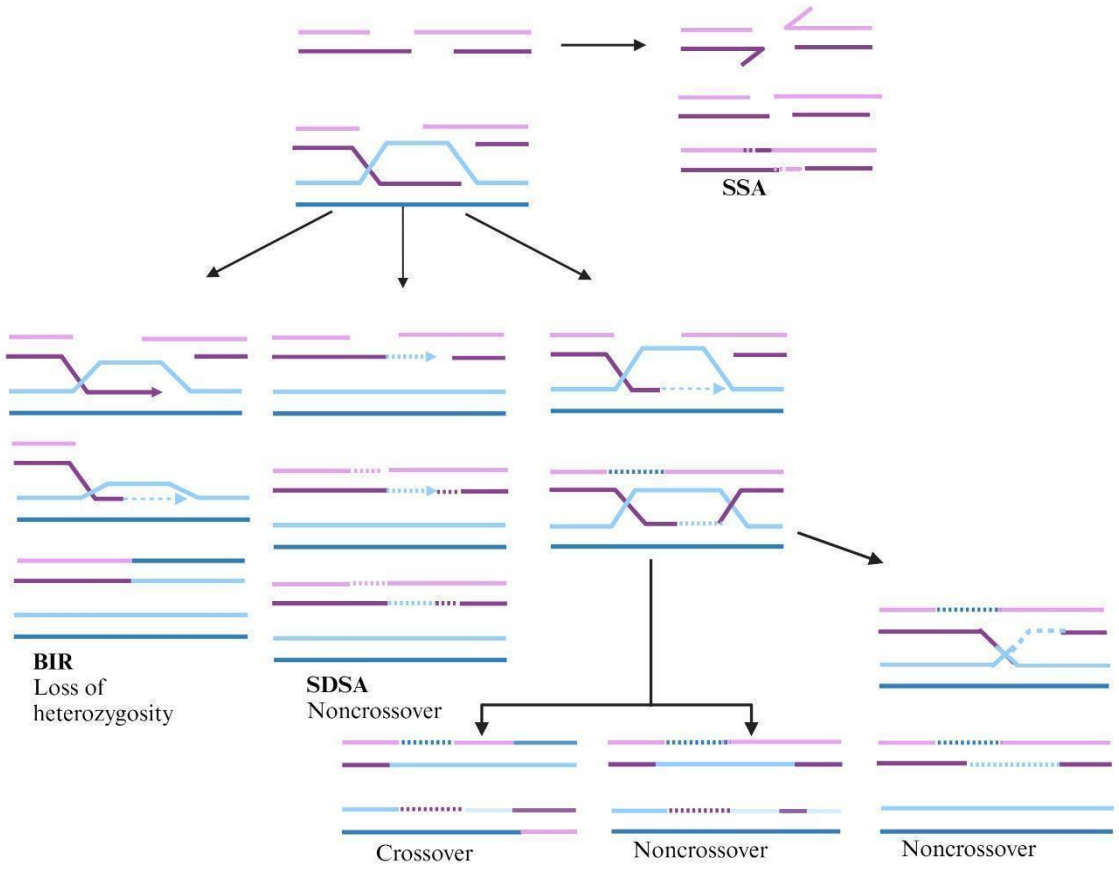

Figure 4: Sub pathways of HR. The DSB repair by HR. upon strand invasion by Rad51 the DSB are repaired in multiple ways which result in gene conversion by forming double holliday junction (dHJ), or by Synthesis-dependent strand-annealing (SDSA) which results mostly into no cross over events. The cleavage of dHJ results into either noncrossover events or cross over event. However, cleavage of the dHJ results in non-crossover events. Additionally, the BIR subtype occurs only when one of the broken ends is present for repair and results LOH. The SSA pathway uses some homology to identify template sequence and ligates the broken ends resulting in erroneous products.

1.3 Meiotic recombination vs Mitotic recombination

The functional difference between meiotic and mitotic recombination (Lalwani et al., 2020) depends on the genetic variability of the mechanisms involved during the initiation of damage, repair pathway choice or cell cycle stage. Meiotic recombination can accurately generate crossing over (CO) events that segregate homologous chromosomes from one another, while mitotic recombination plays a broader role and can rarely generate COs. The proper segregation of

chromosomes during meiosis of the yeast *S. cerevisiae* is dependent on pairing and recombination. Crossovers and gene conversion events occur between 100 and 1000 times more frequently during meiosis than during mitosis. The localized DSBs facilitated by SPO11 that occur during meiosis are the first step in this recombination process. DSBs appear before the formation of joint molecules, and their frequency correlates with the frequency of gene conversion and crossing-over. Mutations in several yeast genes have been shown to block the formation of DSBs and recombination during meiosis. These include general recombination genes, as well as meiotic-specific genes SPO11, DMC1, MER2, REC102, REC104, REC114 and MEI4. Homologs of these genes are present in mammals.

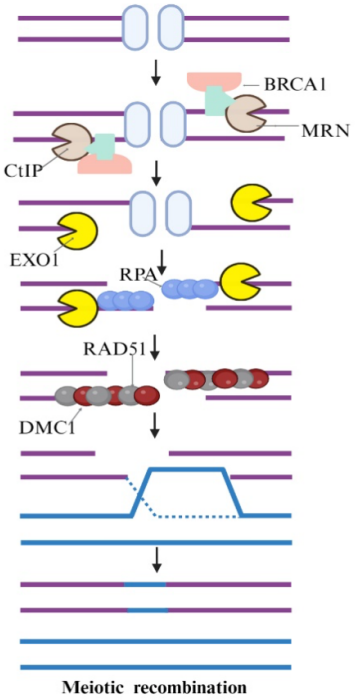

Figure 5: Meiotic recombination pathway. The meiotic HR is initiated by a special potein called SPO11 which induces DSBs. MRN complex and SPO11 initiate 5' resection of the single strand to yield ssDNA on 3' ends. Additional resection is performed by EXO1 protein. DMC1 and Rad51 proteins bind to the ssDNA and search for homology followed by strand invasion. The repair yield either no crossover or crossover products.

Although HR facilitates the segregation of chromosomes during meiosis, it is also used for the repair of spontaneous or induced damage in mitotic cells. There is a predominance of NCO gene conversion events in somatic cells, which contrasts with recombination at meiosis in which COs are frequent, indicating different mechanisms during the two processes. The DSB repair model with Holliday junctions is consistent with DSB-induced recombination during meiosis. The physical structure of isolated intermediates of meiotic recombination supports this model. By contrast, products of mitotic recombination suggest a replication-based model repair a DSB without altering the homologous template for repair. Importantly, NCO mechanisms in mitotic cells may safe- guard the cell against genome scrambling.

1.3.2 Donor sequence dependence on DSB repair pathway choice

The extent of homology (Lalwani et al., 2020) between a DSB end and the homologous donor template is an essential element in the homology search during repair. Eukaryotic investigations have implied that HR between divergent sequences is limited. The frequency of HR declines with the decline in the availability of homologs sequence, as seen in experiments done in budding yeast, mouse embryonic fibroblasts, and fruit flies. Additionally, the location of the template strand is equally important concerning DSB repair via HR. Furthermore, the arrangement of the genome as euchromatin and heterochromatin provides diversification in accessibility to DNA-damaged regions and, therefore, can vary the response pathways involved. High content of open chromatin regions in highly proliferative cells of the developing organism may facilitate interaction between heterologous chromosomes that are required for inter-chromosomal HR.

A plethora of yeast and mammalian studies have demonstrated preferences for sister chromatid donor templates, while recombination across homologous, heterologous, or ectopic chromosomes has also been detected. The intra-chromosomal HR utilizes either the sister chromatid as a template for repair or a repeat sequence in near proximity for repair, such as in the case of MAT switching. Inter-chromosomal HR utilizes a repetitive element or homologous

sequence present on a heterologous chromosome. Intra-chromosomal recombination between direct repeats can be measured up to ≥10−1 per cell generation following a DSB. Similarly, it has been observed in yeast that as the genomic distance between the site of DSBs and homologous templates, the likelihood of intrachromosomal HR declines. This result is consistent with a study in Drosophila, where HR repair occurs more frequently between proximal regions within the same chromosomal as the DSB. They discovered that inter-chromosomal recombination is conceivable and happens as frequently as intra-chromosomal recombination without an intrachromosomal donor template. However, when offered the choice of intra-chromosomal or interhomolog donor templates, the HR repair mechanism prefers intra-chromosomal donor templates to repair the broken ends. The degree of analogy between the double-strand break (DSB) and donor templates substantially impacts the donor template selection. These findings point to a sophisticated repair mechanism that distinguishes between donor templates and can discriminate against heterologous regions independent of chromosomal position (Fernandez et al., 2019). Research from Jasin's lab demonstrated recombination between heterologous chromosomes using embryonic stem cell culture. It was evident that most recombinants repaired the DSB by gene conversion, transferring a tiny amount of sequence information from the unbroken to the broken chromosome. Even though some recombinants conveyed more information than others, no chromosomal abnormalities were found. This further solidifies the idea that mammalian cells search genome-wide for potential DSB repair sequences, and the lack of crossover events leading to translocations supports a paradigm in which recombination is linked to replication.

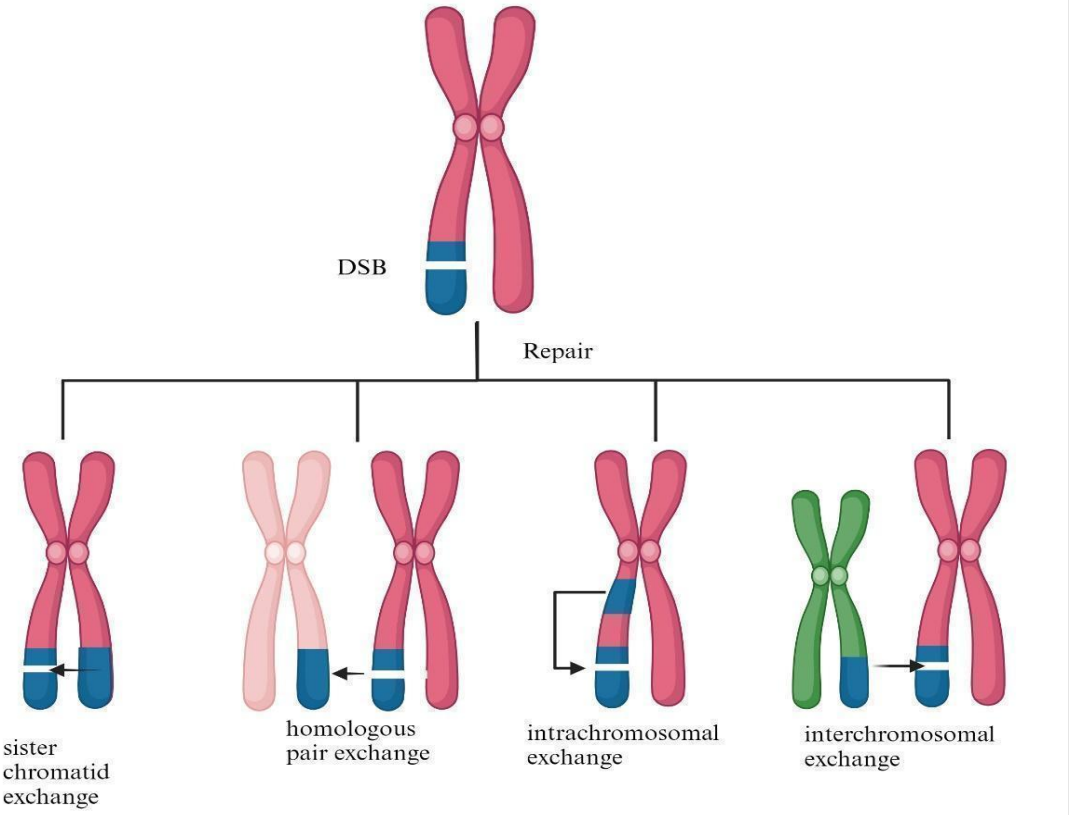

Figure 6: Donor sequence dependence on DSB repair pathway HR requires template sequence to repair the broken DNA. This template strand exchange could occur between homologous sequence on a sister chromatid or on a homologous chromosome. However, the strand exchange can also occur from homologous sequence within the same chromosome or from a homologous sequence from a heterologous chromosome.

1.4 HR-mediated genome instability

In most literature, HR is generally regarded as an "error-free" mechanism for repairing broken DNA duplexes using a homologous sequence as a template (Lalwani et al., 2020). However, despite this perception, HR can give rise to genetic alterations linked to various types of cancers (Reliene & Schiestl, 2003). Gene conversion can result in LOH, where one allele becomes predominant while leading to the extinction of a coding sequence by transferring a stop codon from a pseudogene to a related functional gene. The presence of repetitive sequences within heterochromatin, such as satellites and transposable elements, increases the susceptibility to DSB formation (Elliott & Jasin, 2002; Richardson & Jasin, 2000). CO events between repeated sequences in different genomic regions (non-allelic homologous recombination) can give rise to various genomic rearrangements, including translocations, deletions, amplifications, and inversions. When these repetitive sequences undergo repair through HR, it can result in chromosome rearrangements, characteristic features of tumorigenesis, and certain congenital disorders (Elliott & Jasin, 2002).

Dysfunction of genes involved in HR can result in genome instability, disease, and tumorigenesis. Disruptions in the recombination machinery are expected to lead to several mutations, including increased frequencies of gross chromosomal alterations, unequal sister chromatid exchanges, loss of heterozygosity, and a mutator phenotype, which can confer sensitivity to multiple DNA damaging agents. Consistent with this, patients with chromosome instability syndromes have increased frequencies of chromosome breakage, IR sensitivity, and various malignancies.

Altered function of one or several of the proteins involved in sensing DNA damage, DSB repair, and HR may promote genome instability (Levine, 1997; Lübbert et al., 1992; Vogelstein et al., 1990) (Agarwal et al., 2006; Khanna & Jackson, 2001; Marx, 2002). The ability of cells to modulate damage sensors and repair proteins may depend on the differentiation stage. It will impact

the ability of specific subpopulations to protect against aberrant repair of DNA damage. A striking connection between recombination and tumorigenesis involves hereditary breast cancer syndromes. BRCA1 and BRCA2, proteins encoded by the genes associated with these cancers, interact with the recombination protein Rad51 (Chen et al.,1998), and cells recovered from BRCA1 and BRCA2 mutants are sensitive to DNA damaging agents. These results suggest that BRCA1 or BRCA2 mutations may disrupt Rad51-mediated HR. Germline mutations of the BRCA1/2 and RAD51 genes can result in hereditary breast and ovarian cancer syndrome (Helleday, 2010). BRCA1 interacting protein C-terminal helicase I (BRIP1), along with PALB2 and CHK2, are other facilitators of HR machinery, and their mutations may or may not lead to breast cancer. BRIP1 and PALB2, along with BRCA2 and some of the components of HR, play a vital role in the Fanconi anemia pathway, and defects lead to autosomal recessive Fanconi anemia disorder. For ataxia-telangiectasia, a high level of spontaneous intrachromosomal recombination has been observed and may result from a higher frequency of chromosome breaks or their longer persistence. ATM dysfunction contributes to the development of breast cancer due to its association with the BRCA1 pathway and MRN complex. Mutation of other HR-associated genes, such as RAD54 and CtIP, can result in the development of non-Hodgkin lymphoma and colon cancer. RAD51B mutation is observed in lipoma and uterine leiomyoma. Mutant forms of BLM, WRN, and Nbs1 have been detected in various other cancers (Roy et al., 2011; Prakash et al.,2015). As the pun mouse model indicates that loss of BRCA1 reduces in vivo HR and loss of BLM increases in vivo HR, additional studies using the in vivo HR mouse models in combination with repair gene knockouts are likely to show the role of these proteins in multiple somatic tissues to protect against promiscuous HR events and maintain genome integrity.

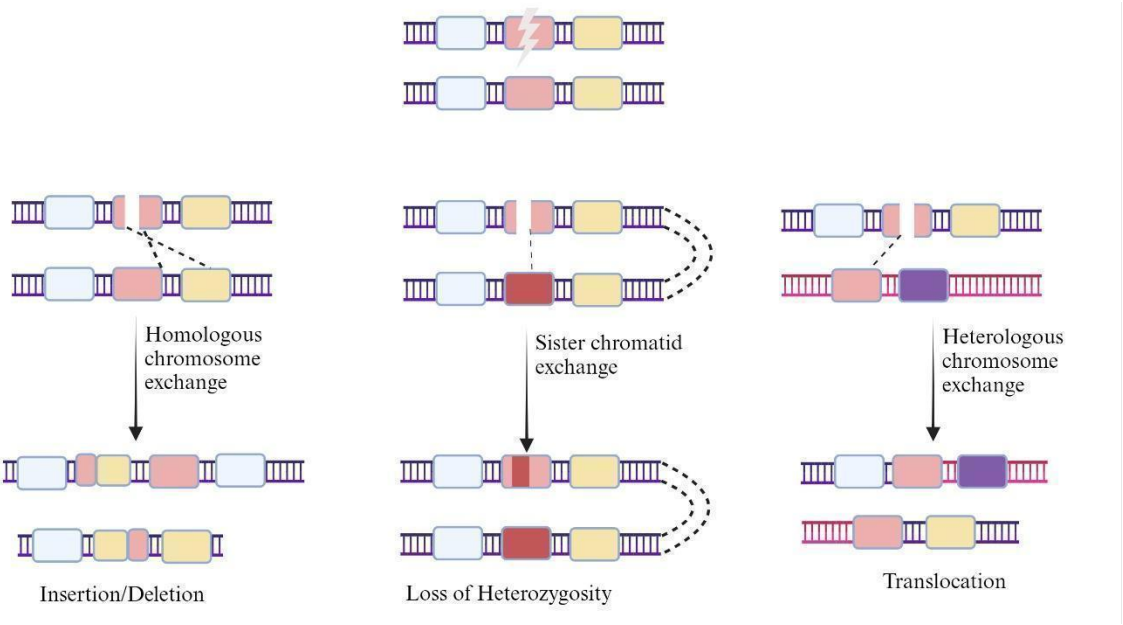

Figure 7: Mutagenic HR outcomes. Homologous exchange between two homologous chromosomes often results in insertions or deletions mutations. The Intrachromosomal recombination that occurs within same chromosome often results in loss of heterozygosity while the inter-chromosomal HR between heterologous chromosomes results in translocation.

1.5 Evolutionary considerations

Rearrangements resulting from DSB repair that occur in germ cells can have evolutionary implications. It has been observed that topo II has a role in DSB formation in spermatids (Har-Vardi et al., 2007), and chromatin loop organization is similar between spermatids and somatic cell types (Kantidze & Razin, 2009). These observations have led to the suggestion (Ashley et al., 2006; Kantidze & Razin, 2009). That this may be universal across multiple kingdoms, is supported by genome analysis of plants that suggests translocations are a regular mechanism of plant evolution (Blanc et al., 2000; Udall et al., 2005). The presence of Alu elements in mammals elevates recombination rates (Witherspoon et al., 2009), and Alu-Alu mediated recombination has been associated with founder mutations and evolution (Hwu et al., 1986; Rudiger et al., 1995; Small, Iber, et al., 1997; Small, Wagener, et al., 1997). In addition, mutation fixation has been implicated

during DSB repair in the first zygotic cell division in mice (Derijck et al., 2008). These findings underscore the importance of understanding the paradigms of repair of DSBs arising on heterologous chromosomes *in vivo*.

1.6 In Vivo Models to study DSB and Repair

In order to explore the potential for repairing DNA double-strand breaks (DSBs), *in vivo* models have been developed. Animal models are particularly valuable for studying this process due to the intricate nature of tissue and cellular differentiation programs, chromatin landscape patterns, and the impact of aging. Moreover, exposing mice to nonspecific agents allows the induction of DSBs in a broader and physiologically relevant context (Lalwani et al., 2022).

One of the first reporter systems developed assesses mutagenic events through the E. coli-derived LacZ gene, which codes for producing β -galactosidase. β -galactosidase cleaves lactose, forming galactose and glucose, but is receptive to substrate 4-bromo-5-chloro-3-indolyl -D-glucopyranoside (X-Gal) and produces blue precipitate when bound to -galactosidase. The blue precipitate is observable through light microscopy (Bariar et al., 2018). Shuttle vectors carrying the bacterial reporter gene include micro-injection of bacteriophages and electroporation of plasmids to develop transgenic mice for mutagenetic assay. Transgenic LacZ+ mice have been dosed with different mutagenic chemical compounds, like ethyl nitrosourea, chlorambucil, and benzopyrene, to observe changes in the production of X-Gal's blue precipitate as an indicator of mutagenicity (Goodenow et al., 2020). The Mutamouse and Big Blue transgenic mouse models were developed via bacteriophages. Mutamouse utilizes bacteriophage DNA (gt10) as a vector for LacZ insertion at an EcoRI restriction site. Excision of the LacZ gene for analysis and a positive agar selection system is used to score clear plaques to identify the mutants. Big Blue also has a bacteriophage shuttle vector for LacZ. However, a non-selectable color screening assay provides a ratio of blue plaques to white plaques and, consequently, a mutation frequency (Vanhees et al., 2011). In the 35.5 transgenic mouse system, the LacZ transgene concameter is in a particularly unstable chromosomal

region near the pseudo-autosomal region on the X-chromosome, resulting in an increased potential for germinal and somatic mutations (Goodenow et al., 2020).

The pun mouse model system is one of the early models used to investigate homologous repair by inducing DSBs. This model focuses on assessing DSB-induced intra-chromosomal recombination, specifically, the deletion of a 70kb segment in the pink-eyed unstable locus, resulting in the appearance of black cells on the transparent retinal epithelium. This heterozygous mouse model can detect mitotic recombination events through the loss of heterozygosity in the Aprt gene (Lalwani et al., 2022).

Nonspecific DNA damaging agents, including chemotherapeutic drugs, environmental agents, and radiation, provide a global understanding of cell function during response to DNA damage and DSBs. Molecular analysis of specific repairs is complex as DNA breaks occur spontaneously in unknown locations. Using tools such as endonucleases and retroviruses can limit off-target effects on the genome. In addition to site-specific damage induced by specific endonucleases, a defective selectable marker or a defective fluorescent protein such as green fluorescent protein (GFP) can be added to develop a reporter system (Levitsky et al., 2013). The endonuclease induces DSBs, and repair can result in a fluorescent or selectable active marker that was previously defective (Lalwani et al., 2022).

A notable mouse model using a fluorescent readout is the fluorescent yellow direct repeat (FYDR) model designed to evaluate a range of DSB-induced intra-chromosomal recombination events in multiple tissues, including the skin. This model employs two truncated enhanced yellow fluorescent protein (EYFP) sequences arranged in tandem. These sequences are prone to DNA damage-induced unequal sister chromatid exchange or replication fork collapse, leading to genetic changes and the expression of EYFP. The FYDR model revealed the frequency of spontaneous intra-chromosomal HR in multiple tissues, estimated to be around 10^{-5} to 10^{-6} per base pair per cell division. However, it should be noted that the expression of the EYFP reporter in most tissues of

the FYDR model is relatively low. A modified version of the model, called Direct Repeat-GFP (RaDR), employs two truncated EGFP sequences integrated into the ubiquitously expressed Rosa26 locus. This modified model allows for detecting spontaneous and DNA damage-induced intra-chromosomal HR in various gastrointestinal and respiratory organs, such as the lung and pancreas, indicating a cell-type and tissue-type specificity in the populations of EGFP recombinant cells. Furthermore, this model showed that older mice exhibit a ten-fold increase in the accumulation of recombinant cells compared to younger mice, highlighting the influence of age in the accumulation of mutated cells and a potential link to age-related cancers and other diseases (Kimoto et al., 2017; Wiktor-Brown et al., 2006).

A recent age-dependent study developed a knock-in R26BHEJ model to determine the efficiency of frequency of intra-chromosomal NHEJ for repair. R26BNHEJ knock-in is a GFP-based NHEJ reporter inserted into the ROSA26A locus. The DSBs are created using ISceI, and repair by NHEJ was analyzed in several tissues using flow cytometry. This model demonstrated a 1.8 to 3.8-fold decline in NHEJ efficiency with increased age (Yang et al., 2006). Another unique model to determine repair pathways in vivo developed earlier this year is the firework mouse model, also known as an IDDoR system (Inducible Dual-Fluorescence-Based Double-Strand Break Repair Reporter). This unique model includes a dual-fluorescence reporter cassette installed at the Rosa26 locus that yields GFP-based readouts for NHEJ repair and mCherry tomato red readouts for HR repair (Chen et al., 2023).

Another study examined the genetic interactions between ATM, BRCA1, and 53BP1 in mice using a hypomorphic mutant, Brca1S1598F (Brca1SF) (Levitsky et al., 2013). A direct repeat GFP (DR-GFP) gene reporter assay allows for the detection of intrachromosomal HR with a full-length non-functional GFP gene containing an ISceI endonuclease site followed by a downstream GFP homologous donor sequence; DSBs induced by ISceI cleavage can promote intrachromosomal HR repair to result in GFP+ cells. Primary fibroblasts from Brca1SF/SF mice and Atm-/- mice were

integrated with a DR-GFP reporter and a doxycycline (Dox)-inducible I-SceI endonuclease. HR repair in Brca1SF/SF and Atm−/− mice showed 3- and 2-fold reductions, respectively, whereas ATM inhibition of WT cells reduced HDR by 1.6-fold. The addition of ATM inhibitor (ATMi) exacerbated the GFP population in Brca1SF/SF fibroblasts compared to WT and Atm-/- fibroblasts. PCR-based assay with the DR-GFP reporter was used to quantify the SSA pathway, which suggested a significant reduction in the Interaction of Atm, Brca, and 53bp1 in HR, demonstrated by RAD51 foci from ear fibroblast. Examination of triple mutants indicated a plausible role of ATM in generating end-resected intermediates for RAD51 filament formation in cells with compromised BRCA1 and 53BP (Levitsky et al., 2013).

In contrast to intra-chromosomal HR, inter-chromosomal HR occurring between sequences on two heterologous chromosomes has the potential to produce chromosomal rearrangements analogous to those observed in cancers, particularly leukemias, lymphomas, and soft tissue sarcomas. Therefore, the development and study of an in vivo model of inter-chromosomal HR has important implications for human health. The Richardson lab created a transgenic mouse model (G2S mouse) to determine the potential for DSB-induced inter-chromosomal HR repair in vivo (White et al., 2013). This G2S mouse model was genetically engineered to contain three distinct transgenes- two non-functional green fluorescent protein (GFP) reporter transgenes on heterologous chromosomes and a bi-cistronic doxycycline drug inducible ISceI transgene. Each GFP reporter construct contains an ISceI recognition site that renders it non-functional and induces a specific DSB. Repair of the DSBs by inter-chromosomal HR generated a functional GFP gene, and fluorescent GFP+ cells were detected in a large spectrum of tissue types and hematopoietic progenitor cell populations visualized by fluorescent microscopy and quantitated by flow cytometry. In the G2S model, in vivo, DSBs stimulated inter-chromosomal HR events across multiple tissues examined --pancreas, liver, spleen, kidney, thymus, heart, and lung- at a frequency of 10-6. The G2S model also showed a decrease in the presence of detectable GFP+ vivo damaged

DNA duplexes that have the mobility and potential to search for homologous sequences genome-wide. Similar to results with RaDR mice and intra-chromosomal HR, aged G2S mice showed reduced inter-chromosomal HR cell populations.

1.7 Aim of this research

For my research assignment, I created a "rainbow mouse" model. The mouse model is the only one that detects mutagenic inter-chromosomal HR repair that results in translocations. The “Rainbow mouse" model consists of three unlinked transgene insertions: two nonfunctional green fluorescent proteins (GFP) with an ISCE1 endonuclease recognition site and an inducible ISCE1 construct that consists of an ISCE1 endonuclease gene. Doxycycline administration results in the ISCE1 gene being expressed and induces DSBs in the two GFP reporters. Inter-chromosomal HR can result in a functional fluorescent GFP.

In this study, I aimed to investigate the repair of DSBs within stem cells via inter-chromosomal HR. *I hypothesized that stem cells and progenitor cells would show the potential to undergo DSB-induced inter-chromosomal HR more frequently than differentiated cells*. My study revealed that the hematopoietic stem cell population, line-/CD34+, utilizes ISCE-induced inter-chromosomal HR. In contrast, terminally differentiated T and B lymphoid cells did not use inter-chromosomal HR to repair the DSBs. Additionally, I explored the potential for inter-chromosomal HR in fetuses due to *in-utero-induced* DSBs from doxycycline ingestion by pregnant females. I observed the occurrence of recombinant cells among the fetal tissues. My analysis results demonstrate variability in GFP+ recombinant cells among fetal tissue and establish inter-chromosomal HR as a probable recombination pathway during fetal development.

I also aimed to evaluate cell type-specific inter-chromosomal HR in the two distinct solid tissue types: the pancreas and the lung. *I hypothesized that both lung and pancreatic tissues would readily utilize DSB-induced inter-chromosomal*. Pancreatic duct cells are more susceptible to DSB-induced inter-chromosomal HR than any other cell type.

My findings significantly impact our understanding of DNA damage repair processes, genomic stability, and the potential implications for tissue-specific disease development and malignancy. These findings add to our understanding of how different cell types, notably stem and progenitor cells, repair DSBs via inter-chromosomal HR. These findings also highlight the importance of cellular plasticity and differentiation status in regulating the proclivity for inter-chromosomal HR repair. Furthermore, the work reveals the difference in reliance on inter-chromosomal HR repair pathways between terminally differentiated cell types and those with more remarkable plasticity. This refined understanding of repair pathways informs strategies for preserving the integrity of the genome and preventing detrimental genetic changes. The consequences go beyond revealing the delicate interplay between genetic stability and cellular responses to environmental factors and dietary choices, influencing disease susceptibility, aging, and cancer formation.

The findings additionally demonstrate that the rainbow mouse model is a valuable tool for studying changes in inter-chromosomal HR repair across developmental stages. This model improves our ability to view and analyze inter-chromosomal HR repair processes within various tissues, contributing to a complete understanding of HR repair dynamics.

Finally, the heterogeneity of GFP+ recombinant cells observed between different cell types and individual mice emphasizes the complex interplay of parameters such as replication rates, predominance rates, and clonal expansion. This variation has evolutionary significance, underscoring the potential significance of genomic instability due to recombination.

CHAPTER 2: MATERIALS AND METHOD

2.1 Rainbow cell line

The Rainbow cell line was engineered by transfecting oGFPs, yGFPs, and TET-ISCE plasmids in a WT mouse embryonic stem cell line. The oGFPs and yGFPs plasmids constitutively expressed DsRed and yellow fluorescent protein (YFP) fluorescent colors, respectively. The Far-Red or (FP602) transgene on the TET-ISCE construct showed conditional expression only in the presence of doxycycline.

Linearized oGFPs plasmid DNA was nucleofected into 1*106 D3 cells using the Amaxa nucleofection kit, following the guidelines provided by Lonza company. Post transfection, the cells were incubated in 8 ml of DME media in a 10 cm Petri plate at 37°C in a 5% CO2 incubator. Four days after transfection, the DsRed+ cells were isolated using fluorescence-activated cell sorting (FACS) with a purity of 98%. These sorted cells were cultured for an additional week to distinguish between stable and transient transfections. After eight days of sorting, the DsRed+ colonies were manually selected and cultured in 96-well plates with 100 µl of DME media. The wells containing DsRed+ colonies were expanded and used for subsequent transfection experiments. Since DsRed emits fluorescence in the red/orange range, this cell line was designated the Orange-Green (oGFPs) cell line. Subsequently, the linearized yGFPs plasmid DNA was introduced into the oGFPs cell line using nucleofection, followed by FACS sorting to select individual colonies positive for both DsRed and YFP. Each of these selected colonies was expanded and utilized for further. Each of these selected colonies was expanded and utilized for further experimentation. This resulting cell line was named the Orange-Green-Yellow (OGY) cell line.

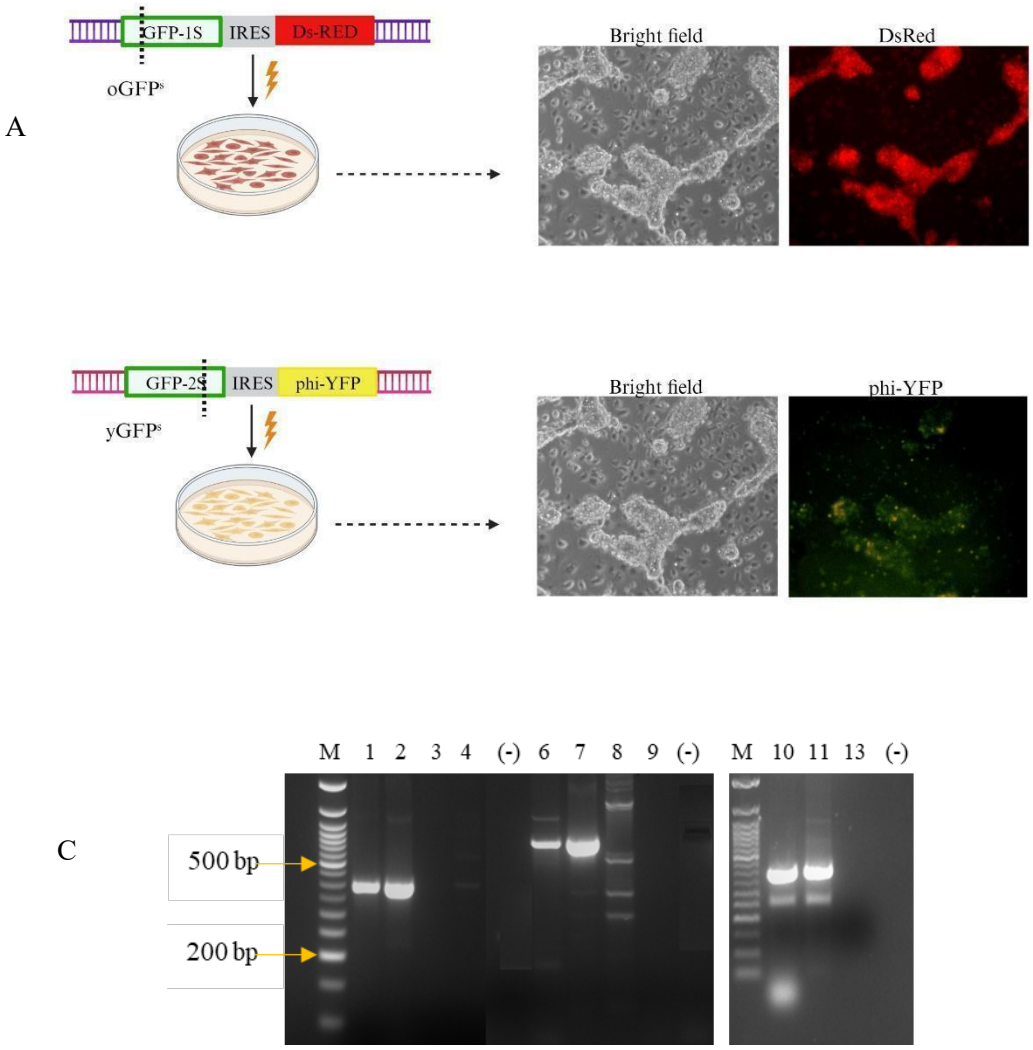

Figure 8: Engineering the rainbow cell line. A. schematic showing transfection of oGFPs (A) and yGFPs (B) constructs into D3 WT mouse embryonic cell line. Right- Images captured using done to visualize DsRed fluorescent gene using inverted Zeiss Axiovert25 microscope and capturing images with Zeiss AxioCam MRc digital camera. 20X magnification 20X, scale bar 300 µm. (C) 3% agarose gel product. (M) 50base pair NEB bp Ladder, (1) OGY cell line, (2) oGFP plasmid, (3) ISCE1 plasmid, (4) WT mouse embryonic stem cell line, (-) water. PCR was done using oGFP primers to amplify the DsRed gene. (6) OGY cell line, (7) yGFP plasmid, (8) ISCE1 plasmid, (9) WT mouse embryonic stem cell line, (-) water. PCR was done using yGFP primers to amplify YFPgene. Right (M) 50base pair NEB bp Ladder, (1) CBAS plasmid, ISCE1 plasmid, (-) OGY cell line, (-) water PCR done using ISCE1 primers to amplify ISCE1 gene.

2.2 Rainbow Mouse model

The three constructs were sent to Taconic/Cyagen Labs to use their unique technology to generate transgenic mouse lines, each with a single copy of the transgenes using the founder mouse strain CG57BL/6. The generated transgenic mice positive of single transgenic constructs were transported and housed at the vivarium facility at the University of North Carolina Charlotte. Each founder was initially mated with a wild-type C57BL/6 mouse. The presence of the transgene construct was confirmed through genotyping each mouse at the weaning age. Genomic DNA was extracted from a 2mm ear punch or tail tips using the Kapa Express Extract DNA extraction kit from Kapa Biosystems. PCR was employed to confirm the presence of each transgene using the following primers: i) yGFPs: forward 5' agttcatctgcaccaccgg 3', reverse 5' ggtaggtcttgcggcaatc 3'; ii) oGFPs: forward 5' gctccaaggtgtacgtgaag 3', reverse 5' agcttggagtccacgtagta 3'; iii) ISCE1: forward 5' tcagcagtttagagttcggac, reverse 5' gatgtctctggcatactggt 3'. The amplified DNA was visualized using gel electrophoresis on a 3% gel.

Positive transgene obligate heterozygote progeny was then backcrossed to founder mice. The resultant positive progeny was crossed and screened by PCR. Positive progenies were crossed for multiple generations and screened by semi-quantitative PCR to generate presumptive homozygous mice. Individual homozygous transgenic lines of each construct were generated and maintained. The results demonstrated that each transgenic line followed Mendelian inheritance. Homozygous oGFPs and yGFPs lines were crossed to produce the double positive oGFPs/yGFPs line. This line was maintained and self-crossed to acquire a homozygous oGFPs/yGFPs line. Finally, to generate mice for experiments, this double positive oGFPs/yGFPs homozygous line was crossed with the ISCE1 homozygous line, resulting in the triple positive oGFPs/yGFPs/ISCE1 obligate

heterozygous progeny for the experiments. Rainbow Mouse model mice were subsequently used for all the experiments.

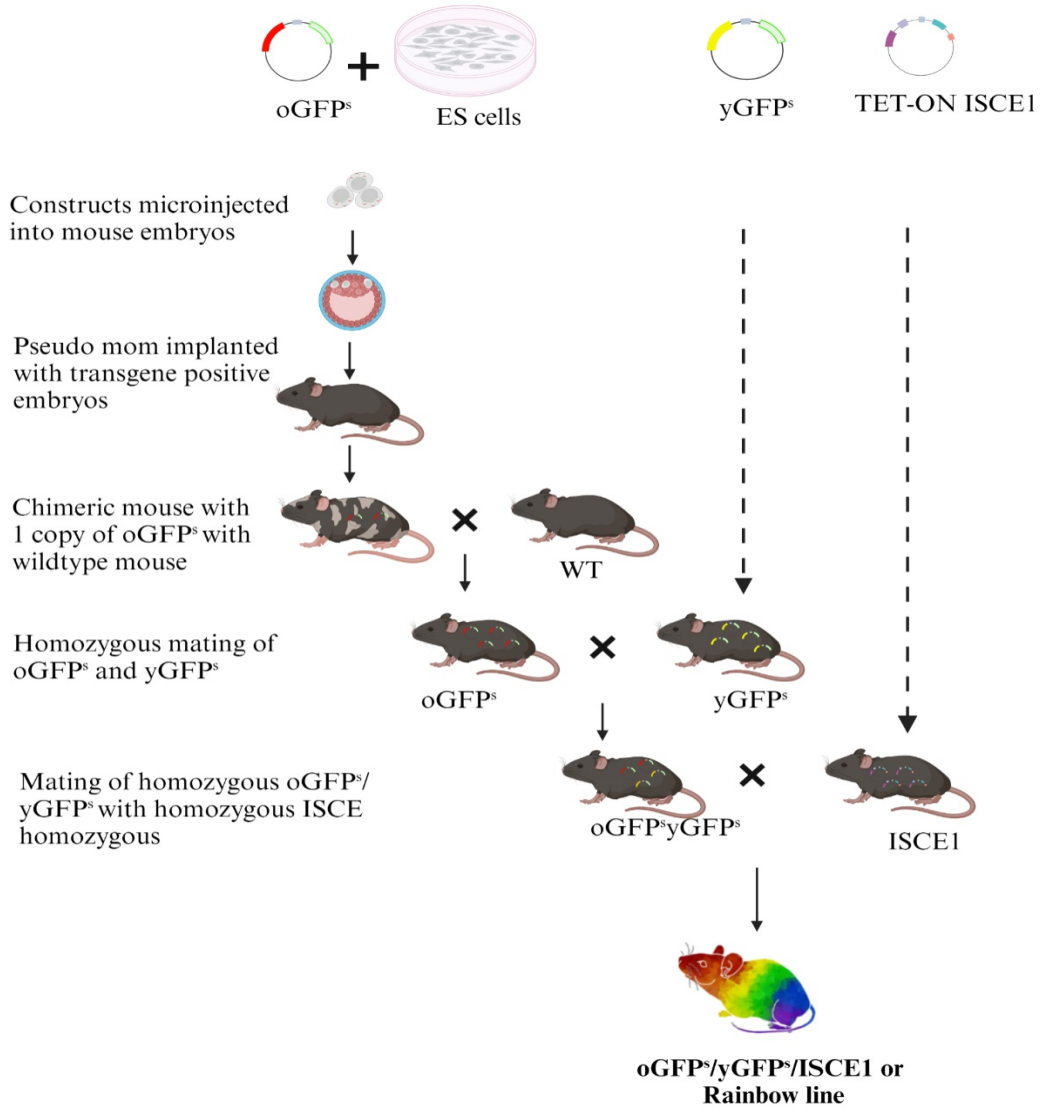

Figure 9: Scheme demonstrating generation of rainbow line. Rainbow constructs were microinjected into mouse embryos. The embryos were then implanted into WT C57BL6 pseudo mother. The offspring were screened for transgenes, positive chimeras were mated with C57BL6 WT mouse to obtain heterozygous mice which were sent to UNCC Vivarium facility. Positive transgene obligate heterozygote progeny was then backcrossed to founder mice. Resultant positive progeny was crossed and screened by PCR. Positive progenies were crossed for multiple generations and screened by semi-quantitative PCR to generate presumptive homozygous mice. Individual homozygous transgenic lines of each construct were generated and maintained. Homozygous oGFP^s and yGFP^s lines were then crossed to produce the double positive oGFP^s/yGFP^s line. Finally, this double positive oGFPs/yGFPs homozygous line was crossed with the ISCE1 homozygous line, resulting in the triple positive oGFPs/yGFPs/ISCE1 obligate heterozygous. (Rainbow mouse)

2.3 Rainbow Mouse embryonic fibroblasts

Rainbow Mouse fetuses were harvested at gestation day E13.5, and fibroblasts were cultured to generate mouse embryonic fibroblasts (MEFs). Briefly, a small portion of the fetus was segregated for DNA extraction and PCR genotyping. The bulk of fetal tissue was minced into smaller pieces and incubated in 3 ml of 0.25% Trypsin-EDTA (Gemini Bio-Products, Sacramento, CA) at 37°C with a 5% CO2 incubator for 15 minutes. The disintegrated tissue with trypsin was neutralized with 3 ml of culture medium (Dulbecco's Modified Eagle Medium (Gibco), 15% FBS (Gemini Bio-Products), 1.0% 200mM L- Glutamine (Gemini Bio-Products), 1.0% Non-essential Amino Acids (Gibco), and 1.0% Penicillin-Streptomycin (Gibco)] and centrifuged at 1000 rpm for 10 minutes. The pellet was resuspended in 4ml of culture medium and plated on 6 well petri-dish that were incubated at 37°C with 5% CO2. Once confluent, MEFs were expanded.

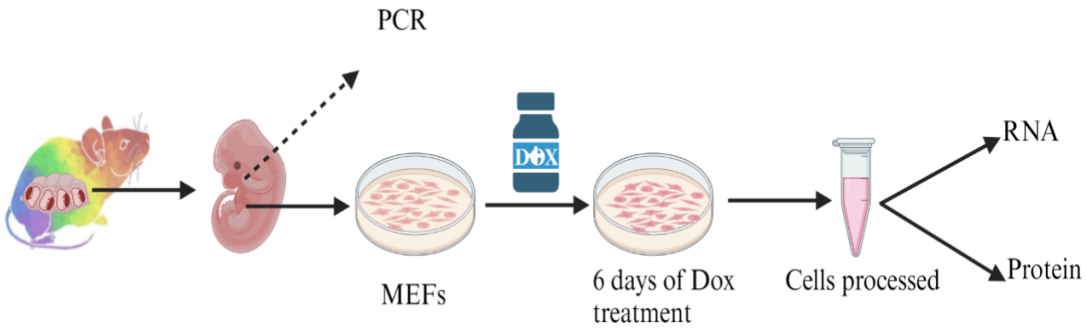

Figure 10: Schematic flowchart for obtaining rainbow MEFS. The MEFs were isolated from fetal tissues on gestation day 13.5. The cultured MEFs were treated with 2ug/ml of doxycycline drug for 6 days and processed for either RNA or protein extractions. The isolated heads from the fetus were used to extract DNA and perform genotyping.

2.4 Validation of the ISCE expression using MEFs

To confirm the expression of transgenes in rainbow mice, we performed multiple molecular techniques, including PCR, rtPCR, and western blot. The rainbow mice expressed DsRed, YFP, and ISCE1, which can be seen from the PCR results.

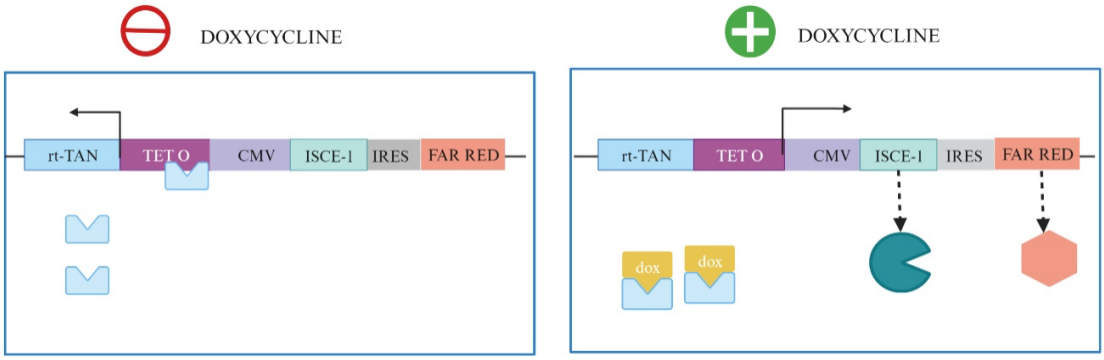

Figure 11: Schematic showing working of TET-ON system. (Left) In absence of doxycycline drug, the reverse transactivator (rtTAN) binds to the TET operator and blocks the transcription of ISCE1 and FarRed genes. In presence of doxycycline the rtTAN binds to the doxycycline and allows transcription and translation of ISCE1 and FarRed genes

PCR

Polymerase Chain Reaction (PCR) was employed to confirm the presence of the three transgenes. For yGFPs, forward (5' agttcatctgcaccaccgg 3') and reverse (5' ggtaggtcttgcggcaatc 3') primers were used to target the YFP sequence. The PCR reaction was carried out for 35 cycles with an annealing temperature of 51°C to amplify the DNA region of interest. The amplification resulted in a 567-base pair product corresponding to the YFP transgene. Gel electrophoresis was performed using a 3% agarose gel to visualize the product. For oGFPs, forward (5' gctccaaggtgtacgtgaag 3') and reverse (5' agcttggagtccacgtagta 3') primers targeted the DsRed sequence. The PCR reaction was carried out through 30 cycles with an annealing temperature of 52°C to amplify the DNA region of interest. The amplification resulted in a 397-base pair product corresponding to the DsRed transgene. For the ISCE1 construct, forward (5' tcagcagtttagagttcggac, 3') and reverse (5' gatgtctctggcatactgg 3') primers were used to target the ISCE1 sequence. The PCR reaction was carried out through 35 cycles with an annealing temperature of 51°C to amplify the DNA region of interest. The amplification resulted in a 567-base pair product corresponding to the ISCE transgene.

Water was used as a negative control, and plasmid DNA, or founder mouse DNA, was used as a positive control for each PCR reaction.

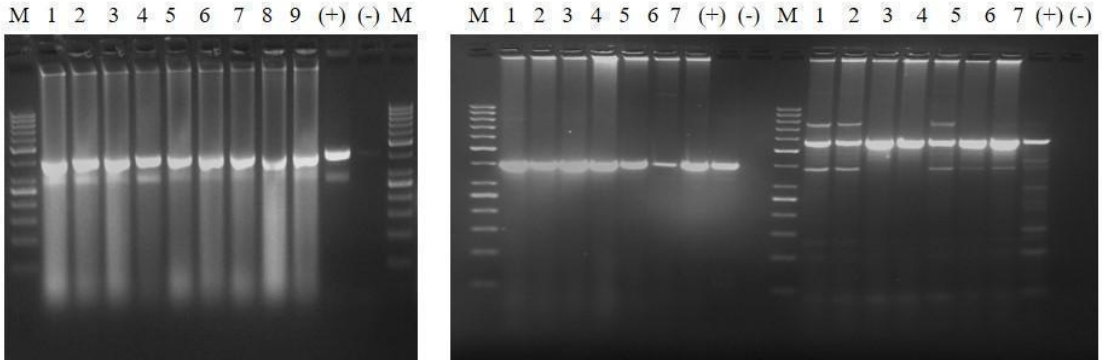

Figure 12: 3% agarose gel electrophoresis of DsRed, YFP and ISCE1 gene product from fetal tissue. (left) ISCE primers to amplify ISCE gene, Rainbow Fetus DNA (pups 1-9), ISCE founder DNA (+), water (-) (M) 50 Base pair ladder

(middle). oGFP primers to amplify DsRed gene, Rainbow Fetus DNA (pups 1-7), oGFP founder DNA (+), water (-) (M) 50 Base pair ladder

(right) yGFP primers to amplify YFP gene, Rainbow Fetus DNA (pups 1-7), yGFP founder DNA (+), water (-) (M) 50 Base pair ladder

Reverse transcription PCR

RNA from fetal tissue or rainbow mice was isolated using Qiagen RNeasy kit according to the manufacturer's protocol and was stored at -80 ^{o}C. 5 µl RNA was used for cDNA synthesis using the OneStep RT-PCR kit (Qiagen) following the manufacturer's protocol. Forward (5' tcagcagtttagagttcggac, 3') and reverse (5'gatgtctctggcatactgg 3') primers (0.6 µM dilutions were made from stock ISCE1 primers) were used targeting the ISCE1 sequence. The rt-PCR reaction was carried out through 35 cycles, each with an annealing temperature of 51°C, to amply templates.

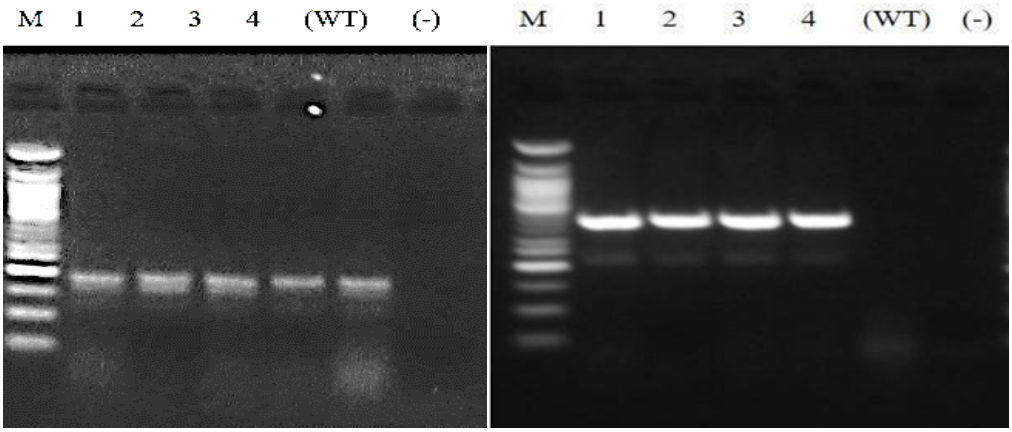

Figure 13: ISCE1 Transcript Analysis Using 3% Agarose Gel Electrophoresis in four Doxycycline-Administered Rainbow fetuses. RNA from ES cell line used as control (WT), water (-) Left GAPDH cDNA products. Right ISCE1 cDNA products. (M) 50 Base pair Ladder. *Note: From post-coitus day 1 to day 13.5, the Rainbow mother received continuous doxycycline until euthanasia and fetal tissue collection.

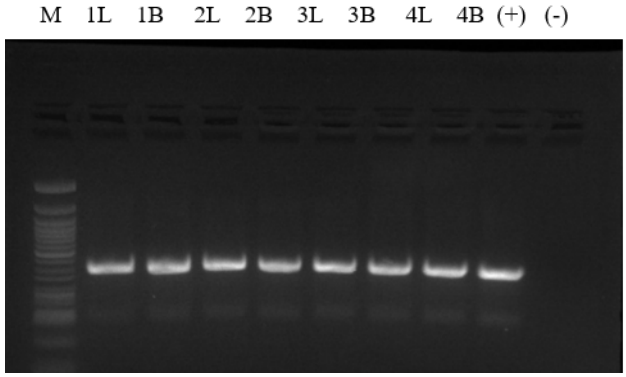

Figure 14: ISCE1 Transcript Analysis Using 3% Agarose Gel Electrophoresis in Doxycycline-Administered Rainbow Mice. Bone marrow was used as a representative for ISCE expression in hematopoietic cells. Lung was used as a representative of ISCE1 expression in sold tissues. 1L and 1B represents ISCE1 transcripts from RNA collected from lung and bone marrow one rainbow mouse after 21 days of dox administration. 2L and 2B represents ISCE1 transcripts from RNA collected from lung and bone marrow second rainbow mouse after 21 days of dox administration. 3L and 3B represents ISCE1 transcripts from RNA collected from lung and bone marrow third rainbow mouse after 21 days of dox administration. 4L and 4B represents ISCE1 transcripts from RNA collected from bone marrow fourth rainbow mouse after 21 days of dox administration. ISCE1 transcripts from RNA collected from bone marrow ISCE1 mouse after 21 days of dox administration used as positive control and water used as negative control. (M) 50 bp Ladder

Western blot

Following the manufacturer's protocol, total protein was isolated from MEF cells using M-PER (for adherent cells) or T-PER tissue Protein Extraction reagent (Thermo Scientific). The cell lysate was then separated on a 12% SDS-page gel and transferred to the PVDF membrane (GE Healthcare Life Sciences). The membrane was blocked with 10% milk-TBST for 30 minutes and washed thrice with 1X TBST buffer. The membrane was probed with HA-antibody at 1:100 overnight at 4 degrees or a monoclonal β-actin HRP conjugated antibody (Invitrogen) 1:2000 dilution for 90 minutes. Then, the membrane previously probed with the Ha-antibody followed by three 10-minute washes with 1X TBST and subsequently probed with secondary antibody anti-mouse IgG HRP conjugated secondary antibody for 90 minutes. This was followed by three 10-minute washes with the 1XTBST buffer. The blots were developed using ECL Amersham (Cytiva) and visualized using a Chemiluminescent machine.

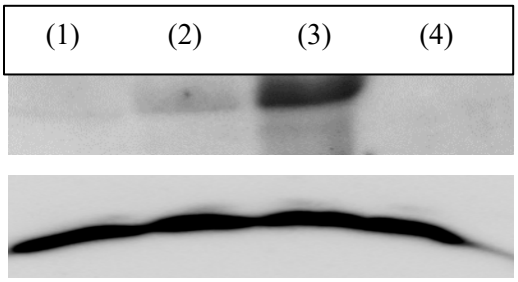

Figure 15: Western blot analysis of ISCE protein from total Rainbow MEF cell lysates. Representative immunoblots show level of ISCE protein from MEFS (1) protein from MEF treated with doxycycline (2 µg/ml) for 48 hours, (2) protein from MEF treated with doxycycline (2 µg/ml) for 96 hours, (3) protein from rainbow fetal tissue, (4) protein from untreated MEF.

*note: fetal tissue was obtained the Rainbow mother who received continuous doxycycline until euthanasia and fetal tissue collection.

2.5 Doxycycline administration

A plethora of literature suggests the 625 ppm of doxycycline dose is the most frequently used dosing, and this ensures maximum induction and distribution in most tissues (Agwuh & MacGowan, 2006; Antaódn et al., 1994) (Redelsperger IM et al., 2016). Doxycycline is generally administered by adding the drug to water or as medicated pellets. The administration of doxycycline in water had some limitations, which were considered before selecting the medium of administration. There are reports describing concerns regarding doxycycline in water, such as light sensitivity of the dox drug, frequent fungal contamination in water bottles, and the taste of the drug itself (Redelsperger IM et al., 2016). Considering all these facts, we decided to administer the dox as pellets. A specialized diet containing 625mg/kg/day of doxycycline was formulated by Harlen-Tekald (Madison, WI) for feeding the mice.

To perform an in vivo analysis of inter-chromosomal HR, age-matched rainbow mice were individually housed in cages to receive doxycycline administration. Before commencing the inter-chromosomal HR experiment, the mice underwent an acclimation process to the doxycycline diet, gradually introducing it alongside their regular diet. Initially, the mice 1/4th doxycycline chow and 3/4th regular chow for 48 hours, followed by 1/2th doxycycline chow and 1/2th regular chow for another 48 hours, and finally, 3/4th doxycycline chow and 1/4th regular chow for an additional 48 hours, after which they were transitioned to a diet consisting of 100% doxycycline chow. The mice were fed with 100% doxycycline chow for 21 days to allow continuous induction of ISCE1 expression.

2.6 Collection of cultured cells for flow cytometry

The cells were processed for flow cytometry 4-6 days post-treatment with doxycycline. For this, first, the DME media from the Petri plates was removed, followed by the addition of pre-warmed Trypsin-EDTA. The petri plates were placed in an incubator for 15 minutes at 37 C; after that, 2 ml of fresh DME media was added to neutralize the trypsin effect and remove the cells from

the Petri plate's surface. The cell suspension was centrifuged for 10 minutes at 1000 rpm. The pellets were resuspended in the appropriate amount of FACS buffer and analyzed using the FACSAriaII flow cytometer.

2.7 Tissue collection for FACS analysis

Twenty-one days of dox administration allowed continuous expression of ISCE1 transgene. The mice were euthanized per the Institutional Animal Care and Use Committee (IACUC) guidelines. After euthanasia, the mice were placed dorsally, and the limbs were secured with tape. The abdominal fur was dampened using 70% ethyl alcohol to prevent hair from entering the thoracic cavity. The surgery began with a V-shaped incision in the abdominal region that extended from the lower abdomen to the diaphragm. Once the cavity was opened, the liver was identified and gently pulled aside to reveal the pancreas and spleen. The pancreas and spleen were removed and placed in a solution of 1XPBS with 0.02% Trypsin-EDTA.

The sternum and frontal ribs were carefully cut off to expose the trachea before lung extraction. The trachea was gently tugged to access and remove the lungs and heart. The lungs were separated from the heart and trachea and put in 1X PBS with 0.02% Trypsin-EDTA.

The femur bone was used for bone marrow harvest. The thigh muscles were trimmed, and the bone above the knee and below the hip's ball socket joint was isolated. A 3 ml injection solution containing 1X PBS was passed through the femur with a 21-gauge needle to push the marrow out of the femur.

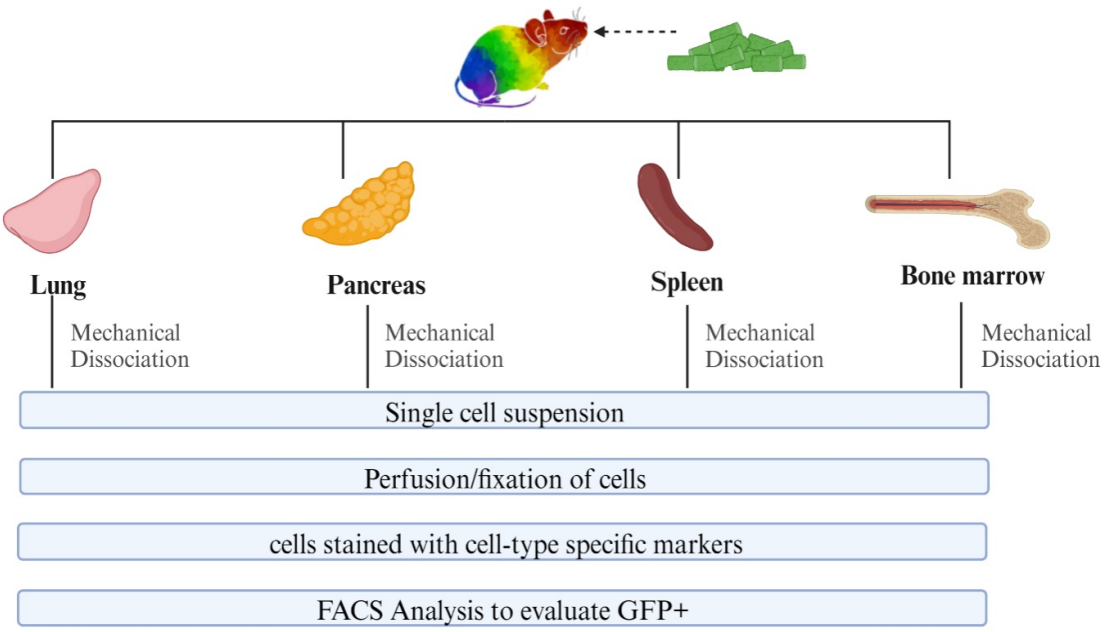

Figure 16: Schematic workflow to demonstrate inter-chromosomal HR in four different tissues. Rainbow mice were fed doxycycline chow for 21 days ad libitum and were euthanized to harvest lung pancreas spleen and bone marrow. The organs were processed to get single cell suspensions. Cells were perfused and fixed before staining with fluorescent cell type specific markers to identify the GFP+ cell subpopulations.

2.8 Organ Fixation and cell suspension

Once the organs were removed from the mice, they passed through a 40 µm cell strainer with 3 ml of 1XPBS/trypsin buffer. This allowed disintegration of the tissues, which was followed by centrifuge for 10 mins at 1000 rpm. The pellet was washed with 3ml of 1XPBS two-three times. The cells were fixed and permeabilized using a BD Cytofix/Cytoperm kit. The pellet was then resuspended 250 µl of Fixation/Permeabilization solution for 20 mins at 4℃. They were washed twice with 1ml of 1X BD Perm/Wash Buffer. The pellet was resuspended in 1ml 1X FACS buffer.

Islet enrichment: To enrich mice islet cells, I followed the protocol outlined in the study by (Corbin et al., 2021) with some minor alterations. In brief, mice were euthanized per the IACUC protocol using the CO2 method. The abdominal cavity was exposed to visualize the pancreas. A total of 3 ml of Solution C (details provided in the publication) was injected into

the pancreas near the duodenum. The entire pancreas was removed and incubated in a 15 ml tube at 37°C for 8 minutes. After incubation, the tube containing the pancreas was shaken to facilitate pancreas dissociation and subsequently filled with 10 ml of G solution. Centrifugation was performed at 1200 rpm for 7 minutes, and the supernatant was discarded.

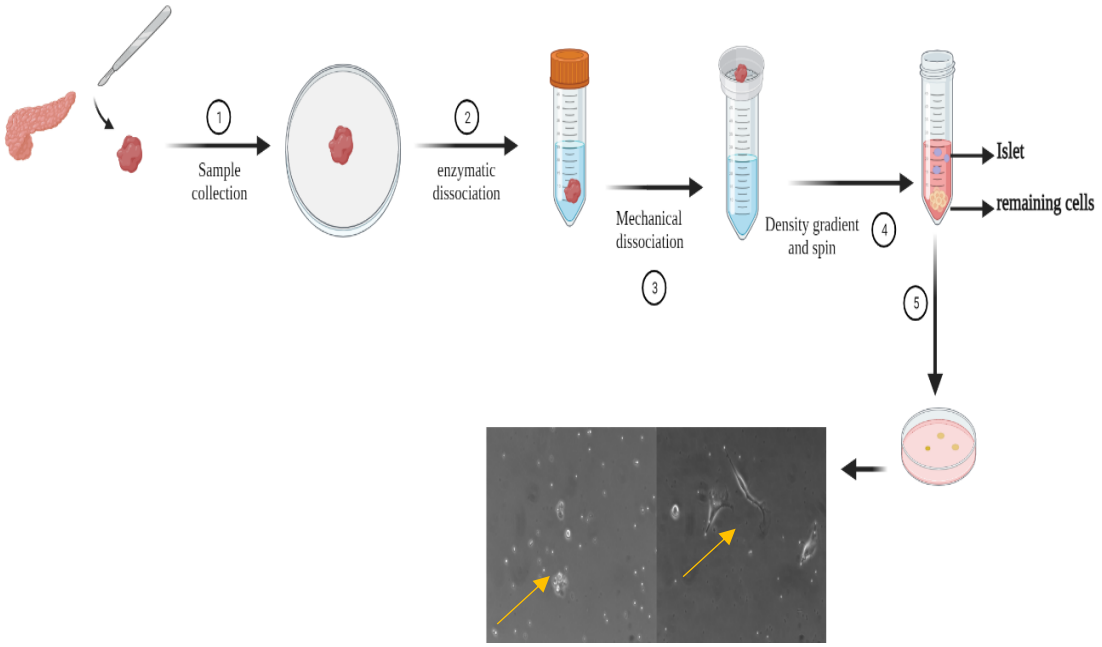

Figure 17: Schematic representation of islet cell isolation. (A) Pancreatic tissue is extracted from the mouse. Tissue is dissociated enzymatically and mechanically, followed by gradient separation. Finally, the islet cells are cultured and observed under inverted fluorescent microscope. Yellow arrow on left points to islet cell group and one on the right points to pancreatic stem cell colony.

The pellet was resuspended with fresh G-solution. This suspension was passed through a 40-µm sieve into a separate tube to eliminate clumps and excessive fat tissue. An additional 10 ml of G solution was added, followed by centrifugation at 1200 rpm for 7 minutes. The resulting pellet was resuspended in 15 ml of Histopaque 1100 (recipe provided in the publication) and centrifuged at 1200 rpm for 20 minutes. The supernatant was discarded, and the pellet was resuspended in 10 ml of G solution. Centrifugation was performed at 1500 rpm for 5 minutes, after which the supernatant was removed. The pellet was then washed to obtain

individual islet cells. Subsequently, 10 ml of prewarmed RPMI media (recipe provided in the publication) was added to the islet cells in a 10 cm petri plate, and the cells were incubated in a 5% CO2 37°C incubator. According to the manufacturer's protocol, islet cells were harvested approximately four days later and fixed using the BD Perm cytofix/cytoperm kit. The fixed cells were stored in an appropriate volume of 1X BD Perm wash buffer.

2.9 Antibody for flow cytometry

The cells were first fixed and permeabilized with a BD cytofix/cytoperm kit. Cells resuspended in 1000 µl of FACS buffer cell into multiple 5ml flow cytometry tubes. Based on the cell type, the cells were stained with specific fluorescent markers for 25 minutes in the dark at 4℃. After the cells were centrifuged for 10 minutes at 1000 rpm, the supernatant was removed, and the pellet was resuspended in 300 µl of FACS buffer. The flow tubes were stored in the dark at 4℃ until analysis. The suspensions were analyzed by BD Biosciences FACSAria AriaII Flow sorter machine with three lasers- violet (405 nm), blue (488 nm), and red (640 nm). Compensation was performed each time to avoid spectral overlapping of fluorophores and distinguish them clearly. (Table shows cell type and specific markers used.)

Table 1: List of all the four organs assessed using flow cytometry. The Cell types, known percentages and markers used to identify the cell subpopulations.

Organ	Cell Type	Cell type-Antibody with dilutions	Fluorophore	Expected Percentage
LUNG	Alveolar type-1 (AEC-1)	PDPN (1:20)	Superbright 600	8-11%

	Total epithelial population	EPCAM (1:25)	SUPERBRIGHT 645	about 70%
	AEC2	SPC (1:50)	ALEXA FLUOR 790	35-37%
	Club cells	SCGB1A1 (1:20)	bv421	3-5%
	Bronchioalveolar stem cells (BASC)	SPC+SCG1A1B1	ALEXA FLUOR 790 + BV421	>1%
PANCREAS	β cells	INSULIN (1:20)	ALEXA FLUOR 647	1%
	α cells	GLUCAGON (1:20)	BV421	>1%
	Acinar cells	AMYLASE (1:20)	ALEXA FLUOR 790	40-50%
	Duct cells	Krt19 (1:20)	ALEXA FLUOR 790	5-10%
BONE MARROW	T cells	Lin+CD4 (1:25)	ALEXA FLUOR 647	1.50%
	T cells	Lin+CD8 (1:25)	BV421	2%
	B cells	Lin+CD45r (1:10)	BV650	1%

	Hematopoietic Progenitor cells (HPCs)	Lin-CD117 (1:20)	BV605	4%
	Hematopoietic Stem and Progenitor cells (HPSC)	Lin-Sca1 (1:100)	ALEXA FLUOR 647	30-50%
	Hematopoietic stem cells (HSC)	Lin-CD34 (1:20)	BV421	1−2%
	Long Term Hematopoietic Stem cells (LT-HSC)	Lin-CD117+ Sca1-CD34+/Lin-	BV605 +BV421+ALEXA 647	>1%
	Short Term Hematopoietic Stem cells (ST-HSCs)	Lin-CD117+CD34+ Sca1	BV605 +BV421+ALEXA 647	>1%
SPLEEN	T cell	Lin+CD4 (1:25)	ALEXA FLUOR 647	1−2%
	T cell	Lin+CD8 (1:25)	BV421	1−2%
	B cell	Lin+CD45r (1:10)	BV650	7-15%
	HPCs	Lin-CD117 (1:20)	BV605	>1%

	HSPCs	Lin-Sca1 (1:100)	ALEXA FLUOR 647	30-50%
	HSCs	Lin-CD34 (1:20)	BV421	>1%
	LT-HSCs	Lin-CD117+ Sca1-CD34+/Lin-	BV605 +BV421+ALEXA 647	>1%
	ST-HSCs	Lin-CD117+CD34+ Sca1	BV605 +BV421+ALEXA 647	>1%

2.10 Mouse perfusion for histological analysis

Mice were put in an isoflurane chamber according to IACUC guidelines, and once aestheticized, mice were given nose anesthesia. Their abdominal fur is wetted with 70% ethanol to avoid hair entering the cavity. The abdomen is opened using scissors in a V-shape, from the lower abdomen to the diaphragm. The diaphragm is punctured, and two cuts from each side of the sternum are made. The sternum is pushed and held in place using a hemostat, exposing the heart. Using a 21-gauge butterfly needle apex of the heart towards the right ventricle, 20 ml of 1X phosphate saline buffer is injected. Maintain the flow rate of about 1ml/10 seconds. After that, 15-20 ml of 4% paraformaldehyde (PFA in 1XPBS) is injected using the butterfly needle while under anesthesia, maintaining the flow rate of 1 ml/10 seconds. Once the perfusion was complete, organs were harvested.

- *Lungs*: Once the trans-cardiac perfusion was complete, the tissue covering the trachea was lifted to expose the trachea. A 21-gauge butterfly needle with 5 ml of 4% PFA in 1XPBS was injected into the trachea to inflate the lung. A suture thread was tied around the trachea to hold the

needle in place. Once the perfusion was complete and the lung was inflated and whitish, the needle was removed, and the thread was tightened. The tied trachea was pulled to lift both lungs and heart, which were slowly removed using forceps. The heart was then removed, and the lungs were put in 2 ml 4% paraformaldehyde.

- *Pancreas*: Once the trans-cardiac perfusion was complete, the liver was lifted to find the pancreas. Pancreatic tissue is soft and whitish in color. The tissue between the duodenum and the spleen was collected for histology (section 3.5.5). To obtain total pancreatic tissue for flow cytometry, the entire pancreas from the duodenum, bile duct, and spleen to the intestinal lining was removed.

2.11 Histological analysis

The fixed tissue samples were placed in a 4% PFA/PBS solution overnight before histological analysis. The 4% PFA solution was replaced with a 30% sucrose solution the next day, and the samples were kept at 4°C overnight. The next day, the tissues were removed from the solution and cut into smaller pieces if necessary. To embed the tissues, 8mm square disposable polyethylene molds were labeled. Following that, these molds were partially filled with optimal cutting temperature (OCT) compound and placed in a box filled with Cold lab armor metallic alloy beads to facilitate flash freezing. After the OCT compound had partially frozen, the tissue was positioned longitudinally onto the mold. Another layer of OCT compound was put on to embed the tissues completely. Following complete tissue freezing, the molds were covered with aluminum foil and stored at -80°C until sectioning. The embedded sections were thawed to -20°C in a cryostat chamber before being sectioned. Using a cryostat, thin sections of 6 micrometers were cut. Each section was collected onto a labeled gelatin-coated slide and stored at -20°C until needed. Different staining techniques were employed to identify the morphology of the cells, nucleus and determine cell types.

2.11.1 Hematoxylin and Eosin Staining

The hematoxylin compound stains the nucleus while the eosin stains cytoplasm. Before beginning the staining process, the tissue section-containing slides were frozen at room temperature for 30 minutes. The slides were first placed in a jar containing deionized water (DI) for 1 minute, which was then repeated. Next that, the slides were incubated for 15 seconds in a jar containing hematoxylin stain, followed by a 2-minute rinse under tap water. This was followed by a 30-second immersion in a jar containing a 95% ethyl alcohol twice. Following that, the slides were immersed in Eosin for 15 seconds. The slides were submerged in 95% ethyl alcohol twice for 30 seconds each. Following this sequence, two 1-minute immersions in 100% ethyl alcohol were performed. The slides were then placed in a container containing Xylene dye for about 3 minutes. Following that, the slides were taken out, cleaned, and a drop of Cytoseal mounting media was applied, followed by the placement of the cover slide. The mounting media was allowed to firm overnight before the sections were viewed under the Thermo Fisher EVOS M5000 microscope with 10X or 20X lenses and RGB channel detection.

2.11.2 DAPI staining

The 4',6-diamidino-2-phenylindole (DAPI) dye binds with minor groove areas of adenine-thymine (A/T) rich double-stranded DNA sequences, making it helpful for fluorescent nuclear labeling. The tissue sections were first thawed at room temperature for 30 minutes, followed by adding 0.2% Triton X-100 in 1X PBS and incubating for 15 minutes at room temperature. Then, the tissues were washed in 1X PBS twice, 5 minutes each. Diamond Antifade mounting solution with DAPI dye was applied to the sections, and coverslips were placed over the slides. The slides were then kept in a dark room at room temperature to allow DAPI to activate and the mounting media to solidify. The slides were viewed under a Thermo Fisher EVOS M5000 microscope with 10X or 20X lenses and DAPI channel detection.

2.11.3 Immunohistochemistry

The slides were thawed at room temperature for 30 minutes. First, the slides were washed with 1X PBS. The tissue sections were marked on the slides using a hydrophobic barrier pen, and the sections were washed twice for 10 minutes with 1% bovine serum albumin (BSA) in 1XPBS-T (0.4% Triton X-100 in 1X PBS buffer). The sections were then blocked with 5% BSA/PBS-T for 30 minutes at room temperature to avoid nonspecific binding. The blocking buffer was removed, and cell-specific primary antibodies were added on top of the tissue. The slides are incubated in a moist closed box placed at room temperature for 90 minutes and later stored at 4C overnight. The next day, the slides were washed twice with 1% BSA/PBS-T for 10 minutes each time. The slides were then stained with fluorescent label conjugated secondary antibodies and incubated in a dark, moist box for 2 hrs. Excess antibodies are washed, a prolonged antifade diamond mounting medium is dropped on the sections, followed by a coverslip. The slides are stored at room temperature to solidify the mounting medium. The slides are then stored at – 20C and analyzed using Confocal microscopy. (Table shows the antibodies used to identify lung cell types.)

Table 2: List of lung cell types identified using immunohistochemistry.

Organs	*Cell Type*	*Primary Antibody*	*Secondary Antibody*
Lung	Alveolar type- 2 cells (AEC2)	SPC (unconjugated) (1:50)	ALEXA FLUOR 750 (1:100)
Lung	Club cells	SCGB1A1 (unconjugated) (1:50)	ALEXA FLUOR 750 (1:100)

CHAPTER 3: GENERATION AND IN VITRO VALIDATION OF RAINBOW MOUSE MODEL

3.1 Creation of rainbow model

In order to develop the rainbow mouse, three individual plasmid transgene constructs were designed. (Figure) These included: i) oGFPs that consist of a mutated GFP with an ISCEI endonuclease recognition site followed by IRES-DsRed. ii) yGFPs, another mutated GFP with ISCE1 endonuclease recognition site followed by IRES-YFP, and iii) tetracycline ON-inducible ISCE1 endonuclease gene followed by IRES-Far red.

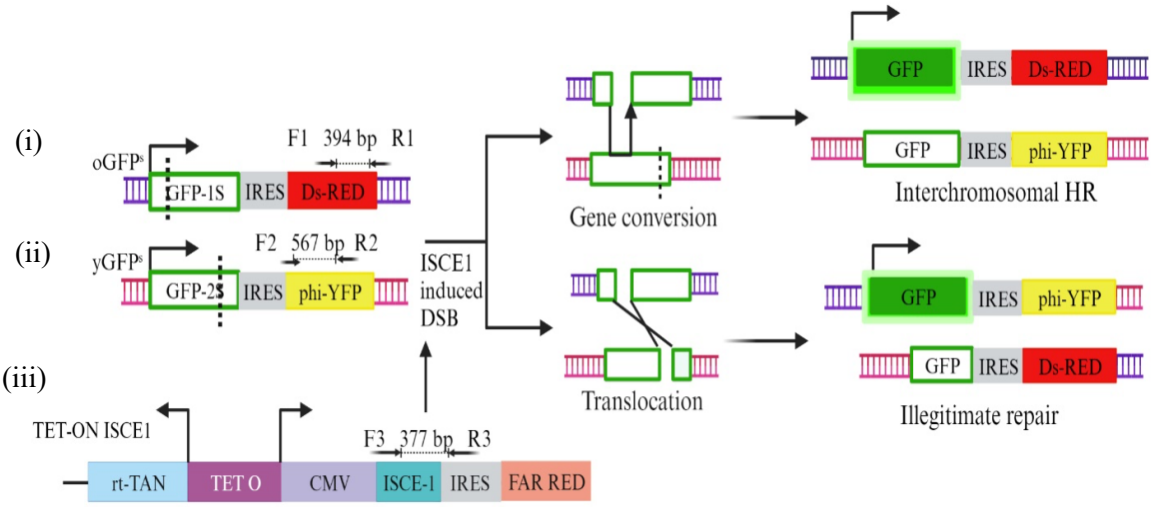

Figure 18: Schematic of the Rainbow model. (i) oGFPˢ, (ii) yGFPˢ, and (iii)TET-ON ISCE1. Addition of doxycycline to the rainbow system induces expression of ISCE1 endonuclease which initiates site directed DSBs at the two GFP (ISCE1-recognition site highlighted by dotted lines) The repair via inter-chromosomal HR results in fluorescent GFP.

3.1.1 yGFPs construct

This reporter construct utilized the turbo-green fluorescent protein (GFP) derived from the Green pTurboGFP-PRL plasmid as the GFP component. The plasmid DNA was subjected to restriction digestion using the NOT1 restriction enzyme, resulting in a linear DNA fragment. A 7-base pair oligonucleotide linker, Not-Hpa-EcoR1, was ligated to the Not1 site on the turboGFP-PRL plasmid. The ligated plasmid was then cloned and introduced into TOP10 competent E. coli

cells through transfection. The DNA extracted from the cells was subsequently digested with the EcoR1 restriction enzyme, resulting in the isolation of turbo GFP fragment, confirmed through 1% agarose gel electrophoresis. This GFP fragment was inserted into a backbone plasmid, pBluscript SK+, using the T4 ligase kit, creating the BlueGreen-WT Ecor1 vector. Furthermore, a 23-base pair SCE1 blunt oligonucleotide sequence was inserted downstream of the EcoR1 site at position 1881 base pairs of the GFP fragment, leading to the generation of the BSKgreenfoSce construct. The entire GFP fragment and the ISCE site region were isolated from the BSKgreenfoSce plasmid at EcoR1 sites and then inserted into the pEF2a-IRES vector.

The phiYellow-PRL vector was subjected to digestion with the Sal1 restriction enzyme to linearize it. A Sal-Xba-Sal linker was inserted downstream of the yellow fluorescent protein (YFP) gene. The pEF2a-GFPs IRES vector was digested using the Xba restriction enzyme, and the YFP fragment was subcloned into it, creating the BlueGreenfoSce-YFP construct (referred to as yGFPs). This yGFPs plasmid was then introduced into competent E. coli cells and allowed to grow overnight. The DNA extracted from the E. coli colonies was amplified using YFP-specific primers (forward: 5’ agttcatctgcaccaccgg, reverse: 5’ ggtaggtcttgcggcaatc), resulting in a 567-base pair amplified product. The amplified product was observed using 3% agarose gel.

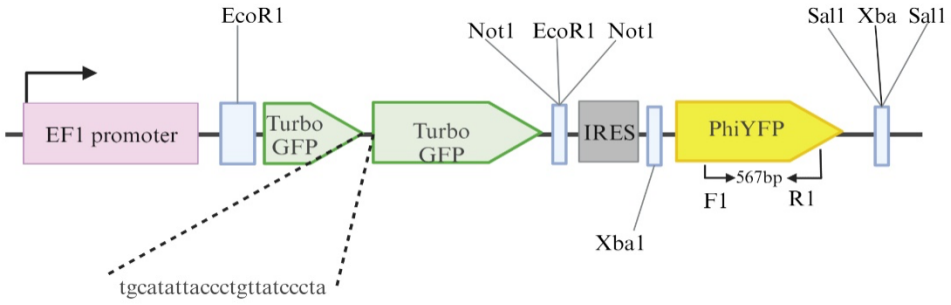

Figure 19: Schematic of yGFP^s construct. The yGFP^s plasmid consists of a turbo GFP with 23 bp ISCE1 sequence which makes the gene nonfunctional. It also consists of the IRES region for continuous transcription of GFP and YFP genes. The F1 and R1 are forward and reverse primers used to amplify 567 bp long YFP amplified product.

3.1.2 oGFP^{s} construct

A 23-base pair SCE1 linker was inserted into the Green pTurboGFP-PRL vector at position 334 base pairs downstream of the EcoR1 site on the turboGFP sequence, resulting in the generation of the green pTurboGFPxs-PRL vector. The Orange pEF1-DsRed express vector was obtained commercially. It was initially digested using the Xba restriction enzyme, and the turboGFPxs fragment was subsequently subcloned into it, giving rise to the OrangeGreenxs vector (referred to as oGFPs). The DNA extracted from the E. coli colonies was amplified using DsRed-specific primers (Forward 5' gctccaaggtgtacgtgaag 3' reverse 5' agcttggagtccacgtagta 3'), resulting in a 394-base pair amplified product. The amplified product was observed using 3% agarose gel.

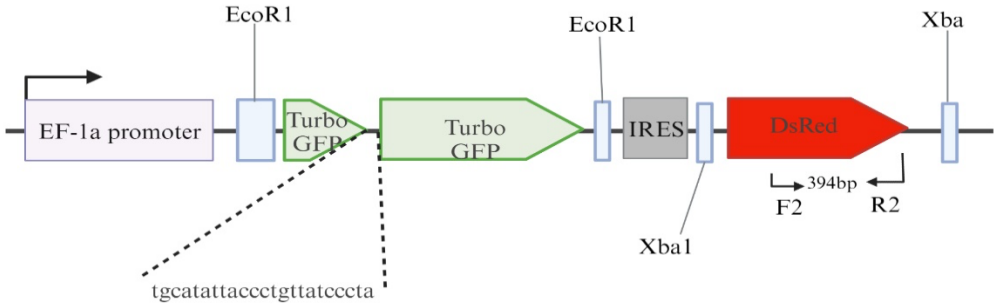

Figure 20: Schematic of oGFP^{s} construct. The oGFP^{s} plasmid consists of a turbo GFP with 23 bp ISCE1 sequence which makes the gene nonfunctional. It also consists of the IRES region for continuous transcription of GFP and DsRed genes. The F2 and R2 are forward and reverse primers used to amplify 394 bp long DsRed amplified product.

3.1.3 TET-ON ISCE construct

Concurrently, the ISCE gene derived from the CBAS vector was fragmented at the Xba1 and Bgl2 restriction sites. This fragment was subsequently inserted into the pBIG3i bicistronic TET-ON vector at the BamH1-Nhe1 site, generating the pBIG3i-ISCE1 vector. The pTurboFP602-PRL vector was obtained commercially and subjected to fragmentation using Sal1 and Not1 restriction enzymes, yielding the turboFP02 sequence. This sequence was then inserted into the blue pEF2a-IRES vector at the Sal1/Not1 site, creating a subclone known as the blue EF2a-IRES-TurboFP602

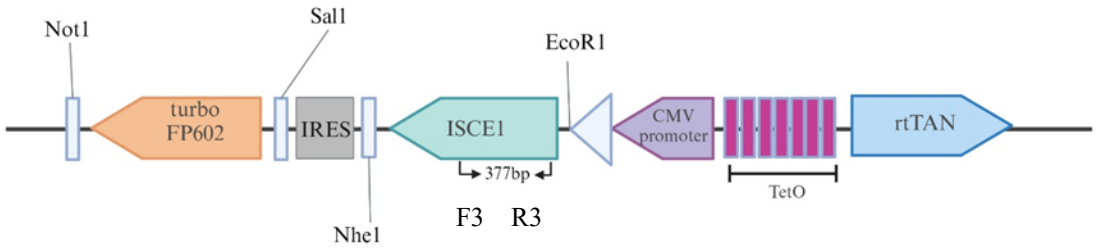

Figure 21: Schematic TET-ON ISCE1 construct. The TET-ON ISCE1 plasmid is bicistronic plasmid consisting of tetracycline operator with reverse transactivator gene on one side and CMV promoter on the other side. The ISCE1 is followed by IRES region and turbo FP602 gene. The F3 and R3 are forward and reverse primers used to amplify 377 bp long ISCE1amplified product.

vector. IRES-pTurboFP602 fragment from the blue EF2a-IRES-TurboFP602 vector was then inserted into the pBIG3i-ISCE1 vector at the Not1-Spe1 site, resulting in the formation of the pBIG-SCE-FP602 vector, which will be referred to as the TET-ON ISCE vector. Following the introduction of the constructs into E. coli cells, DNA was extracted from the colonies, and amplification was performed using ISCE-specific primers (ISCE: tcagcagtttagagttcggac, reverse: 5’ gatgtctctggcatactggt). This amplification resulted in a 377-base pair product, which was visualized using 3% agarose gel electrophoresis.

3.2 In vitro validation of rainbow model

3.2.1 Experimental setup for investigation of inter-chromosomal HR in OGY cell line

The cells were divided into groups: (i) group received only ES DME media, (ii) received GFP plasmid vector, (iii) received CBAS plasmid vector, and (iv) received TET-ISCE1 vector. Each plasmid vector was transfected into the OGY cells using an electroporation technique. Once the cells were electroporated with the necessary concentration of plasmid sequences, the cells were incubated at 37°C, 5% CO2 overnight. The media was changed the following day. Group (iv) received 2ug/ml doxycycline in 1X PBS daily for four days. The cells were initially scored for GFP+ colonies using an inverted Zeiss Axiovert25 microscope and capturing images with a Zeiss AxioCam MRc digital camera. The GFP+ cells were quantified using a BD Science FACSAriaII flow sorter machine.

3.2.2 Results:

The inverted microscopy revealed GFP+ colonies in four of the treatment groups: (i) control group with only ES DME media, (ii) received GFP plasmid vector, (iii) received CBAS plasmid vector, and (iv) received TET-ISCE1 vector. As expected, flow cytometry analysis revealed that the first group with only DME media had the least or no GFP+ cells, and the second group with a GFP+ vector had the highest percentage of GFP+ cells, about 15.9%. The third group with the CBAS vector had about 2.1% GFP+ cells, and the TET-ISCE1 vector with doxycycline drug had 1.6% GFP+ cells. The results from the in vitro cell line experiment demonstrate that in the presence of a functional ISCE1 endonuclease, the two nonfunctional GFPs accurately create double-stranded breaks at the ISCE1 recognition sites on the two GFPs and inter-chromosomal HR between the two GFPs results into functional GFP.

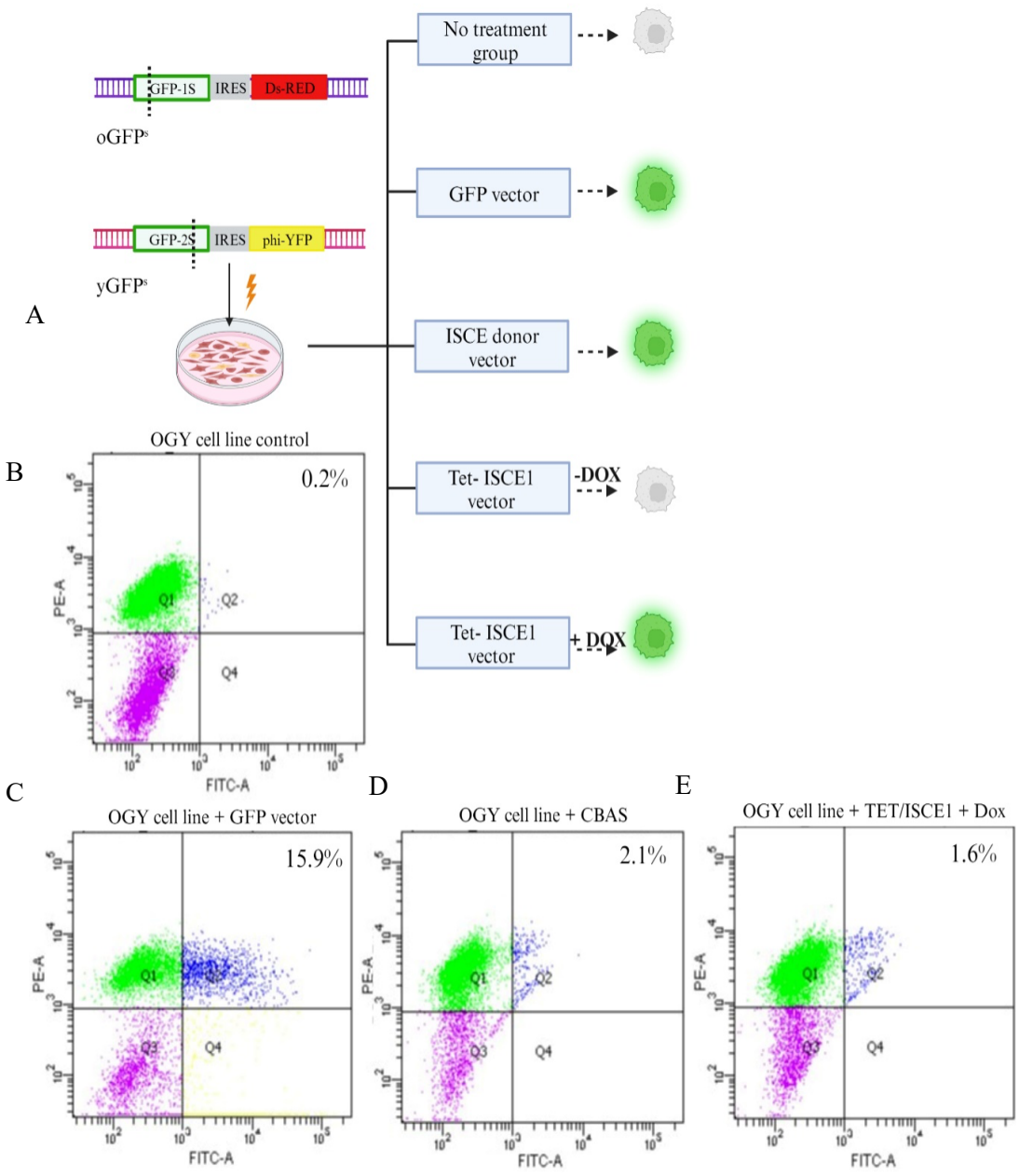

Figure 22: in vivo validation of rainbow constructs. A Schematic figure of showing experimental groups, i) control group with only ES DME media, (ii) received GFP plasmid vector, (iii) received CBAS plasmid vector and (iv) received TET-ISCE1 vector.

Representative FACS plots of OGY experimental groups. A-D plots represents forward/ side scatter plots of 4 experimental groups, (The dot plot profile of DsRed+ cells shown in Quadrant 1 (Q1) dot plot profile of DsRed/YFP/GFP+ cells are shown in Q2, dot plot profile of YFP/GFP+ cells are shown in Q4, dot plot profile of WT cells shown in Q3.

3.3 Experimental setup for investigation of inter-chromosomal HR in MEF

Mouse embryonic fibroblasts (MEFS) were harvested from triple-positive rainbow mice on gestation day E13.5. The cells were divided into groups: (i) group received only MEF DME media, (ii) received GFP plasmid vector, (iii) received CBAS plasmid vector, and (iv) received 2 µg/ml doxycycline in 1X PBS every day for six days. Based on the manufacturer's guidelines, each vector was nucleofected into the MEFs using the Lonza MEF nucleofection kit. Once the cells were incubated at 37℃, 5% CO2 overnight. I performed rt-PCR and western blot to validate the expression of dox-induced ISCE1 in MEFs. The cells were initially scored for GFP+ colonies using an inverted Zeiss Axiovert25 microscope and capturing images with a Zeiss AxioCam MRc digital camera. The GFP+ cells were quantified using BD Science FACSAriaII flow sorter.

3.3.1 Results:

MEFs were harvested from triple-positive rainbow mice on day E13.5. The cultured MEFS were divided into three groups: (i) receiving DME media without Doxycycline, (ii) group transfected with GFP expression vector, or (iii) CBAS ISCE1 expression vector, (iv) receiving DME media with two µg/ml of Doxycycline to induce DSB through ISCE1 expression, and. The detection of GFP+ cells was done by fluorescent inverted microscopy and flow cytometry.

The gating system for determining GFP positivity was set up such that negative controls showed no detectable GFP-positive events, with a calculated value of less than 2 events per million. This same gating system was applied to the MEF samples that were transfected with GFP vector or ISCE1 vector or treated with or without doxycycline drug. The MEF group transfected with the GFP vector had about 6.6% GFP+ cells. The MEF group transfected the ISCE1 vector with about 1.02% GFP+ cells. The MEF group treated with Doxycycline had 0.8% GFP+ cells. Statistical significance was calculated using one-way ANOVA followed by the Kruskal-Wallis nonparametric test. A similar trend was observed in both qualitative and quantitative analysis, determining the efficiency of the TET-ON ISCE1 system.

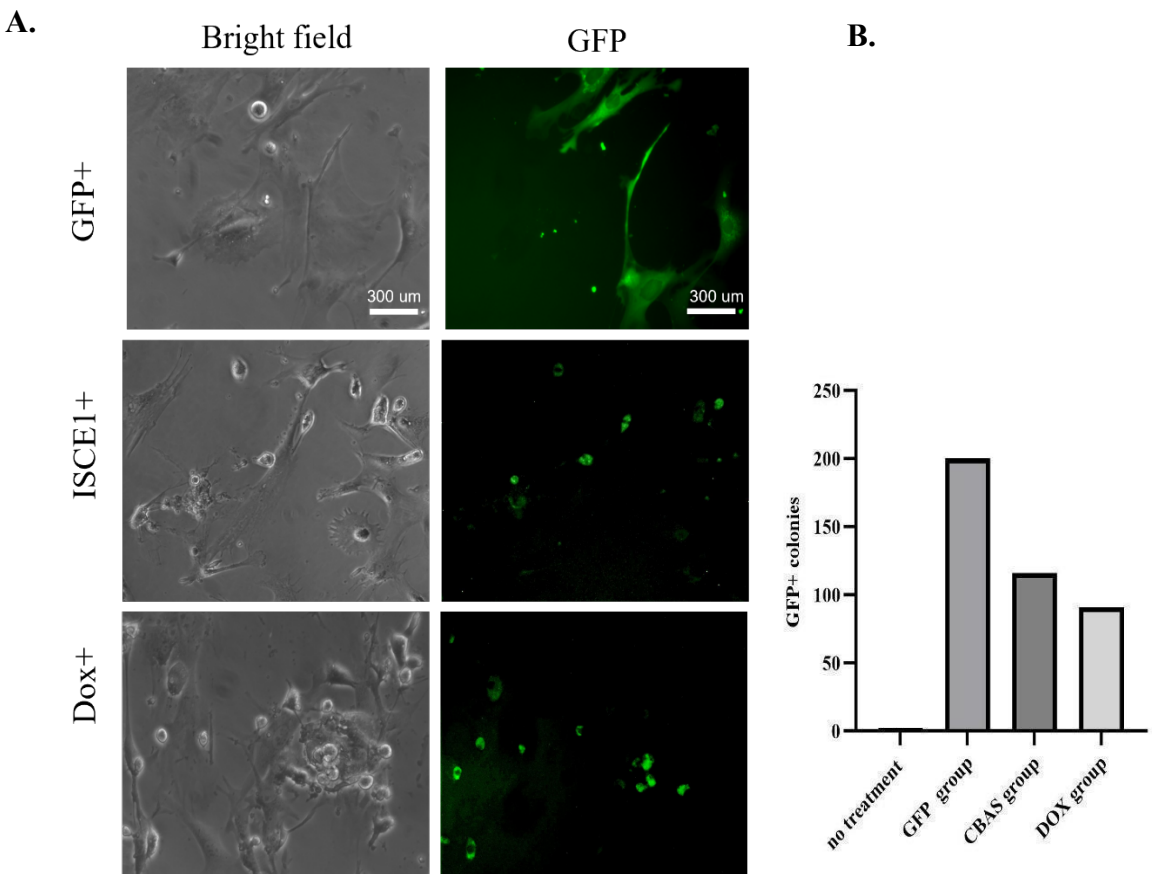

Figure 23: Validation of interchromosomal HR in MEFs by microscopy. (A) Microscopy from MEF experiments. Bright-field and matched fluorescent microscopy images of GFP+ colonies among MEF experimental groups, 20X magnification. Top- GFP+ colonies in the GFP group as a control, (center) GFP+ colonies in the CBAS ISCE expression group, and (bottom) GFP+ colonies in the treatment group. (B) Representative bar graphs depicting the number of GFP+ colonies counted from each treatment group on day 6. As observed from the microscopy and the representative graphs, the highest number of GFP+ colonies were observed in the GFP transfected group, which was 200 colonies. This was followed by the ISCE plasmid group with 116 GFP+ colonies and the least in the Dox group with

Table 3: Results from MEF experiments. To investigate inter-chromosomal HR in MEF tissues, the cultured cells were divided into 4 groups. This experiment was performed in four replicates. Each replicate received exact treatment for 96r and analyzed for flow cytometry. See figure 23 for FACS analysis.

Replicates	*No Treatment*	*GFP Group*	*ISCE1 Group*	*Dox Group*
1	0	3.9	0.4	0.1
2	0	14.9	1.2	1.2
3	0	4.4	1.3	1.3
4	0	3.2	1.2	N/A

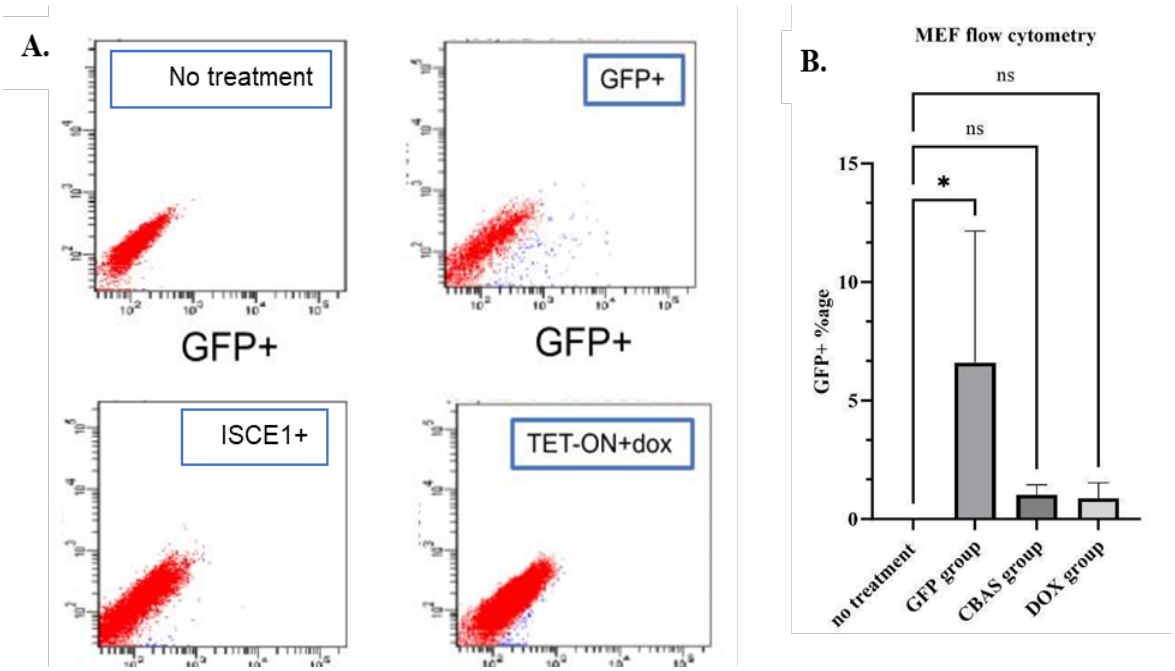

Figure 24: Validation of inter-chromosomal HR in MEFs by flow cytometry. (A) FACS representative plots of each of the experimental groups. The total number of events observed was 30K. The X-axis depicts logarithmic GFP positivity, and the Y-axis depicts cell count. (D) Graphical representation of GFP+ from each experimental group. As observed from the FACS plots and the bar graph, there was a clear indication that the group administrated with doxycycline had a GFP recombinant population. The FACS plots are indicative of a very similar trend observed via microscopy. The GFP+ group had the highest percentage of GFP+ cells (average 6.6%), followed by the percentage of GFP+ from the ISCE group (1.03%) and the percentage of GFP+ from the dox group (0.87%).

Data (No treatment N=3, Treatment group N=3) are presented as Individual values and Median (with ranges). Differences in GFP+ (%) between treatments were tested using non-parametric KW and post-hoc determined by the Dunn test (*p<05; **p<0.01).

3.3.2 Conclusion

This initial validation of the rainbow constructs involved using rainbow mouse embryonic cell lines and the rainbow MEFs. ES and MEF cells were cultured in controlled conditions and treated similarly to induce ISCE breaks and repair. The FACS analysis was performed on a small population of 30,000 events, which revealed detectable HR recombinant events. Microscopic analysis of the ES cells also revealed GFP+ colonies in the TET-ISCE1 group, similar to GFP+ colonies from the CBAS group, suggesting a non-leaking TET-ON system.

CHAPTER 4: *IN VIVO* INTER-CHROMOSOMAL HR IN HEMATOPOIETIC CELLS

Introduction

Stem cells are characterized by their ability to replicate into another stem cell and a more differentiated cell that can generate specialized cell lineages (D. J. Rossi et al., 2008; Tichy & Stambrook, 2008). During development, embryonic stem cells (ESC) form from the blastocyst's inner mass, have unique replication potential and form an entire organism. In addition, ESCs have unique characteristics like a high replication rate, specific cell cycles, and DNA damage repair mechanisms (Tichy & Stambrook, 2008). ESCs are incredibly proficient in repairing DNA damage, resulting in a considerably decreased mutation rate—approximately 100 times lower—compared to other specialized cells such as MEFs (Tichy & Stambrook, 2008). However, the increased replication rate of ESCs increases the risk of passing on damaged DNA to daughter cells. To repair DSBs in DNA, ESCs predominantly use homologous recombination; however, the specific molecular mechanisms behind this robust repair process are less defined (Tichy & Stambrook, 2008).

Similar to ESC, adult stem cells can undergo differentiation to generate multipotent and lineage-committed cells, although usually within specific organ systems. Hematopoietic stem cells (HSC) mainly reside in the bone marrow and differentiate to continually replenish red blood cells, myeloid cells, and immune cells (Ramaiah et al., 2013; Schmitt et al., 2014). HSCs play a central role in hematopoiesis due to their distinct characteristics as multipotent and self-renewing cells (Seita & Weissman, 2010). Hematopoiesis occurs in two major stages: primitive hematopoiesis, which occurs during early embryogenesis and gives rise to the blood system, and definitive hematopoiesis, which occurs during fetal development and postnatal development and generates stem cells for the formation of all lineages (Seita & Weissman, 2010). In mice, the appearance of hematopoietic cells initially occurs in the yolk sac at gestation day 7.5, followed by secondary

hematopoiesis in the aorta-gonad-mesonephros (AGM) at gestation day 10 (Ramaiah et al., 2013). Later, the HSCs migrate to colonize the fetal liver, which is a significant hematopoietic organ that can be observed from gestation day 12-16, where they undergo approximately 38-fold expansion and eventually settle and colonize into the bone marrow towards the end of gestation and postnatally (Ema & Nakauchi, 2000). Other than BM, HSCs can also be found in the thymus and spleen and may contribute to extramedullary hematopoiesis under specific circumstances (Barker et al., 1969; Marié et al., 2022).

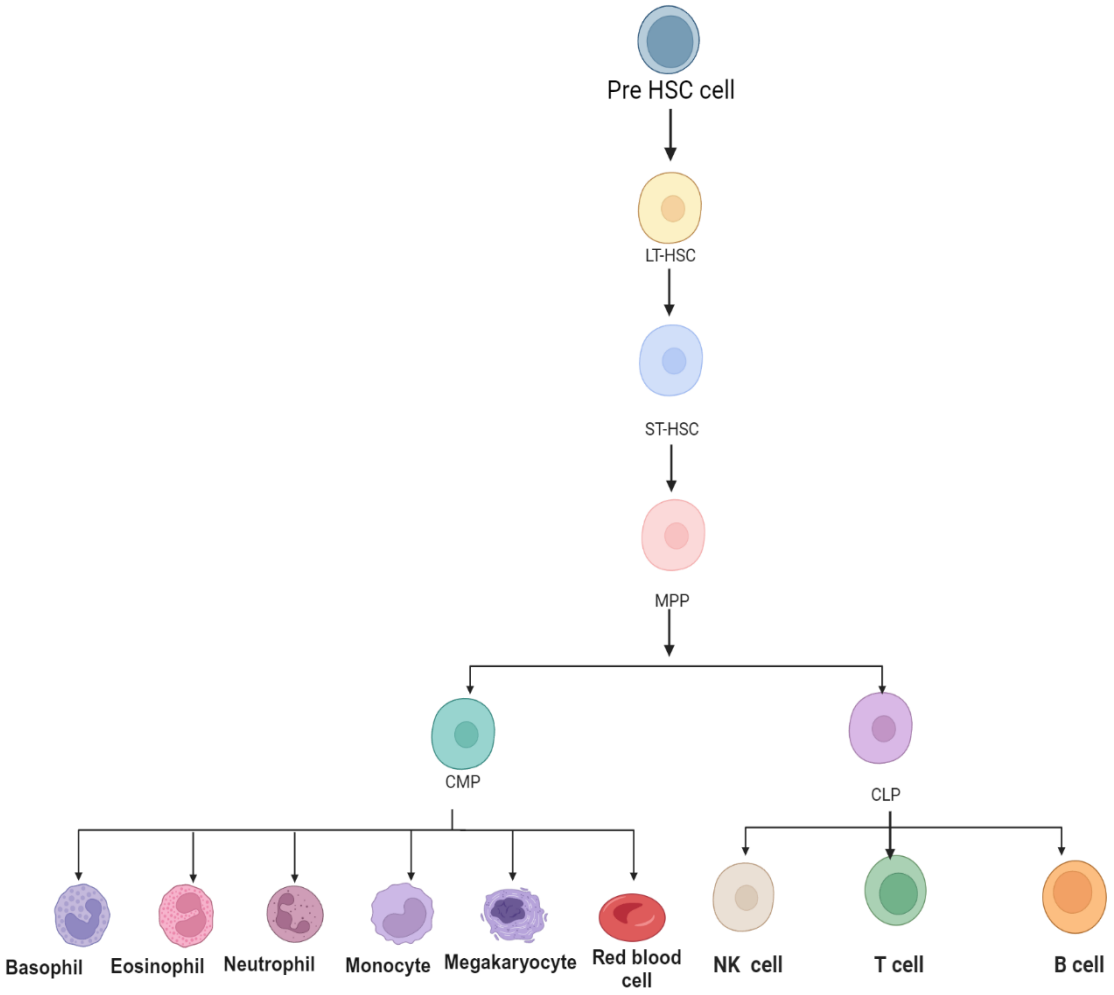

Figure 25: Schematic flowchart of hematopoietic lineage.

In adult BM, long-term HSC (LT-HSC) can produce various progenitor cells and more differentiated cell lineages but are mostly quiescent, dividing once every 145 days (Pietras et al., 2011). However, HSCs can be mobilized to enter the cell cycle and undergo massive expansion under stress, such as inflammation or exposure to cytotoxic or genotoxic agents (Beerman et al., 2014; Li et al., 2016). Multipotent progenitor (MPP) cells are more differentiated, with a lower capacity for self-renewal (Li et al., 2016). They are often called short-term HSC (ST-HSC) (L. Rossi et al., 2011).

The rapid rate of proliferation of hematopoietic cells is driven by the constant requirement for renewal of blood, hemostatic, and immune cell production, which also increases their vulnerability to DNA damage (Ramaiah et al., 2013; L. Rossi et al., 2011). FL HSC has an increased rate of metabolism and energy consumption compared to BM HSC, resulting in a higher frequency of ROS production, which is associated with genotoxicity (Manesia et al., 2015). Another study used IR to induce damage in HSCs of FL and adult BM. The chromosomal analysis of LT-HSCs using multicolor fluorescence in situ hybridization (mFISH) showed that chromosomal aberrations induced by radiation in adult BM were about 2.4 times higher than alterations in fetal HSCs. Results from these experiments highlight that even though FLs are sensitive towards DSB, they are more resilient in resolving DSBs than adult HSCs, which tend to accumulate damage (Hamasaki et al., 2023).

In this study, I aimed to investigate the *in vivo* repair of DSBs via inter-chromosomal HR within hematopoietic cell lineages and progenitor and stem cell-enriched populations from bone marrow and spleen. I hypothesized that stem cells and progenitor cells would show the potential to undergo DSB-induced inter-chromosomal HR more frequently than differentiated cells.

Further, I began to explore the potential for inter-chromosomal HR in fetuses due to *in utero* induced DSBs from doxycycline ingestion by pregnant females.

4.1 In vivo investigation of DSB-induced Inter-chromosomal HR in bone marrow and spleen.

Following 21 days of doxycycline diet supplementation, Rainbow mice were euthanized, and bone marrow and spleen cells were harvested. Single-cell suspensions were fixed, and cell suspensions were enriched. Depletion of lineage-committed cells using the Mouse Hematopoietic Progenitor (Stem) Cell Enrichment Set-DM kit BD enrichment/depletion kit, as guided by the manufacturer's instructions. Some aliquots of lineage + (Lin+) cells were analyzed as total Lin+, a population that includes terminally differentiated myeloid (monocyte, macrophage, and granulocyte cells) and lymphoid cells (T and B cells). Some aliquots were stained with Pacific Blue conjugated anti-CD4 antibodies and APC conjugated anti-CD8 antibodies to identify T cells or with PE-Cy conjugated anti-CD45R antibodies to identify B cells. Lineage – (Lin-) cells were stained with Bv421 conjugated anti-CD34, Alexa Fluor 647 conjugated anti-Sca1, and BV 605 conjugated anti-CD117 antibodies to identify stem- and progenitor-enriched populations.

4.1.1 Results from Bone Marrow

Cell-specific fluorescent antibodies and flow cytometry were used to probe the cell suspensions for GFP+ recombinants within specific hematopoietic sub-populations/lineages. Negative controls were used to create gates with <3 GFP+ cells per 1 million cells analyzed, and these gates were used to identify GFP+ recombinant cells from doxycycline-supplemented mice (n=11). 10 of 11 mice had readily detectable GFP+ recombinant cells indicative of DSB-induced inter-chromosomal HR ranging from 0% to 9.4% in the total BM suspension (median 1.2%). Of Lin+ cells, 11 of 11 mice had readily detectable GFP+ recombinants ranging from 0% to 6.8% (median 0.6%). Of Lin- cells, 6 of 11 mice had readily detectable GFP+ recombinants ranging from 0% to 2.1% (median 0.4%). Although total BM cell suspensions and Lin+ enriched cell populations contained GFP+ recombinants, none of these events occurred within terminally differentiated T or

B cell subsets (CD4+, CD8+, or CD45R+). This result supports the idea that the Lin+ GFP+ recombinant cells are of myeloid origin.

Further, I wanted to determine the potential for progenitor cell subpopulations to utilize inter-chromosomal HR to repair DSBs. Of Lin+ cells, 11 of 11 mice had detectable GFP+ recombinants ranging from 0.07% to 6.8% (median 0.6%). CD34+ cells are further enriched for progenitor cells and typically comprise approximately 1-10% of Lin-enriched populations in humans and mice. In this study, within the Lin-enriched cells, all 11 of 11 mice contained detectable GFP+ recombinants within the CD34+ population ranging from 0.4% to 7.8% (median 1.4%). Identification of more HSC-enriched subsets was performed by further identification of Sca+ and c-kit+ subsets. Within the Lin-enriched cells, triply CD34+/Sca1+/ckit+ populations ranged from almost undetectable (<0.1%) up to 3.4%. Within this gated HSC-enriched subpopulation, a small but variable number of GFP+ recombinant cells indicative of DSB-induced inter-chromosomal HR was detected in 7 of 11 mice.

The inter-chromosomal HR cell frequency distribution among rainbow mice was non-normal across mice of different genders and age groups within the bone marrow subpopulations. To assess the variance between total GFP+ recombinants within the non-enriched whole bone marrow suspension, as well as in lin-/GFP+ and lin+/GFP+ populations, the Kruskal Wallis nonparametric test was applied with Dunn's test as post hoc analysis. Upon comparing the means, it appeared that the highest percentage of GFP+ recombinants existed within whole bone marrow suspension, followed by the percentage of GFP+ recombinants among lin+/GFP+, and the lowest percentage of GFP+ recombinants among the lin-/GFP+. However, this observed trend lacked statistical significance, possibly because the GFP+ recombinants whole bone marrow suspension encompasses the lin+ and lin- populations, Kruskal Wallis nonparametric test was applied with Dunn's test as post hoc analysis to compare the lin-/GFP+ population with the lin-/CD34+GFP+ populations, revealing a statistically significant trend.

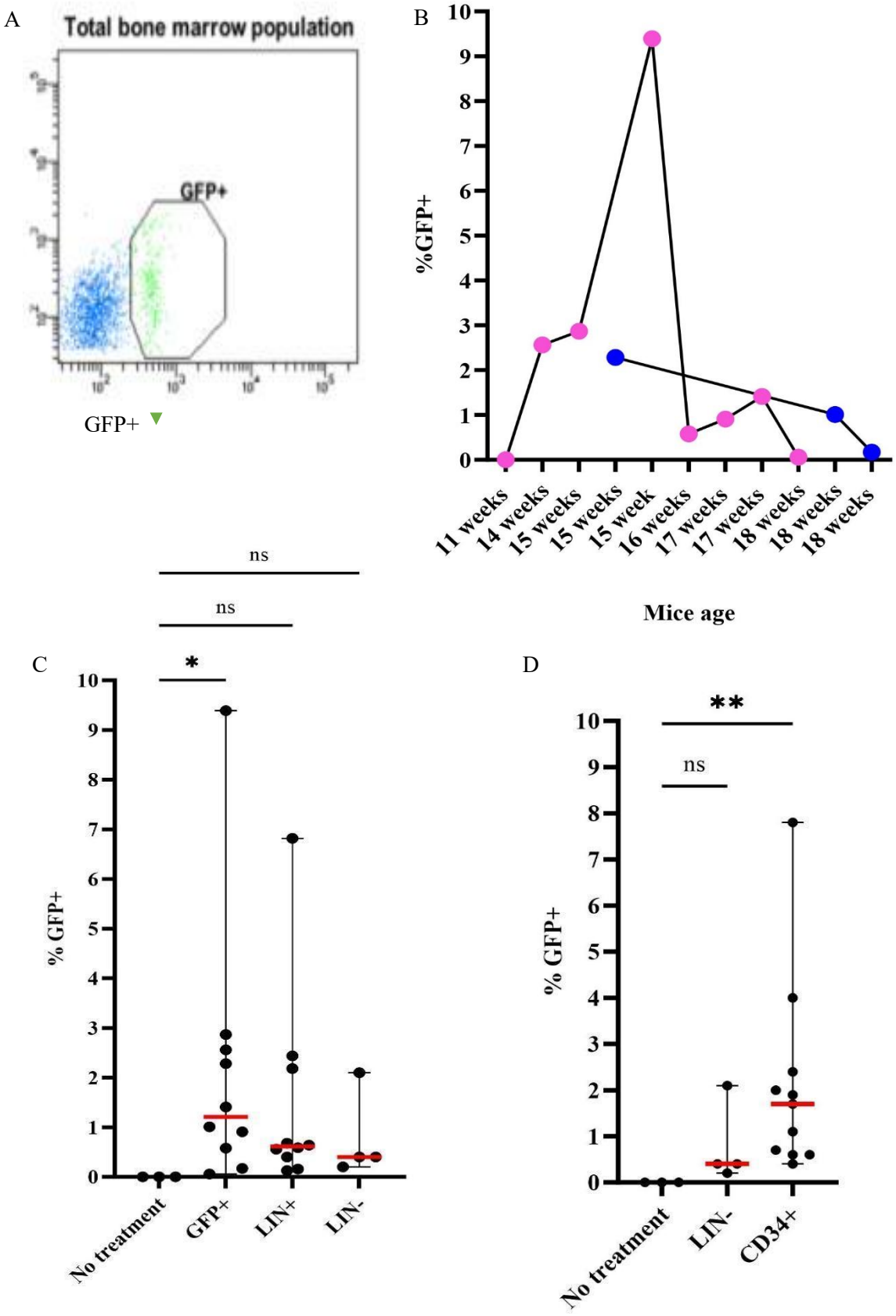
A
Total bone marrow population
GFP+
GFP+
B
%GFP+
11 weeks
14 weeks
15 weeks
15 weeks
15 week
16 weeks
17 weeks
17 weeks
18 weeks
18 weeks
18 weeks
Mice age
C
ns
ns
*
% GFP+
No treatment
GFP+
LIN+
LIN-
D
**
ns
% GFP+
No treatment
LIN-
CD34+

Figure 26: Investigating inter-chromosomal HR in bone marrow. (A) FACS representative plot depicting GFP+ recombinant population from whole bone marrow tissue suspension. (30k events analyzed) The X-axis represents logarithmic GFP positivity, and the Y-axis represents the cell count. (B) graphical representation of GFP+ recombinant populations (Y-axis) plotted based on mice gender and two age groups (X-axis). Blue dots represent the male population; pink dots represent the female population. Comparing the %GFP+ recombinant population from mice between 11-18 weeks age doesn't seem to follow any particular trend. (C) graphical representation of GFP+ recombinant populations among non-enriched whole bone marrow suspension, lin-/GFP+, and lin+/GFP+ populations, the no treatment group was used as control. The highest percentage of GFP+ recombinants was observed among entire bone marrow suspension (median 1.2%), followed by the percentage of GFP+ recombinants among lin+/GFP+ (median 0.6%), and the lowest percentage of GFP+ recombinants among the lin-/GFP+ (median 0.4%) As compared to the no treatment group (n=20) all the GFP+ recombinant populations had a higher percentage of GFP. This trend was statistically significant for total bm suspension but not for the other cell suspensions. (D) Graphical representation of GFP+ recombinant populations among lin-/GFP+ and GFP+/CD34+ population (median 1.7%). Comparing the no-treatment group with the lin-/CD34+ population was found to be statistically significant. ns= not significant, *p<05; **p<0.01

Data (No treatment N=20, Treatment group N=11) are presented as Individual values and Median (with ranges). Differences in GFP+ (%) between treatments were tested using non-parametric KW and post-hoc determined by the Dunn test (*p<05; **p<0.01).

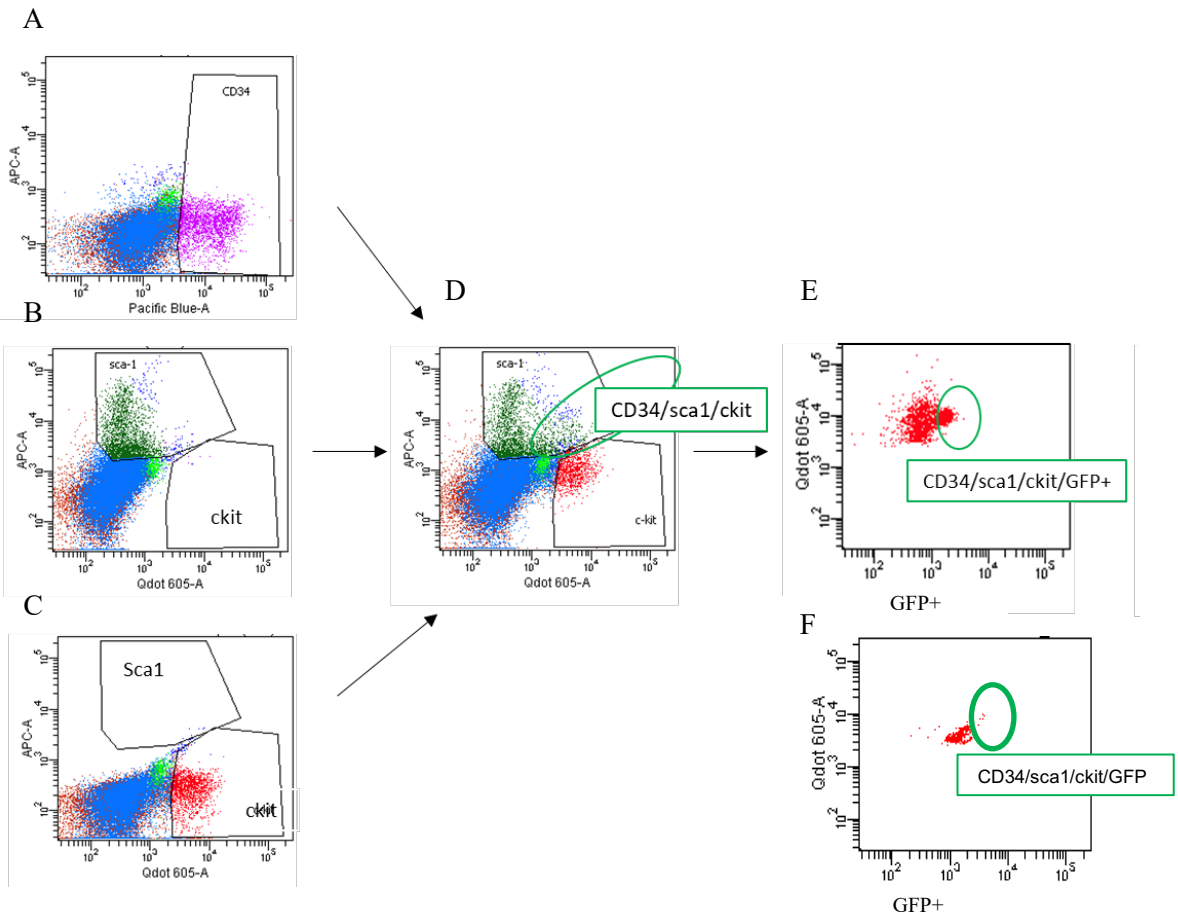

Figure 27: FACS representative plots to demonstrate the gating scheme for identification of lin-/sca+/CD34+/ckit+ cells. (A) FACS plots depict gating for the CD34+ population on the X axis, plotted against the Y axis non-significant fluorescence marker (B) FACS plots represent gating for the sca+ population on the Y axis plotted against non-significant fluorescence marker (C) FACS plots depict gating for kit population on the X axis plotted against non-significant fluorescence marker. (D) FACS plots show gating for the CD34+/ckit+/sca+ positive population. The CD34+ population was selected, and the ckit+ population was plotted on the X-axis against the sca+ population plotted on the y-axis. The resultant triple-positive population is circled in green. (E-F) FACS representative plots of the GFP+ recombinant lin-/sca+/CD34+/ckit+ populations from two different mice. As seen from the plot, it is possible to observe the GFP+ recombinant lin-/sca+/CD34+/ckit+ population, but this population was tiny (<1%) and was not detected in all 11 mice. (N=11)

4.1.2 Results: Spleen

Cell-specific fluorescent antibodies were used to probe the isolated spleen cell suspension for GFP+ recombinants, and flow cytometry was employed for analysis. The gating system for

determining GFP positivity was set up such that negative controls showed no detectable GFP-positive events, with a calculated value of less than 2 events per million. This same gating system was applied to the rainbow mice samples fed doxycycline. Of all the 13 mice, two had no detectable GFP+ percentages, ranging from 0.2% to 17.7%, with the median being 1.7%. 6 of 14 mice exhibited easily visible GFP+ recombinant cells, and the observed range of recombinant cells was 0.2% to 2.4%, with the median being 1.25%. 13 of 14 mice had readily identifiable GFP+ recombinant cells, and the observed range of recombinant cells was 0.4% to 14.5%, median being 1.45%. Within the Lin-enriched cells, all 14 of 14 mice contained detectable GFP+ recombinants within the CD34+ population ranging from 0.7% to 13.4% with a median of 5.3%. Although total spleen cell suspensions and Lin+ enriched cell populations contained GFP+ recombinants, none of these events occurred within terminally differentiated T or B cell subsets (CD4+, CD8+, or CD45R+). This result supports the idea that the Lin+ GFP+ recombinant cells are of myeloid origin.

The inter-chromosomal HR cell frequency distribution among rainbow mice was non-normal across mice of different genders and age groups within spleen subpopulations. To assess the variance between total GFP+ recombinants within the non-enriched whole spleen suspension, as well as in lin-/GFP+ and lin+/GFP+ populations, Kruskal Wallis nonparametric test was Dunn's test at post hoc was applied. Upon comparing the means, it appeared that the highest percentage of GFP+ recombinants existed within whole bone marrow suspension, followed by the percentage of GFP+ recombinants among lin+/GFP+, and the lowest percentage of GFP+ recombinants among the lin-/GFP+. However, this observed trend lacked statistical significance, possibly since the GFP+ recombinants whole bone marrow suspension encompasses both the lin+ and lin- populations. Kruskal Wallis nonparametric test was applied with Dunn's test as post hoc analysis to compare the lin-/GFP+ population with the lin-/CD34+GFP+ populati ons, revealing a statistically insignificant trend.

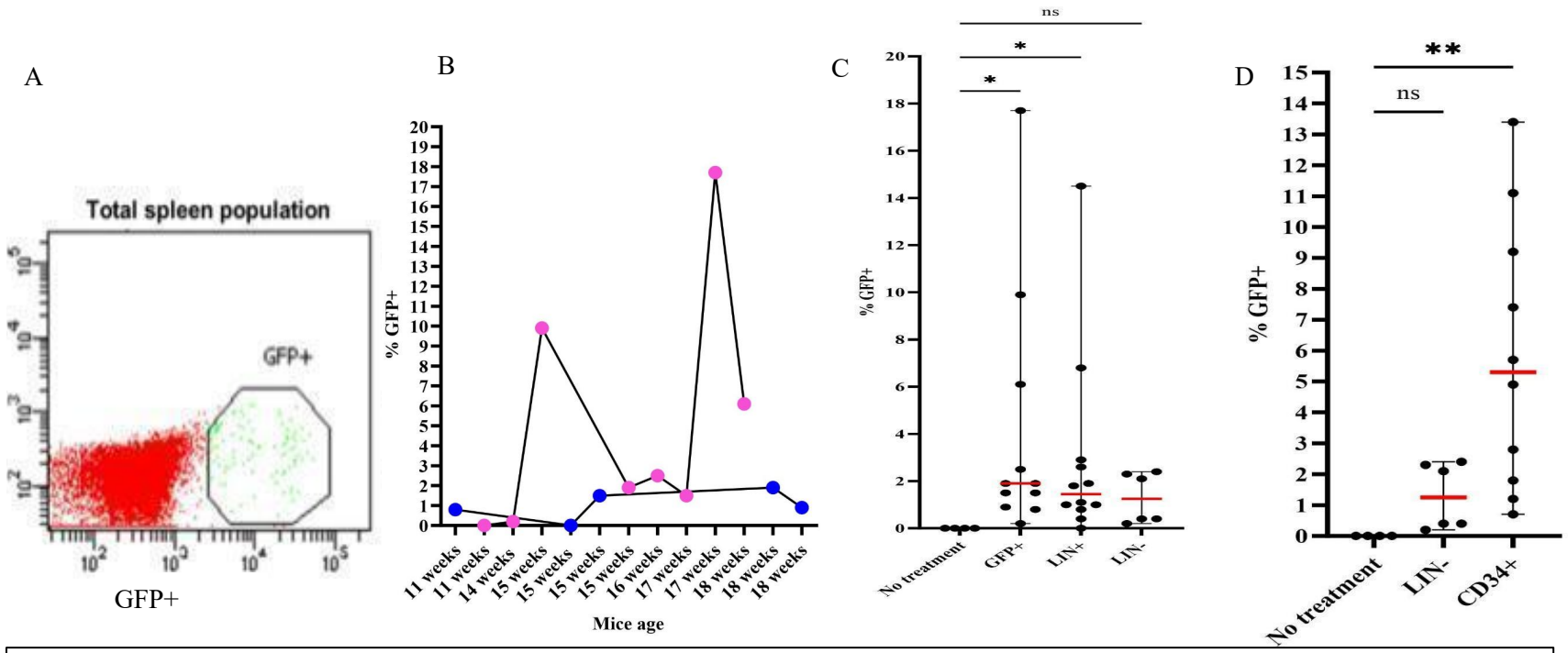

Figure 28: Investigating inter-chromosomal HR in the spleen. (A) FACS representative plot depicting GFP+ recombinant population whole spleen tissue suspension. (30k events analyzed) The X-axis represents logarithmic GFP positivity, and the Y-axis represents the cell count. (B) graphical representation of GFP+ recombinant populations (Y-axis) plotted based on mice gender and age (X-axis). Blue dots represent the male population; pink dots represent the female population. Comparing the %GFP+ recombinant population from mice between 11-18 weeks age doesn't seem to follow any particular trend, however it appears that females between 14-16-week-old age group did have a higher percentage of GFP+ recombinant population as compared to males from the same age group as well as from the mice from the other age group.(C) graphical representation of GFP+ recombinant populations among non-enriched spleen suspension, lin-/GFP+ and lin+/GFP+ populations. The highest percentage of GFP+ recombinants was observed among spleen suspension (median 2%), followed by the percentage of GFP+ recombinants among lin+/GFP+ (median 1.5%) and the lowest percentage of GFP+ recombinants among the lin-/GFP+ (median 1.2%) Comparing the cell types with no treatment group (n=20) suggested that was trend, which was statistically significant. (D) Graphical representation of GFP+ recombinant populations among lin-/GFP+ and GFP+/CD34+ population (median 5.3%). Comparing the no-treatment group with the lin-/CD34+ population shows a statistically significant trend. Data (No treatment N=20, Treatment group N=11) are presented as Individual values and Median (with ranges). Differences in GFP+ (%) between treatments were tested using non-parametric KW and). post-hoc determined by the Dunn test (*p<05; **p<0.01)

4.1.3 Conclusion

Overall, our in vivo evaluation of inter-chromosomal HR in the major hematopoietic organs, namely the bone marrow and spleen, revealed a prevalence of inter-chromosomal HR among stem cells and progenitor cells populations. Using flow cytometry, we identified GFP recombinant from major hematopoietic populations: lin-/CD34+, lin-/Sca+, lin-/CD117+ stem and progenitor populations. These populations had varying percentages of GFP+ recombinants, the highest being Lin-/CD34+. I also identified the lin+ population such as lin+/CD4+, lin+/CD8+ and lin+/CD45r+ lymphoid populations. I did not observe GFP+ recombinant populations among the terminally differentiated populations, however it should be noted that we did have GFP+ recombinant population among the total lineage positive population in both bone marrow and spleen suggesting the that the Lin+ GFP+ recombinant cells are of myeloid origin.

4.2 Potential of DSB-induced Inter- HR to occur in utero.

I began to explore the potential for inter-chromosomal HR to occur in fetal hematopoietic cells as a result of *in utero* induced DSBs from doxycycline ingestion by pregnant females. It is known that doxycycline passes the placental barrier reaching the developing fetus (Moutier et al., 2003). Extensive examination of low doxycycline dosages, such as those used in our study, has established their non-toxic adverse effects on fetal developmental processes, effectively ruling out any speculation about doxycycline-induced fetal toxicity (Moutier et al., 2003). Following doxycycline diet supplementation for one-week, female mice mated, and continued with doxycycline diet supplementation for 14 days of gestation. At E14.0 pregnant mice were euthanized, and fetuses harvested. Single cell suspensions of fetal tissue and isolated fetal livers were analyzed. In addition, single cell suspensions of placental tissues were isolated from 3 fetuses of a single litter. Negative controls were used to create gates with <3 GFP+ cells per 1 million cells analyzed. (Figure 29 A)

These gates are used for identification of GFP+ cells from whole fetal tissue, fetal liver, and placental samples.

4.2.1 Results:

To extend my findings in hematopoietic cell populations in BM and spleen, I investigated fetal liver cells that are the site of ongoing hematopoiesis during mid-gestation. For my investigation I analyzed fetal liver cells from all the three litters, however for the placental tissue and fetal tissue I analyzed a single litter. Shown below is the data obtained from flowcytometry analyzed of 3 liters.

Table 4: This table lists three litters analyzed for in utero inter-chromosomal HR evaluation. Overall, litter #1 did not have detectable GFP+ recombinant cells (< 2 GFP events per million cells) in fetal liver suspensions, no other tissues were analyzed for GFP+ recombinant cells from these fetuses. Litter# 2 also did not have any GFP+ recombinant cells (< 2 GFP events per million cells) in fetal liver suspensions, and none of the other tissues were analyzed for GFP+ recombinant cells. From Litter #3, fetus 3_2 and 3_3 had detectable GFP+ recombinant cells in fetal liver and fetal tissue. Furthermore, placental tissue of fetus 3_2 had detectable GFP+ recombinants. *Note: The total events analyzed using flow cytometry for each of the tissues was 1 million.

	Litter #1				**Litter #2**				**Litter #3**		
	fetal tissue	fetal liver	Placenta		fetal tissue	fetal liver	placenta		fetal tissue	fetal liver	placenta
1_1	NA	0	NA	2_1	NA	0	NA	3_1	0	0	0
1_2	NA	0	NA	2_2	NA	0	NA	3_2	42	11	157
1_3	NA	0	NA	2_3	NA	0	NA	3_3	9	7	0
				2_4	NA	0	NA				

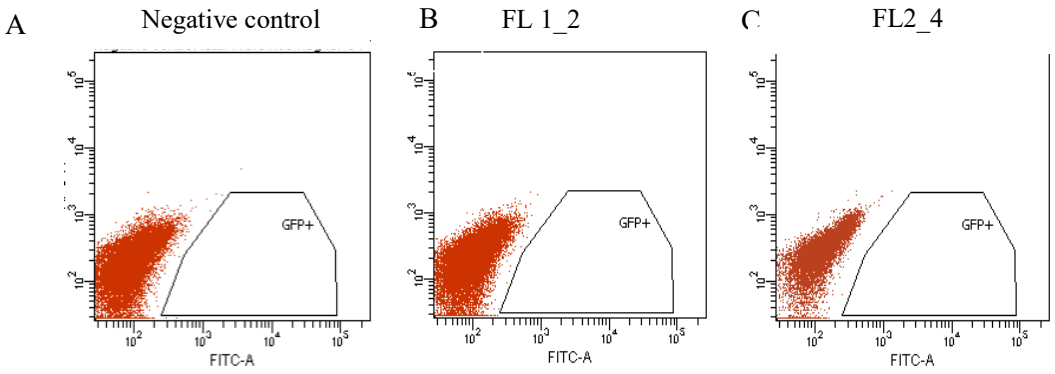

Figure 29: Evaluation of in utero inter-chromosomal HR using flow cytometry. (A) FACS Representative plots depicting GFP+ gating using WT FL as control (GFP events <1 per million). (B) FACS Representative plots depicting GFP+ gating for fetal liver from 1_2 fetus. (C) FACS Representative plots depicting GFP+ gating for fetal liver from 2_4 fetus. Litters # and#2 did not have detectable GFP+ recombinant cells.
Y-axis represents cell count and x-axis represents logarithmic GFP positivity.

I compared the GFP+ recombinant populations from all three tissues from litter#3 using one-way ANOVA with Kruskal Wallis non-parametric test. The highest GFP+ recombinant cells were observed in placenta (52 events/million) followed by fetal tissue (17 events/ million) and then in the fetal liver (6 events/million).

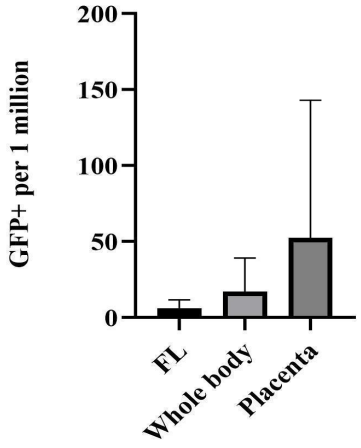

Figure 30: Comparison of GFP+ events in different fetal tissues to investigate in utero inter-chromosomal HR. FL had the lowest number of GFP+ events per million, followed by whole body and highest events observed in Placenta. Since the data was unequally distributed, one-way ANOVA was used followed by Kruskal Wallis non-parametric test. (N=1)

4.2.2 Conclusion

In utero evaluation of inter-chromosomal HR revealed fetal tissues such as FL and total tissue showed a low frequency of GFP+ recombinants although detectable in some cases as well as within one placental tissue.

CHAPTER 5: INTER-CHROMOSOMAL HR IN SOLID TISSUES: LUNG AND PANCREAS

Introduction

DSBs have been identified as the most common type of DNA damage in somatic cells, and erroneous repair may result in mutations, genomic instability, or apoptosis. Organs and tissues are exposed to diverse insults due to their environment, which results in DNA damage (Blokzijl et al., 2016; Ferreira da Silva et al., 2021) (Sun et al., 2019). Highly replicative tissues, such as hematopoietic tissues, are considerably more sensitive to DNA damage, and by contrast, the colon is significantly more resistant (Ferreira da Silva et al., 2021). The liver, lung, and pancreas have steady states of cell replication and are characterized by continued tissue recovery post-damage. Understanding how such organs respond and mediate DSBs is imperative in developing therapeutic strategies to prevent or treat disease states.

Although DNA repair pathways are frequently diagrammed as linear, they operate within a dense signaling network often influenced by cell type and differentiation state. For example, terminally differentiated neural cells preferentially use NHEJ to repair DSBs instead of the HR pathway (Mujoo et al., 2017). Furthermore, gene mutation in HR enhances the risk of cancer development in multiple organs (Kass et al., 2016; Palacio et al., 2019). The severe clinical effects of mutations in genes governing DSB repair pathways in mammalians and humans emphasize the pivotal significance of these DNA repair processes for overall tissue integrity and function.

Generally, terminally differentiated cells in a tissue cannot differentiate into any other cell type. However, some cells have the potential to differentiate into a different cell type or revert the cells into progenitor or multipotent states. Cellular plasticity is usually stimulated in response to tissue damage or disease (Clairambault & Shen, 2020). It has been shown that the ability to trans-differentiate is similar to a stem cell-like state and makes these cells more vulnerable to DNA-damaging insults (Aponte & Caicedo, 2017). Several stem cell-like properties are also closely

associated with tumorigenesis (Aponte & Caicedo, 2017; Ayob & Ramasamy, 2018; Clarke & Fuller, 2006).

In this study, I aimed to evaluate cell type-specific inter-chromosomal HR in the two distinct solid tissue types: the pancreas and the lung. Both solid tissue types are filtering organs responsible for the clearance of ingested environmental toxins, which may induce DNA damage, including DSBs. Both organs comprise specific cellular subtypes capable of trans-differentiation and containing stem-cell-like features, allowing for mutagenic repair and accumulation of DNA damage. I hypothesized that lung and pancreatic tissues would readily utilize DSB-induced inter-chromosomal HR. The prognosis for pancreatic and lung malignancies is poor, emphasizing the importance of exploring the molecular and cellular mechanisms to repair DSBs, maintain genome integrity, and inhibit carcinogenesis.

5.1 PANCREAS

The pancreas is a vital organ composed of endocrine and exocrine compartments, where exocrine cells comprise more than 80% of the total volume of the tissue (Stanger & Hebrok, 2013; Wiktor-Brown et al., 2006). Acinar and duct cells are exocrine cells; the acinar cells secrete digestive enzymes into the duodenum, while the duct cell organizes the epithelial lining between the duodenum and the branched tubes. The endocrine cells include- α, β, δ, ε, and pancreatic polypeptide (PP), which together form the islet of Langerhans. These cells are vital for the regulation of metabolism and glucose homeostasis.

Lineage tracing experiments demonstrate common pancreatic progenitor populations for the origin of all the endocrine and exocrine cells. Initial development of the pancreas occurs on day 9.5 in mice from the embryonic foregut. The development of the pancreas is tightly regulated. Initial pancreatic bud formed as identified by the Pancreatic and duodenal homeobox 1 (PDX1+) undergoes the "first transition phase" to give rise to multipotent progenitor cells and bipotent progenitor cells, which later differentiates into exocrine, ductal, and endocrine cells respectively (Herrera et al., 2002; Malinova et al., 2021). The later stage of development, also called the "second transition," is when the differentiation of endocrine cells into α, β, δ, ε, and pancreatic polypeptide (PP) is prominently observed. In mature mice, approximately 90% of the islet cells are cells that are concentrated in the center of the islet and surrounded by other types of endocrine islet cells (Choi et al., 2004). The duct cell lineage emerges directly from the PDX1-positive cells somewhere around day E 9.5-11.5 (Burke et al., 2007; Reichert & Rustgi, 2011).

Even though the duct cells are differentiated cell types, multiple embryonic rodent, and primate studies have shown these terminally exocrine cells consist of cellular plasticity, giving rise to other exocrine as well as endocrine cell types (Gao et al., 2022; Murtaugh & Keefe, 2015). Duct cells in pancreatic tissue are often considered as the originators of the Pancreatic Ductal Adenocarcinomas (PDAC) tumors (Guerra et al., 2007; Kopp et al., 2012; Pour et al., 2003). Since adult duct cells are stem-like and have the potential to differentiate into duct-acini (Grippo et al., 2003; Kopp et al., 2012) and duct-islet (El-Gohary et al., 2016; Gao et al., 2022), they are considered as a key target for pancreatic cancer origin and cell-based therapy.

Other Molecular analyses of PDAC demonstrated mutations in genes involved in core cellular pathways, including DNA damage response (DDR), cell signaling pathways, and DNA damage repair pathways (Perkhofer et al., 2021; Stoof et al., 2021; Zhang et al. 2022). Genetic profiles of several PDAC patients show mutations of ATM, BRCA1, BRCA2 PALB2 RAD51C, BLM, RAD50 genes essential for DDR and homologous recombination repair (HR), MSH2, MSH6, and

MLH1 genes in mismatch repair pathway (MMR), FANCC, FANCA, RAD51D, and XRCC2 genes from. It was observed that pancreatic cancer patients with a familial history had increased germline mutation of BRCA2 (Teo & O'Reilly, 2016; Waddell et al., 2015). Since these genes are strongly associated with genomic instability caused by DNA-damaging agents, understanding the frequency of mutagenic HR pathways in pancreatic subpopulation cells would provide greater insight into cellular and molecular signatures of pancreatic tumorigenesis and the potential development of HR specific therapy.

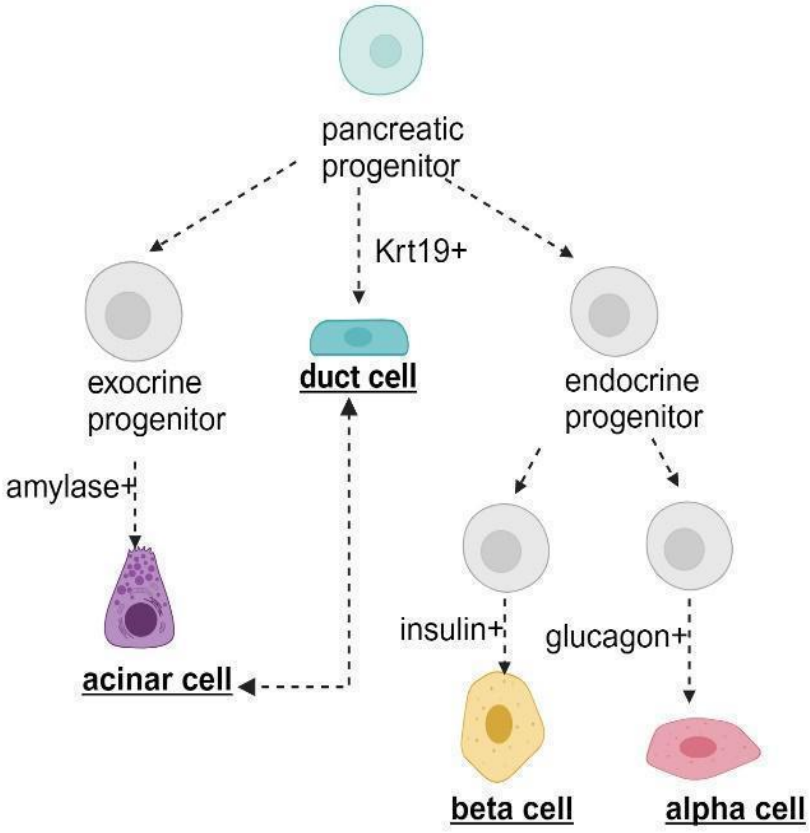

Figure 31: Schematic flowchart of pancreatic lineage with cell type specific markers.

5.1.1 Experimental setup for investigation of inter-chromosomal HR in pancreas

Following 21 days of doxycycline diet supplementation, Rainbow mice were euthanized, and pancreatic tissue was harvested. Single cell suspensions were fixed, and cell suspensions were fixed and stained with cell type specific markers to identify GFP+ recombinant population among pancreatic cell subpopulations. To assess acinar subpopulation Alexa Fluor 790 conjugated Amylase antibody was used; for duct cells, Alexa fluor 790 Cytokeratin 19 (Santa Cruz) was used; for β cells Alexa Fluor 647 mouse anti-insulin was used; and for α cells BV412 Mouse Anti-Glucagon (BD Science) was used. Additionally, Islet cell enrichment protocol was employed to analyze a greater population of islet cells. Furthermore, histological analysis of frozen pancreatic tissues was performed to gain additional insight on GFP+ recombinant population among pancreatic cell sub-types.

5.1.2 Results:

Cell-specific fluorescent antibodies were used to probe the isolated pancreatic cell suspension for GFP+ recombinants, and flow cytometry was employed for analysis Negative controls were used to create gates with <3 GFP+ cells per 1 million cells analyzed, and gates used for identification of GFP+ cells from doxycycline supplemented mice (n=15). Out of 15 mice, 4 had no detectable GFP+ cells indicative of DSB-induced inter-chromosomal HR. Among the remaining 11 mice, detectable GFP+ recombinant cells were detected in 0.21% - 5.16% of the total cell population, with median of 1.9%. 8 of 11 mice exhibited GFP+ recombinant acinar cell population, ranging from 0.04% to 0.9%, median being 0.2%. 7 of mice exhibited GFP+ recombinant duct cell population, median being 0.4%. 7 of 11 mice exhibited GFP+ recombinant β cell population ranging from 0.02% to 0.4%, median being 0.4%. 4 of 11 mice exhibited GFP+ recombinant α cell population ranging from 0.06 to 0.5% median being 0.12%. The highest percentage of GFP+ recombinants existed within whole pancreatic tissue followed by percentage of GFP+ recombinants among insulin+ β cell population, KRT19+ ducts cell population followed

by amylase+ acinar population and lowest was the glucagon+ alpha cell population. Kruskal-Wallis non-parametric with Dunn's post hoc test performed. The results did show a trend however, these were not statistically significant.

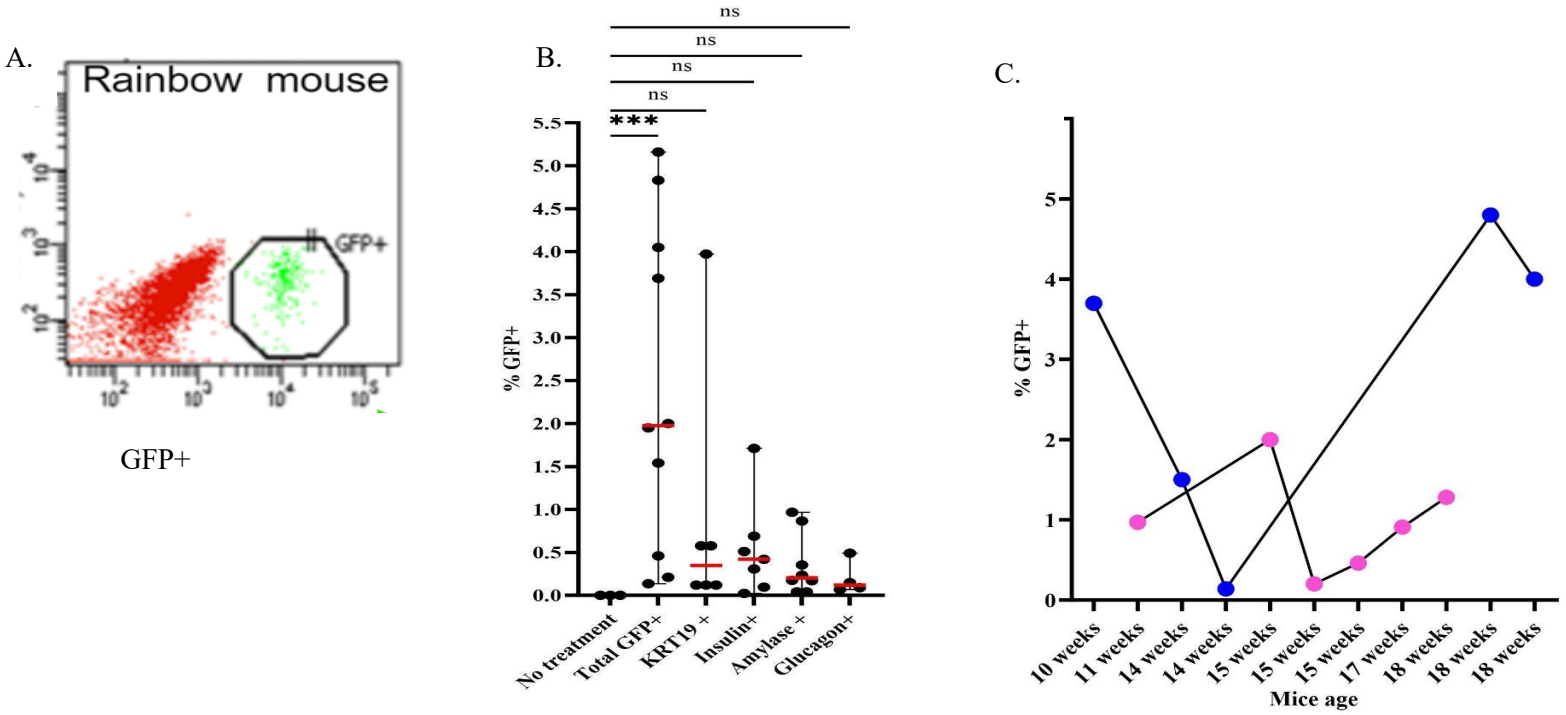

Figure 32: Investigating inter-chromosomal HR in pancreatic tissue. (A) FACS representative plot depicting GFP+ recombinant population from whole pancreas tissue suspension. (30k events analyzed) X axis depicts logarithmic GFP positivity, and the Y axis depicts the cell count. (B) graphical representation of GFP+ recombinant populations (Y-axis) plotted based on mice gender and age groups (X-axis). Blue dots represent the male population; pink dots represent the female population. Comparing the %GFP+ recombinant population from mice between 10-18 weeks age doesn't seem to follow any particular trend however it does appear that the GFP+ recombinant events in older males is higher as compared to females. (C) graphical representation of FACS analysis. GFP+ recombinant populations among pancreatic suspension, KRt19+/GFP, Amylase+/GFP+, insulin+/GFP+ and Glucagon+/GFP+ recombinant populations. The highest percentage of GFP+ recombinants were observed among pancreas population (median 1.9%) followed by percentage of GFP+ recombinants among KRT19+ (median 0.4%) and followed by percentage of GFP+ recombinants among insulin+ population (0.4%) followed by percentage of GFP+ recombinants among amylase+ population (median 0.2%) lowest percentage of GFP+ recombinants among the glucagon+ population (median 0.12%) Comparing the total pancreatic cell suspension group (N=11) with no treatment group (n=20) was significant (p=0.0024). While comparing the cell types with no treatment group (n=20) suggested a trend, which was not significant.

The flow cytometry analysis revealed that the overall frequency of islet cells, including α and β cells, was lower compared to duct and acinar cells. One possible explanation for this discrepancy is the limited efficiency of our current markers and flow cytometry technique in isolating a larger proportion of islet cells. Therefore, we explored an alternative method based on the protocol described by Corbin et al, with minor modifications. Using this modified protocol, we were able to isolate 1.2 times more islet cells that were GFP-positive compared to the total pancreas collection method. In the enriched population, the percentage of insulin-positive cells that were also GFP-positive was 0.26%, while the percentage of glucagon-positive cells that were GFP-positive was 0.18%. We observed a small difference in the β cell population between the enriched and non-enriched samples, with regards to insulin+/GFP+ cells. Over 96 hours a small but consistent population of GFP+ islet cells were observed that did not decrease over time. These cells were readily distinguishable by their larger size (approximately 20μm in diameter) from other pancreatic cells.

GFP+ recombinant cells occurred as clusters typically surrounding the ductal cultures also contained a small population of very small adherent cells, consistent with stem cell morphology. I observed a small population of GFP+ recombinant cells in all three lumen and some were individually scattered throughout the pancreatic tissue types.

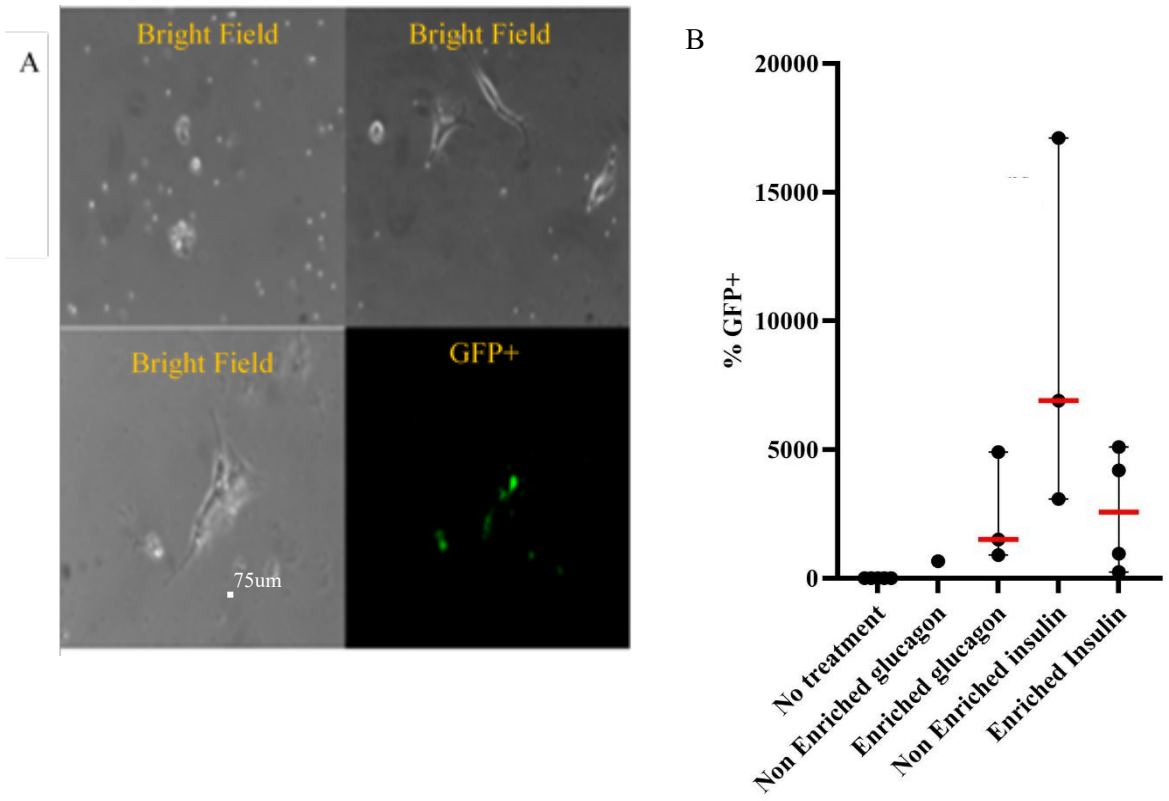

Figure 33: Evaluation of inter-chromosomal HR in islet cell population. To islet cells were enriched using density gradient and mechanical separation technique. The islet cells were plated on a 10 cm plate with RPMI media and observed for GFP+ recombinant islet cells for 4 consecutive days. The islet cells appeared to be round and about 20 µm in diameter. Small but steady number of GFP+ recombinant islet cells were observed. (A) Some pancreatic stem cells appeared on day 6, however, there were no GFP fluorescing stem cell colonies were observed. These cells did not appear to proliferate since the average number of cells remained the same throughout the culture. microscopy. magnification 40X, scale bar: 75µm

Further the cells were harvested for flow cytometry. (B) FACS representative bar graph, comparing GFP+ recombinant cells per million from Enriched islet cell population vs the non-enriched islet cell population. It was observed that the number of GFP+ recombinant declined by enriching for islet cell population, however the number of GFP+ glucagon recombinant cells increased by enriching for islet population. This trend was not statistically significant.

Data (No treatment N=20, Treatment group N=5) are presented as Individual values and Median (or Average ±SEM). Differences in GFP+ (%) between treatments were tested using non-parametric KW and post-hoc determined by Dunn test (*p<05; **p<0.01).

Furthermore, frozen pancreatic tissue sections from 3 mice were assessed for GFP+ cells indicative of DSB-induced inter-chromosomal HR. Based on the morphological analysis of cells by H&E and DAPI staining, the observed GFP+ cells resembled morphology of acinar cells and

cells surrounding intraductal regions. The acinar cells have truncated pyramid like shape with secretory granules on the tip and nucleus on the base of cells. The GFP+ recombinant cells appeared in proximity which could be due to clonal expansion. By contrast, none of the observed GFP+ cells were within islet cell populations. The islet of Langerhans appears as circular patches scattered around the pancreatic tissue. While my flow cytometry investigation identified the insulin+ β cell population to be one of the most prevalent regarding GFP+ recombinant events, this pattern did not hold true when assessed through confocal microscopy. This disparity could be explained by the idea that individual GFP+ recombinant cells do not release enough fluorescence intensity to provide a visible signal under the confocal microscope.

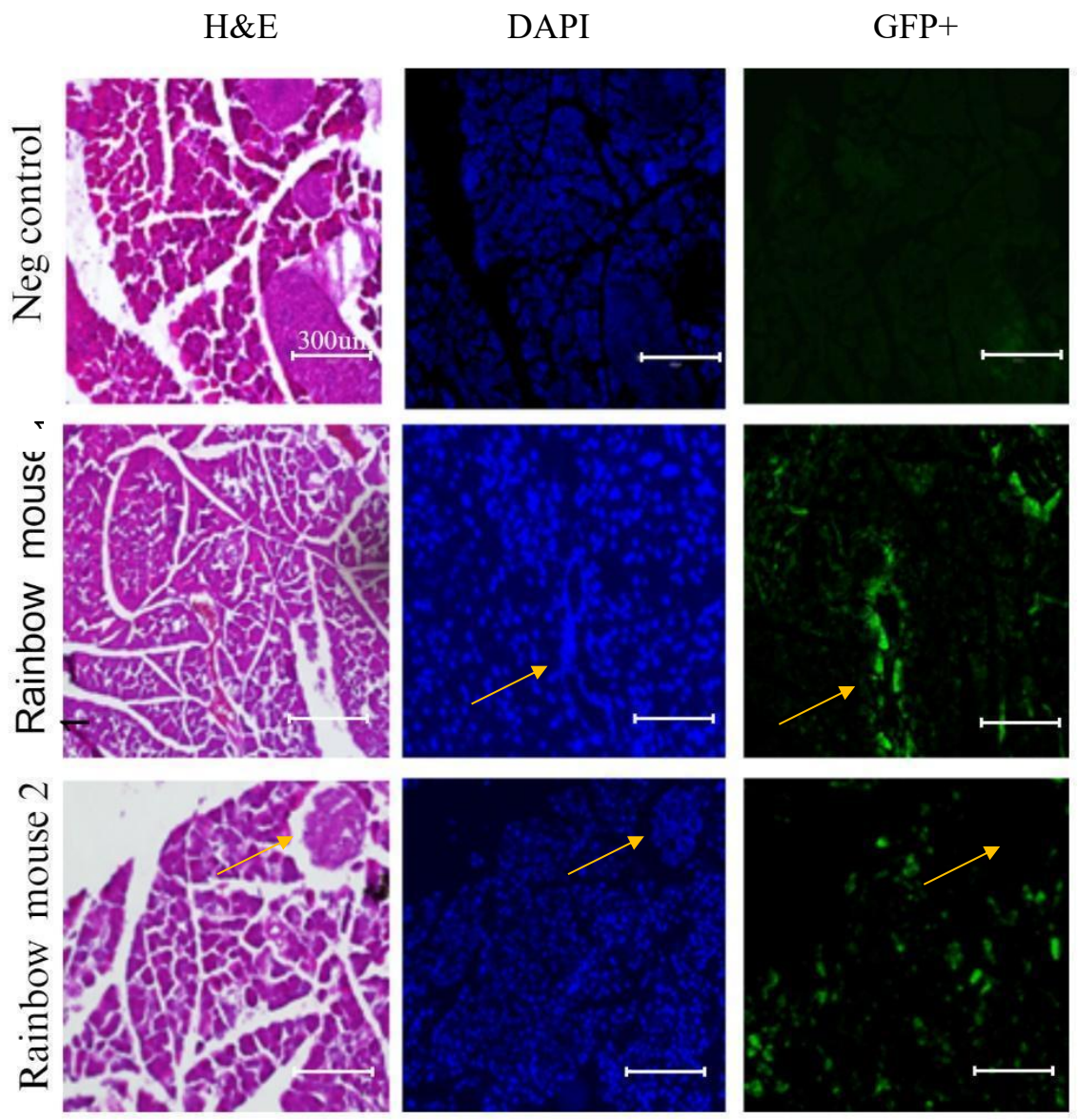

Figure 34: Fluorescent frozen pancreatic tissue section analysis from 3 mice. Row 1 shows fluorescent microscopy analysis of frozen pancreatic tissue section from ISCE (negative control), morphology of the cells can be seen by the H&E and DAPI staining. magnification 20X, scale bar: 300 µm

Middle row demonstrated fluorescent microscopy for a rainbow mouse. The morphology of the cells can be seen by the H&E and DAPI staining, GFP+ recombinant cells were observed surrounding the intraductal region. The intraductal region is highlighted with yellow arrow. magnification 20X, scale bar: 300 µm

Bottom row demonstrates fluorescent microscopy analysis for another rainbow mouse. The morphology of the cells can be seen by the H&E and DAPI staining, GFP+ recombinant cells were observed in in close proximity here as well. The arrows point show islet of Langerhans which did not fluoresce green. magnification 20X, scale bar: 300 µm

5.1.3 Conclusion:

Overall, both quantitative and qualitative analysis of pancreas revealed prevalence of inter-chromosomal HR. We sort to use flowcytometry to identify four distinct cell populations: β cells, α cells, duct cells, and acinar cells. Our flow cytometry data revealed that duct cells exhibit a higher propensity to utilize the inter-chromosomal HR repair mechanism as compared to the other cell types. However, when comparing KRT19+/GFP+ cells with the total GFP+ recombinant population, there was no statistically significant difference in other cell types. Furthermore, flow cytometry analysis revealed insulin+ β cell subpopulation of another cell type with higher GFP+ recombinant cells, ranking second cell type after duct cells to have increase inter-chromosomal HR. Histological analysis revealed GFP+ recombinant cells were among the acinar populations and tend to occur cultures possibly due to clonal expansion of the GFP+ recombinant acinar cell. GFP+ islet cells were not detected using fluorescent microscopy however, flow cytometry revealed high percentage of GFP+ recombinant insulin+ population as compared to acinar and alpha cell populations.

5.2 LUNG

The lung epithelium consists of multiple differentiated cell types based on their function and location. The alveolar region is a tree-like compartment consisting of alveolar type 1 (AT1) and alveolar type 2 (AT2) cells which are essential for gas exchange and synthesizing surfactants to maintain alveolar structure respectively (Bantikassegn et al., 2015). The upper airway consists of luminal cells including unciliated club cells, ciliated cells, goblet cells along with tuft cells and neuroendocrine cells (Weeden et al., 2017; Zheng et al., 2013). Pulmonary neuroendocrine cells and tuft cells have immune and chemosensory functions; club cells secrete anti-inflammatory, antimicrobial proteins; ciliated cells work with goblet cells, the principal mucus-producing cells in the airways (Hogan et al., 2014; Weeden et al., 2017).

During postnatal growth the basal cells differentiate to develop upper airway cells. The adult lung tissues have a small population of bronchio-alveolar stem cells (BASC) which can differentiate into both upper airway and distal alveolar compartment cells (Hogan et al., 2014). Furthermore, the terminally differentiated epithelial cells in the lung have self-renewal and de-differentiating capacities to maintain normal homeostasis or during lung injury (Zheng et al., 2013). The club cells can not only differentiate into ciliated cells or goblet cells but also into alveolar cells and are often considered as progenitor cells in the lung (Kathiriya et al., 2020; Spella et al., 2019). AT1 and AT2 also have self-renewal capacity and can differentiate into one another in case of alveolar injury.

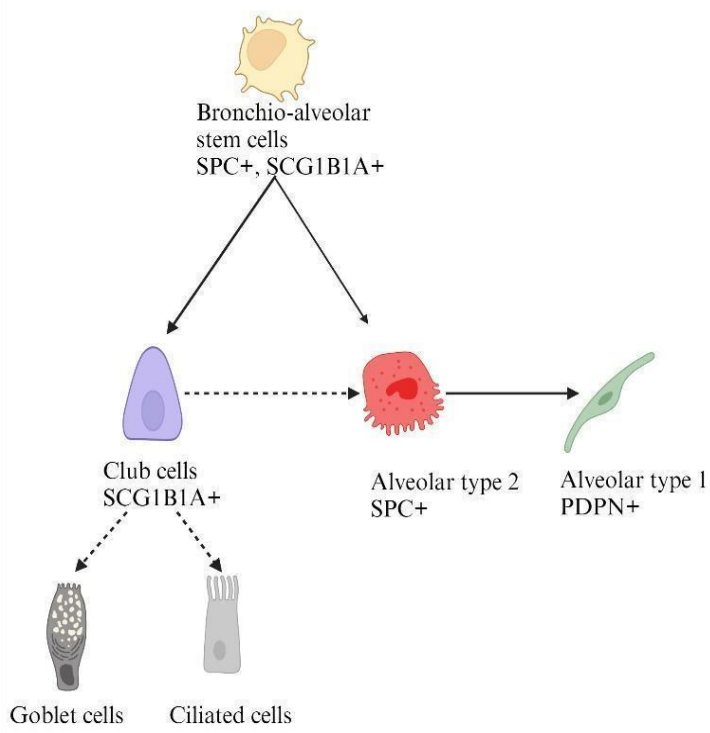

Figure 35: Schematic flowchart of lung lineage and cell type specific markers.

Although this cellular plasticity is key to recovery from damage or injury in the lung that is constantly exposed to chemical or environmental insults, on the other hand, this ability to trans-differentiate and proliferate can be linked to tumor development.

Cellular response to chemical or environmental insults, accumulation of DNA damage and mutagenic repair of DSBs also has the potential to cause genome instability, aging and disease. BASC cells were initially associated with development of lung cancer; however, recent mouse model studies investigated club cells and AT2 cells could give rise to lung adenocarcinomas (Spella et al., 2019). A recent rat study demonstrated that DSBs accumulated in AT2 cells promoted bronchopulmonary dysplasia (BPD) which affects the development of alveoli in infants. Accumulation of oxidative stress induced DSBs ultimately led to diminished repair efficiency and cell cycle arrest of AT2 cells resulting in BPD (Ferone et al., 2020; J. Lee et al., 2006). Increased incidence of DNA mutations due to tobacco smoking have been seen in lung cancer patients who smoke vs nonsmokers (Furrukh M, 2013). Base substitutions within cancer-related genes such as KRAS and TP53 are also observed in many patients. Furthermore, aneuploidy and gene duplications are also associated with non-small cell lung carcinomas (NSCLC) (Choma et al., 2001; Diossy et al., 2021). While environmental variables are thought to play a role in the development of lung cancer, there is evidence that both germline and somatic cell mutations within DNA repair genes themselves can enhance susceptibility to lung carcinoma. Among 741 lung cancer patients examined for one study, mutated HR-specific genes such as MRE11, RAD50, ATM, ATR, FANC1were identified in about 25% of patients (Diossy et al., 2021; Zhang et al., 2022).

5.2.1 Experimental setup for investigation of inter-chromosomal HR in lung

Following 21 days of doxycycline diet supplementation, Rainbow mice were euthanized, and pancreatic tissue was harvested. Single cell suspensions were fixed, and cell suspensions were fixed and stained with cell type specific markers to identify GFP+ recombinant population among pancreatic cell subpopulations. To assess for AT1 cell population fluorescent Superbright-600 conjugated PDPN antibody was used, for AT2 cell population ALEXA FLUOR 790 conjugated SPC antibody was used, for club cell population CC10 BV421 conjugated antibody BASC

population SPC and CC10 antibodies were used. Histological analysis and IHC for lung sections were performed.

5.2.2 Results

Cell-type specific fluorescent antibodies and flow cytometry were used to characterize which lung cell types had the potential to undergo inter-chromosomal HR to repair DSBs. Negative controls were used to create gates with <3 GFP+ cells per 1 million cells analyzed, and gates used for identification of GFP+ recombinant cells from doxycycline supplemented mice (n=15). Out of 15 mice, none of the mice had detectable GFP+ cells from total lung cell suspensions indicative of DSB-induced inter-chromosomal HR. However, we noted that our previous G2S model also showed that inter-chromosomal HR within the total lung tissue, the relative frequency of GFP+ recombinants were much lower as compared to some of the other tissues. Thus, we considered that technical reasons could be the cause that we did not identify GFP+ cells. One possible reason could be that the mechanical dissociation of lung tissues affected the morphology of the lung epithelial cells and hindered proper binding of the cell surface markers. Alternatively, euthanizing the mice must have caused collapse of the airspace of the lung causing cell lysis.

To address this, tissue sections were assessed for GFP+ recombinant cells indicative of DSB-induced inter-chromosomal HR. We observed intact morphology of air sacs and lung epithelial cells and architecture.

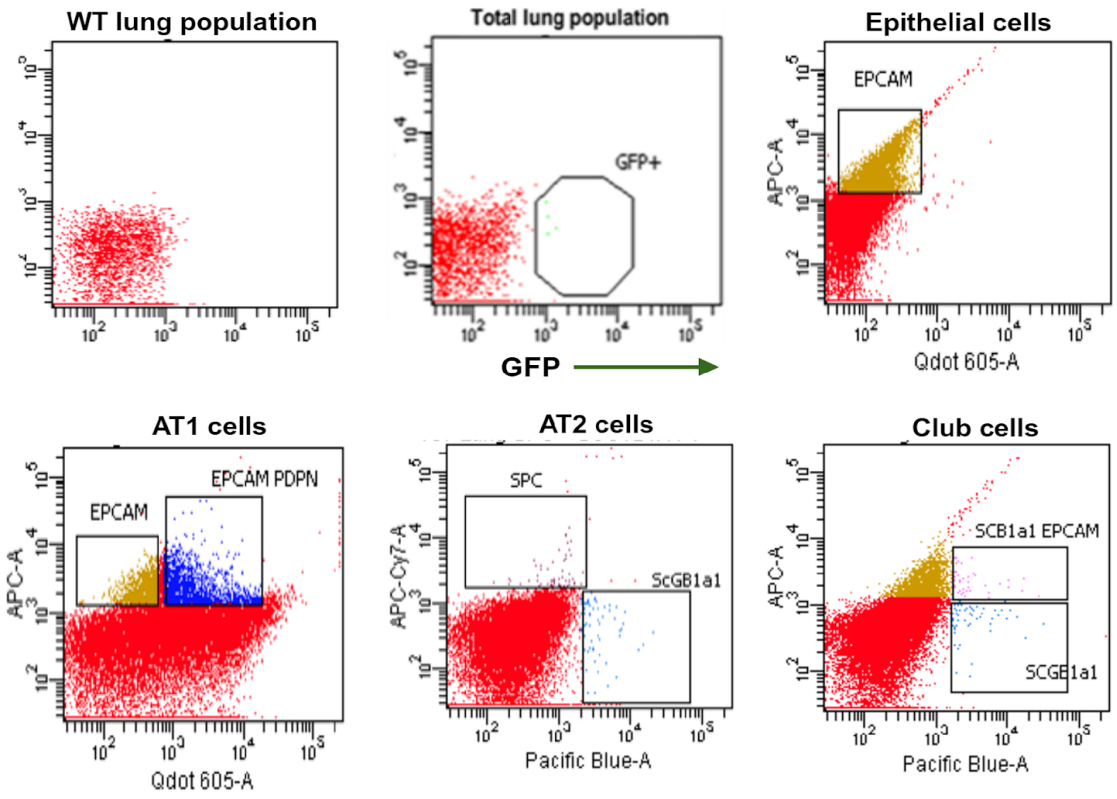

Figure 36: Evaluation of inter-chromosomal HR in lung tissues (A) FACS representative plot depicting GFP+ gating from WT mouse lung. (B) FACS representative plots depicting GFP+ for GFP+ gating from total lung tissue from rainbow mouse lung. X- The axis depicts the logarithmic GFP positivity, and the axis depicts the cell count. (30K events are shown)

The bottom row demonstrates a scheme for the identification of lung populations. (C) FACS plots depicting EPCAM positive population plotted on the y-axis against nonspecific fluorescent marker. The EPCAM was used to select for epithelial cell populations (D) FACS population representing EPCAM+PDPN labeled AT1 population where EPAM has plotted y-axis and gated for double positive population, (E) FACS plots showing SPC labeled AT2 population plotted on the y-axis and SCG1B1A labeled club cell, the highlighted blue arrow points to possible SCG1B1A+/SPC+ BASC population. (F) FACS population depicting EPCAM+ SCG1B1A labeled club population where EPAM is plotted on-axis and SCG1B1a on the x-axis.

Tissue sections of 5 doxycycline administered mice were analyzed using IHC staining technique. The AT2 cell is generally cuboidal small cell types occurring near the alveolar septum, while club cells occur near terminal bronchioles of the 5 presented with detectable GFP+ recombinant cells. In addition to using H&E and DAPI staining, IHC was employed to observe GFP+ recombinant cells among two cell types, AT2 and club cells. Histological examination

revealed an overall presence of GFP+ recombinant cells in lung populations, with an ability to cluster, presumably due to clonal proliferation of these GFP+ recombinant cells. These GFP+ recombinant cells were most noticeable in the alveoli closest to the bronchiole entrance. Additionally, the club cells and AT2 cells were fluorescently labeled with SCG1B1A and SPC antibodies respectively.

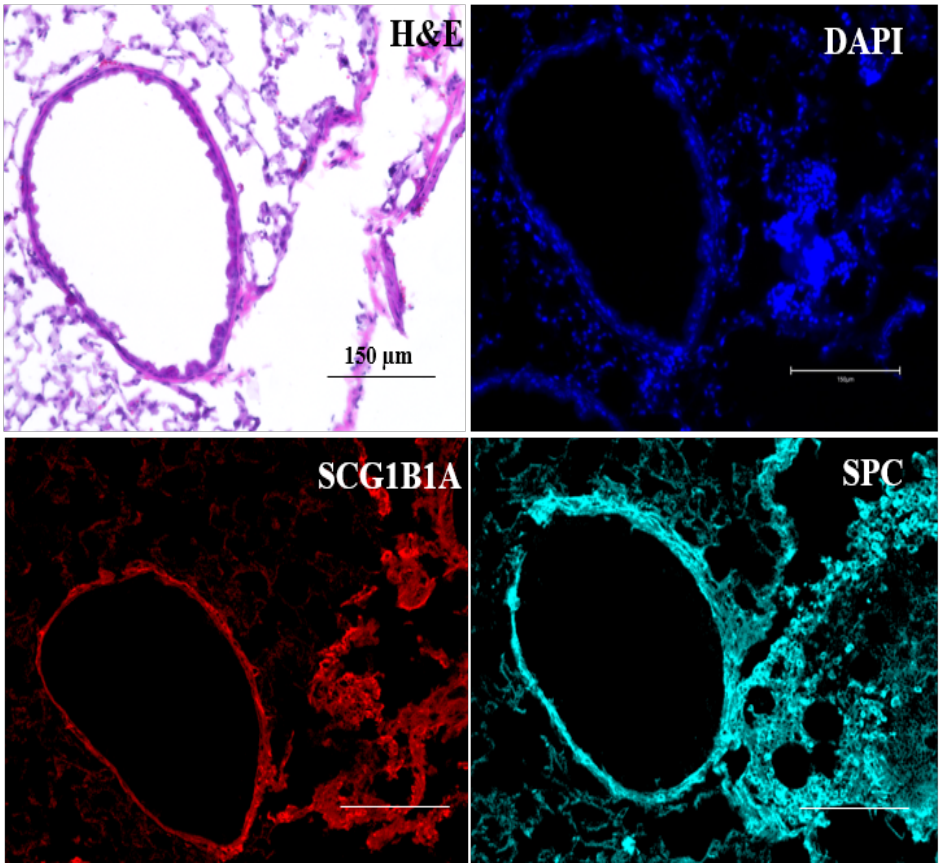

Figure 37: Fluorescent frozen lung tissue section analysis from one ISCE1 mouse. The left lobes were embedded on O.C.T and frozen until sectioned. A 6 µm thick section was used to perform histological analysis. The morphology of the cells can be seen by H&E and DAPI staining. Immunohistochemistry (IHC) was performed to stain with cell type-specific antibodies: club cells were stained with SCG1B1A antibody (1:50), and for AT2 cells, SPC antibody (1:50) was used, followed by probing with fluorescent secondary antibody Alexa Fluor 750 (1:50). Slides were observed using Confocal microscopy (Olympus Fluoview FV1000). magnification 20X, scale bar:150 µm.
Top images illustrate the H&E and DAPI stained section of an alveoli. Consecutive sections were stained for club cells or AT2 cells.

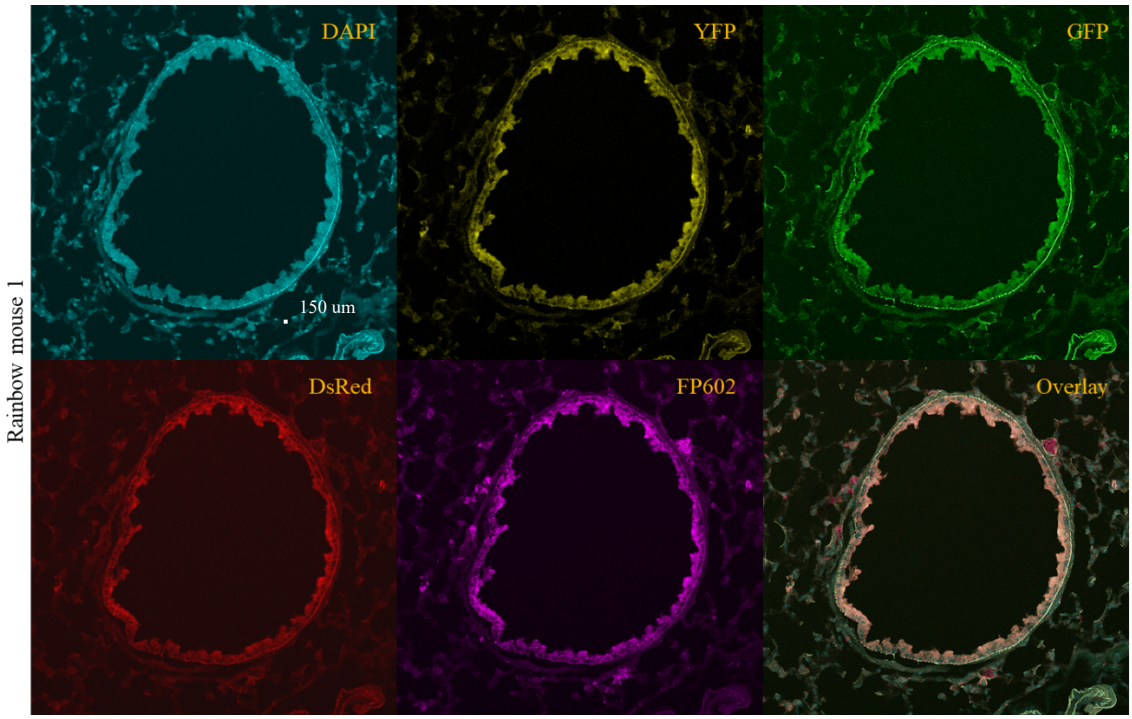

Figure 38: Fluorescent frozen lung tissue section analysis from one of the rainbow mice using Leica imaging system. One of the slides stained that was previously stained with DAPI was used to observe the fluorescent rainbow markers using the STELLARIS confocal imaging system (Leica Microsystems). magnification 20X. Scale bar: 150 µm

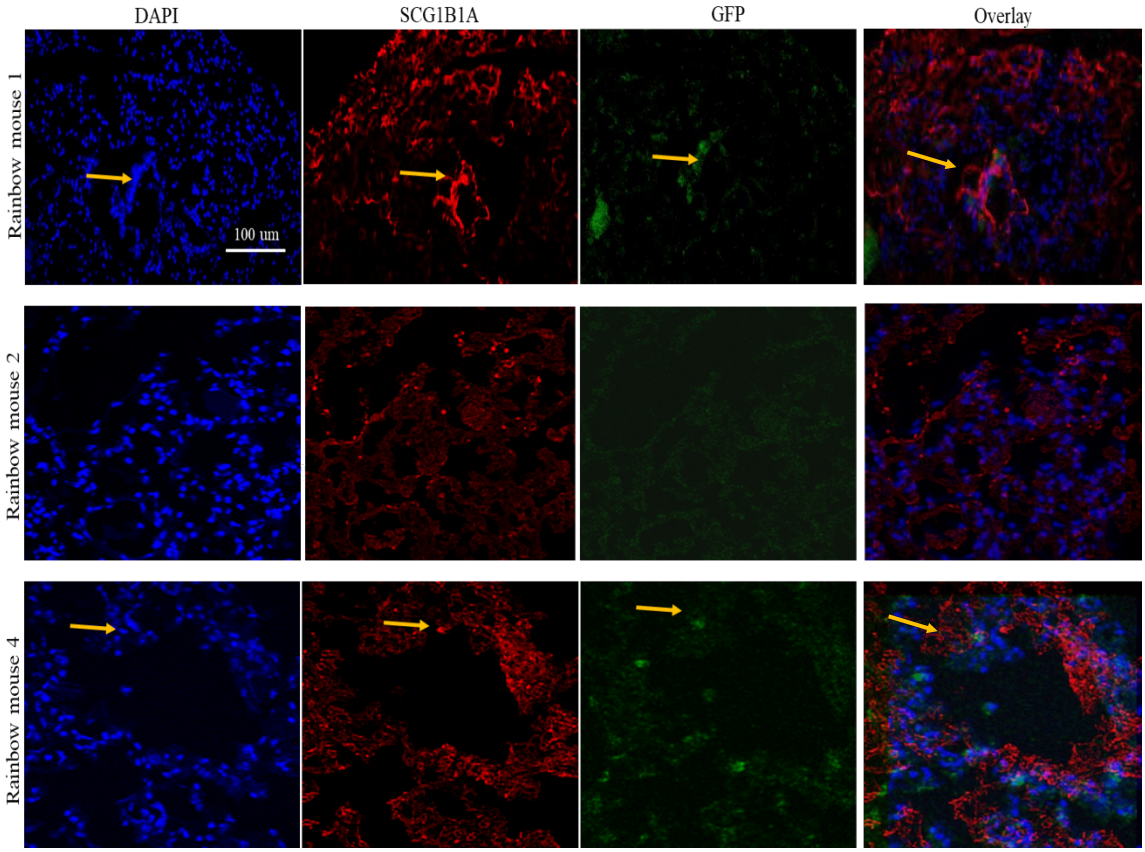

Figure 39: Fluorescent analysis of SCG1B1A labeled cells from frozen lung tissue section from three rainbow mice. The left lobes were embedded on O.C.T and frozen until sectioned. A 6 µm thick section was used to perform histological analysis. The morphology of the cells can be seen by DAPI staining. IHC was employed to label the two stains with cell type-specific antibodies: club cells were stained with SCG1B1A antibody (1:50) overnight, followed by staining with fluorescent secondary antibody Alexa Fluor 750 (1:50). Slides were observed using Confocal microscopy (Olympus Fluoview FV3000). magnification 20X, scale bar:100 µm. Slides stained with cell-type specific antibodies were scanned for GFP+ recombinant cells.

The top row illustrates images from fluorescent microscopy for a rainbow mouse. The tissue was labeled with SCG1B1A marker to identify club cells. The same area was scanned for GFP. Notably, the yellow arrows highlighted GFP+ cells were also observed to be in approximately the same position in the SCG1B1A labeled image. Suggesting that these cells might be GFP+/SCG1B1A+ recombinant cells.

The middle row illustrates images from fluorescent microscopy for another rainbow mouse. The tissue was labeled with SCG1B1A marker to identify club cells. The same area was scanned for GFP. No detectable GFP+ recombinant cells were observed in this particular mouse lung section.

The bottom row illustrates images from fluorescent microscopy for the third rainbow mouse. The tissue was labeled with SCG1B1A marker to identify club cells. The same area was scanned for GFP. Notably, the yellow arrows highlighted GFP+ cells were also observed to be in approximately the same position in the SCG1B1A labelled image. Suggesting that these cells might be GFP+/SCG1B1A+ recombinant cells.

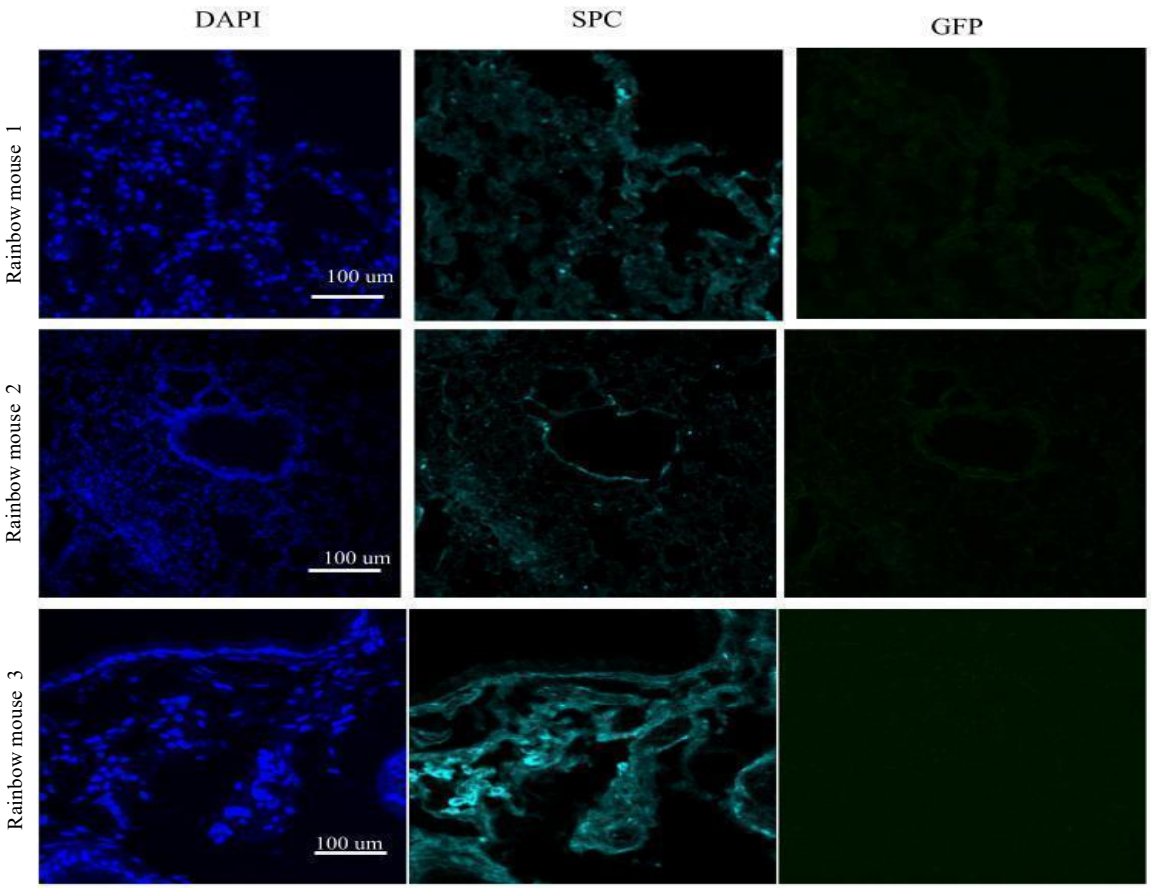

Figure 40: Fluorescent analysis of SPC labeled cells from frozen lung tissue section from three rainbow mice**.** The left lobes were embedded on O.C.T and frozen until sectioned. A 6 µm thick section was used to perform histological analysis. The morphology of the cells can be seen by DAPI staining. IHC was employed to label to stain with cell type-specific antibodies: club cells were stained with SPC antibody (1:50) overnight, followed by staining with fluorescent secondary antibody Alexa Fluor 750 (1:50). Slides were observed using Confocal microscopy (Olympus Fluoview FV3000). magnification 20X, scale bar:100 µm. Slides stained with cell-type specific antibodies were scanned for GFP+ recombinant cells.
The top row illustrates images from fluorescent microscopy for a rainbow mouse. The tissue was labeled with an SPC marker to identify AT2 cells. The same area was scanned for GFP. The same area was scanned for GFP. No detectable GFP+ recombinant cells were observed in this particular mouse lung section.

The middle row illustrates images from fluorescent microscopy for another rainbow mouse. The tissue was labeled with an SPC marker to identify AT2 cells. The same area was scanned for GFP. No detectable GFP+ recombinant cells were observed in this particular mouse lung section.
The bottom row illustrates images from fluorescent microscopy for the third rainbow mouse. The tissue was labeled with an SPC marker to identify AT@ cells. The same area was scanned for GFP. No detectable GFP+ recombinant cells were observed in this particular mouse lung section.

5.2.3 Conclusion:

Histological and fluorescent microscopy analysis showed some preferences towards cell types in mutagenic DSB repair which were otherwise not identified using flow cytometry. GFP+ population was identified from cells that were potentially club cell type. Overall, the data was additional evaluation is required to gain more insight on inter-chromosomal HR in cell subtypes.

CHAPTER 6: DISCUSSION

I aimed to evaluate inter-chromosomal HR in vivo with a unique mouse model. In this study, I have discussed the development and application of the "rainbow mouse" line by incorporating three distinct constructs: two non-functional GFPs and a single TET-ON ISCE1 system meticulously positioned within the open euchromatic region. In the presence of doxycycline, the ISCE1 initiates site-directed DSB at the GFP loci. Subsequently, repair of these DSBs through the inter-chromosomal HR pathway yields a fluorescent GFP. Additionally, these constructs include constitutively expressed fluorescent DsRed and YFP genes, which ensure the continuous expression of GFP and ISCE1 transgenes.

The initial validation of the rainbow constructs was done by developing the mouse ES cell line- OGY cell line. Additionally, MEFs were harvested and cultured the MEFs from rainbow fetuses. Both cell lines were divided into four distinct groups for analysis. The first group served as the untreated control, receiving only DMEM media. The second group was transfected with a GFP vector, which served as a positive control for GFP expression during flow cytometry. The third group, transfected with a CBAS vector, acted as another positive control, as it allowed for constitutive expression of ISCE1, facilitating continuous induction of site-specific double-strand breaks (DSBs) in the rainbow system. The last group was treated with doxycycline for 96 hours to induce conditional expression of ISCE1.

The GFP+ recombinant cell percentages between the groups with constitutive ISCE1 expression and those with conditional ISCE1 expression were comparable, suggesting the ISCE induction efficiency by the TET-ON ISCE1 inducible construct. This result was consistent in both the primary systems. Furthermore, the total frequency of HR recombinants may be attributed to the smaller sample size and fewer replicates used in the analysis. Nevertheless, it should be noted that we observed percentages of inter-chromosomal HR events in mESC cells and primary cells

harvested from the rainbow mice. The percentage of GFP+ recombinants in ESC was greater than GFP+ recombinants in the MEFs.

Results from the *in-utero* experiments revealed GFP+ events within various fetal tissues, including the fetal body, FL, and placenta, suggesting the prominence of inter-chromosomal HR in the fetal tissue. These observations underscore the involvement of inter-chromosomal HR during fetal development. Comparing the three tissues, the GFP+ recombinants were least prevalent within the FL, followed by the fetal body, and highest in the placenta. Stem cells in FL are known for their exceptionally high replication rate (Manesia et al., 2015). The rapid replication process might have eliminated the mutational products, and the damage was not passed to daughter cells, which could be a reason for lower recombinants (Mansell et al., 2019). Alternatively, it is possible that the FL cells with ISCE1-induced DSBs went through the apoptotic pathway rather than undergoing the mutagenic HR repair. Previous research supports this hypothesis that embryonic stem cells undergo cellular apoptosis to prevent DNA damage from passing on to daughter cells, which is a well-established mechanism (Liu et al., 2014) (Manesia et al., 2015).

Plenty of evidence points to the association of in-utero exposure of DNA damaging agents from mother to fetus that increase the chance of childhood cancer (Belson et al., 2007; Heyer et al., 2000a; Pachkowski et al., 2011). One of the initial studies from 1956 reported that exposures to ionizing radiation received in utero for diagnostic radiography had subsequently increased the risk of childhood cancer, especially Acute myeloid leukemia (AML). Since then, several studies have demonstrated that damaging agents such as ionizing radiation, topoisomerase II inhibitors, Benzene, and Pesticides cause an increased risk of childhood leukemia (Belson et al., 2007; Heyer et al., 2000). A more recent study by Els Mansell and colleagues looked at the role of the placental barrier in DNA damage induction as a potential cause of leukemia initiation (Mansell et al., 2019). They demonstrated that the placental barrier participated in releasing chemicals that caused DSB and chromosomal aberrations in the HSC. They used an antioxidant, MitoQ, which prevented the

barrier from releasing damaging factors. This study showed that the placenta likely causes DNA damage to the HSCs in a bystander signaling response which could be linked to leukemia initiation (Dickey et al., 2009; Mansell et al., 2019).

Furthermore, the *in-utero* exposure to DNA-damaging agents causing DSBs was mainly repaired by 4 weeks postnatally. Still, some residual DNA damage in the HSC suggested a possible transgenerational effect. Although we detected GFP+ events from placental tissues, more experiments need to be done to understand the role of the placenta in mutagenic repair since placental dysfunction is a significant cause of many obstetrical syndromes. Also, several placental abnormalities show the incidence of chromosomal aberrations that are hallmarks of DSB-related genome instabilities (Brosens et al., 2011).

Next, I aimed to evaluate inter-chromosomal HR in vivo in hematopoietic organs, mainly the bone marrow and spleen. I analyzed inter-chromosomal HR in HSCs and terminally differentiated T and B cells. Notably, GFP+ recombinant events were observed in the stem and progenitor populations but not in the terminally differentiated T and B cell populations. Previous research using transgenic ES cell lines has highlighted the potential for inter-chromosomal HR to generate translocations (Richardson & Jasin, 2000). Similar investigations using multipotent stem cell enriched hematopoietic stem cells also demonstrated reciprocal translocation as a result of ISCE1-induced inter-chromosomal HR (Francis & Richardson, 2007). I observed a higher percentage of GFP+ recombinants in the lin-/CD34+ HSCs than in other HSCs. CD34+ HSCs have also been associated with cancer leukemia and are considered one of the markers for AML (Quek et al., 2016). However, it is unclear whether CD34+ HSC initiated leukemia transforming into leukemic stem cells or CD34- leukemic stem cells undergoing transformation. These studies further support the hypothesis that progenitor cells are more susceptible to DSBs and potentially mutagenic repairs.

I observed a small population of the LT-HSC, enriched Sca+/CD117+, and the progenitor stem cells enriched Sca+/CD117+ /CD34+ populations. A murine study was undertaken to compare the quantity of LT-HSC in young and old mice with mutant Ku80- and TR genes, which are necessary for the NHEJ repair pathway and the BER respectively, showed that, despite these mutations, the overall number of stem cell population remained mostly unaltered, contradicting previous assumptions about NHEJ being the primary DSB-induced repair route for HSCs (Rossi et al., 2007). However, the impacts of these mutations were more pronounced in more differentiated progenitor cells despite no substantial reduction in the LT-HSC population. This shows that the LT-HSC repair route is tightly regulated regardless of age. While the lin+ population had detectable GFP+ events, we did not observe GFP+ events in the terminally differentiated T cells (lin+/CD4 or lin+/CD8) and B cells (lin+/CD45r). Suggesting that other lineage+ populations, such as committed myeloid and the differentiated myeloid population, might utilize inter-chromosomal HR as a repair pathway.

Accumulation of DNA damage over time is associated with aging. In my study, I analyzed three older mice to assess ISCE1-induced DSBs in hematopoietic tissues. Surprisingly, no detectable GFP+ events were observed in hematopoietic populations. This was unexpected as there are multiple reports of DNA damage accumulation and clonal expansion in hematopoietic stem cells. This outcome suggests an alternative mechanism accounting for the absence of GFP in our rainbow and previously designed G2S models (White et al., 2013). A comparable mouse model-the RaDr model investigated age-dependent intrachromosomal HR in vivo in lung tissue suggests the hematopoietic stem cells from older mice might also use intrachromosomal HR or other repair pathways to ISCE1-induced DSBs (Kimoto et al., 2017).

Additionally, I aimed to evaluate inter-chromosomal HR-induced repair in vivo in two solid tissues: pancreas and lung. We observed detectable GFPs in both tissues; however, the ISCE1-

induced inter-chromosomal HR was more prevalent in pancreatic tissue than in the lung tissue, as confirmed by quantitative and qualitative analysis.

My flow cytometry analysis of pancreatic tissues revealed that pancreatic duct cells exhibit a higher propensity to utilize the inter-chromosomal HR repair mechanism than the other cell types, which supported my hypothesis. The duct cells have cellular plasticity and are known to possess stem cell-like features, making them susceptible to DNA damage. Prior studies have emphasized the stem cell-like properties of duct cells, and rodent investigations have demonstrated their potential to function as pancreatic progenitor cells in adult mice (Kopinke & Murtaugh, 2010; Lardon et al., 2004). Moreover, these cells can undergo trans-differentiation into other cell types under cellular stress conditions, exhibiting stem cell characteristics (Criscimanna et al., 2011; Gao et al., 2022; Reichert & Rustgi, 2011). It is well-established that stem cells tend to accumulate damage and evade apoptosis, resulting in increased genome instability (R. Francis & Richardson, 2007b) (Blanpain et al., 2011; Liu et al., 2014b; Sjakste & Riekstiņa, 2021). The prominence of duct cells using DSB-induced mutagenic inter-chromosomal HR supports the hypothesis that cells with more progenitor-like properties are more susceptible to mutagenic repairs.

Flow cytometry revealed insulin+ β cell subpopulation, another cell type with detectable GFP+ recombinant cells, ranking second cell type after duct cells to have increased inter-chromosomal HR. Although no evidence of DSBs in normal β cells has been reported, it is plausible that β cells are more susceptible to DSBs, which could explain the higher percentage of GFP+ insulin+ cells observed in our study. However, this observation was not consistent with the histological analysis. This discrepancy may be because individual GFP+ recombinant cells do not release enough fluorescence intensity to provide a visible signal under the confocal microscope. Recent studies in mice have emphasized the significance of DNA damage in β cells concerning diabetes (Tay et al., 2019). They demonstrated that a more significant number of DSBs in β cells of type two diabetic mice affects the survival of this cell type.

Conversely, I did not see a similar trend in the alpha cell subpopulation, which could be attributed to the lower percentage of the total glucagon+ population. By modifying the overall cell isolation procedure, we successfully obtained a significantly greater number of total islet cells. I observed small stem cell-like colonies on the Petri plates even in the absence of stem cell growth factors in the culture medium. It is well-established that adult islets possess self-replication and regeneration capabilities (Dor et al., 2004; Romer & Sussel, 2015). To further investigate this phenomenon, it would be intriguing to label these stem cells with pancreatic stem cell markers, such as PDX1, in conjunction with markers for differentiated cells. This approach could be further exploited to determine specific cell types that could potentially develop stem cell-like colonies and shed light on adult pancreatic stem cells.

Flow cytometric analysis showed a surprisingly low percentage of GFP+ acinar cells compared to the other cell types, contradicting our histological findings. This observation further highlights the well-known cellular plasticity of acinar cells (Ferreira et al., 2017; Kopp et al., 2012). Previous reports described acinar cells undergoing dedifferentiation into metaplastic ducts, which can lead to the development of PDAC.

Utilizing flow cytometry to detect GFP+ events within lung tissue yielded limited success, as a very minor and infrequent GFP+ population was discernible in the total lung tissue. Furthermore, GFP+ populations were not observed in the selected cell types. Histological analysis of the lungs unveiled a small GFP+ cell population in two of the mice, while the remaining three exhibited no GFP presence. Our findings suggest the likelihood of clonal expansion, though a more substantial sample size would enhance the conclusiveness of these observations. Paradoxically, our current outcomes from aged mice lung analysis oppose the results from the RaDr mice, which demonstrated DNA damage accumulation with age. This implies the utilization of alternative repair pathways in older mice (Kimoto et al., 2017).

The RaDr model serves to assess the frequency of intrachromosomal HR, a mechanism employing sister chromatids or homologous chromosomes for mending broken ends. Intrachromosomal HR has associations with LOH mutations. Interestingly, a small subset of lung adenocarcinomas displays mutations in HR-specific genes, namely BRCA1 and BRCA2. A genomic investigation employing whole genome sequencing of non-small cell lung cancer (NSCLC) patients unveiled LOH of BRCA1 or BRCA2, coupled with deficiencies in the BRCA genes (Remon et al., 2020). Recent research evaluated DNA damage repair efficiency in basal stem cells within the lung. These cells, considered one of the lung's more progenitor populations, possess enhanced differentiation potential compared to alveolar type 2 cells. They have also been implicated in initiating lung squamous cell carcinoma (SqCC). This investigation revealed that basal stem cells exhibited a stronger inclination towards the NHEJ repair pathway than AT2 cells (Weeden et al., 2017). Another study scrutinized DNA damage in AT2 cells from the lungs of emphysema patients. Western blot analysis targeting DNA damage-specific genes, such as 53BP1 and DNA ligase III specific for NHEJ and XLF for Alt-EJ repair, indicated substantial reductions. In contrast, Rad51 protein levels remained unaltered. These findings pointed towards impaired NHEJ and Alt-EJ, potentially compromising the overall genome stability of AT2 cells and suggesting an inefficacy of the HR pathway for double-strand break repair in these cell types (Kosmider et al., 2019).

Overall, gaining a deeper understanding of the inter-chromosomal HR repair capacity in vivo in multiple tissues is crucial for unraveling the intricacies of DNA damage mechanisms genome and their role in tissue-specific disease and cancer development. In general, the findings of this study offer valuable genetic insights into the repair processes employed by most of the stem and stem-like cell types when encountering DSBs in an in vivo system. Their characteristic features affect their propensity towards inter-chromosomal HR repair. By elucidating how these cell types effectively repair DSBs, they ensure the preservation of genetic integrity and prevent potentially

harmful genetic rearrangements. Furthermore, results from my experiments elucidate that terminally differentiated cell types with minimal or no cellular plasticity do not majorly rely on DSB-induced inter-chromosomal HR pathway and may employ other pathways to repair DSBs. This study significantly advances our knowledge of the fundamental mechanisms underlying the rejoining of DSBs at the chromosomal level, thereby contributing to our understanding of genome stability.

My study has established the rainbow mouse model as a unique and successful in vivo model for investigating potential alterations in inter-chromosomal HR repair throughout different stages of development. The rainbow mouse model allows us to observe and analyze the repair processes within different tissues, providing valuable information on how HR repair may vary across the developmental spectrum. Finally, the rainbow model has implications for understanding how environmental exposures and dietary choices, including the consumption of supplements such as bioflavonoids, can impact cellular responses and the maintenance of genome stability and mitigate the risk of DNA damage-related diseases, aging, and cancer.

Future directions

I observed a small population of the MPPs, CMPs, and lin-/ckit+ lin-/sca+ HSCs. The percentage of GFP+ populations proved to be challenging to obtain. A long-term culture-initiating cell (LTC-IC) assay must be performed as an additional study. This would further identify the primitive HSCs and score GFP+ populations at multiple stages of differentiation. This would further elucidate the clonal expansion capacities of these cell types.

I observed in utero inter-chromosomal HR in multiple fetal tissues. We observed GFP+ events in overall fetal tissues, which warrants further investigation. Furthermore, it is feasible to explore in utero inter-chromosomal HR at different time points of fetal development. It is known that fetal hematopoiesis is not as organ restricted as adult hematopoiesis, occurring majorly in the bone marrow and occasionally in medullary organs like the spleen and thymus. The Placental tissue

is speculated to be one of the hematopoietic organs during fetal development, harboring large pools of HSCs. A study showed that the 12.5 Day placenta has a high population of CD34medckithimarkers similar to the fetal liver, suggesting the occurrence of HSCs phenotypically similar to fetal HSCs (Lee. et al. et al., 2010). Our rainbow mice analysis showed detectable GFP+ events from flow cytometry analysis of total placental tissue in one of the litters. As a part of future study, the placental cells harvested on gestation day 12.5 would be labeled the placental cells stem cell type-specific markers to determine whether the HSC from placental cells is undergoing inter-chromosomal HR.

Additionally, I plan to employ total placental tissues to visualize the distribution of GFP+ recombinant populations across the placenta. Frozen placental tissues will be sectioned vertically and stained with H&E and DAPI staining techniques to achieve these. The sections are labeled with fluorescent stage-specific embryonic antigen-3 (SSEA3) and c-KIT antibodies to elucidate the stem cell populations further.

In addition to the LT-HSCs, neural cells exhibit a slower replication rate and are commonly associated with DNA damage due to neural plasticity (Heyer et al., 2000b; Konopka & Atkin, 2022). Even though earlier neural studies proposed that the neural cells use NHEJ or BER as major repair pathways, recent research showed that mutation of the Rad52 protein affected genome stability in neurons, which was phenotypically similar to that seen in Alzheimer's disease (Welty et al., 2018). Assessing ISCE1-induced inter-chromosomal HR in brain cells would be insightful in understanding inter-chromosomal HR frequency in brain tissue and its potential contribution to double-strand breaks (DSBs) accumulation with advancing age. My proposed methodology involves investigating brain cells from two different age groups of mice. Neurons glial and neural stem cells will be identified using cell type-specific antibodies. Furthermore, frozen whole brain tissue can be sectioned and observed for GFP+ cells to observe whether the GFP+ are detectable

and form clusters in brain tissues, providing insights into the occurrence and accumulation of GFP+ recombinants in brain tissue.

Understanding the frequency of mutagenic HR pathways in vivo in multiple tissues would provide greater insight into cellular and molecular signatures of solid tumorigenesis and the potential development of HR-specific therapy. Mutation of HR genes such as BRCA1 often elevates genomic instability and renders the cells more prone to damage by exogenous agents. Notably, pancreatic cancer patients with familial history demonstrate higher germline mutation of BRCA2 (Teo & O'Reilly, 2016; Waddell et al., 2015). Another genomic investigation employing whole genome sequencing of non-small cell lung cancer (NSCLC) patients unveiled LOH of BRCA1 or BRCA2, coupled with deficiencies in the BRCA genes (Remon et al., 2020). In our research framework, we propose expanding our current rainbow model by incorporating a BRCA knockout line (Teo & O'Reilly, 2016; Waddell et al., 2015). This unique BRCA knockout rainbow line would allow for the evaluation of inter-chromosomal HR frequencies across several organs, directly comparing the results acquired from our current approach.

Finally, the rainbow mouse model is an excellent tool to identify which environmental and dietary compounds have the potential to induce DSBS and undergo mutational repair, thereby resulting in overall genomic instability. Research from our lab has demonstrated several dietary supplements, primarily bioflavonoids, that act like topoisomerase II inhibitors and cause DSBs, and have the potential to induce translocations (Bariar et al., 2013, 2018; Goodenow et al., 2020; Welty et al., 2018). A recent endeavor successfully provoked DSBs in rainbow mice through a 28-day oral administration of genistein. Flow cytometry and microscopy analyses revealed the presence of detectable GFP+ recombinants across multiple tissues. Moving forward, our laboratory intends to leverage this model to assess other bioflavonoids, such as quercetin, to induce DSBs, and the resultant mutagenic repairs could be quantified through the observation of GFP+ recombinants.

REFERENCES

1. Agarwal, S., Tafel, A. A., & Kanaar, R. (2006). DNA double-strand break repair and chromosome translocations. *DNA Repair*, *5*(9–10), 1075–1081. https://doi.org/10.1016/j.dnarep.2006.05.029
2. Agwuh, K. N., & MacGowan, A. (2006). Pharmacokinetics and pharmacodynamics of the tetracyclines including glycylcyclines. *Journal of Antimicrobial Chemotherapy*, *58*(2), 256–265. https://doi.org/10.1093/jac/dkl224
3. Antaódn, A., Martinez-Larrañaga, M. R., Diaz, M. J., Bringas, P., Fernandez, M. C., Fernandez-Cruz, M. L., Iturbe, J., & Martinez, M. A. (1994). Pharmacokinetics of doxycycline in broiler chickens. *Avian Pathology*, *23*(1), 79–90. https://doi.org/10.1080/03079459408418976
4. Aponte, P. M., & Caicedo, A. (2017). Stemness in cancer: Stem cells, cancer stem cells, and their microenvironment. In *Stem Cells International* (Vol. 2017). Hindawi Limited. https://doi.org/10.1155/2017/5619472
5. Ashley, T., Gaeth, A. P., Inagaki, H., Seftel, A., Cohen, M. M., Anderson, L. K., Kurahashi, H., & Emanuel, B. S. (2006). ARTICLE Meiotic Recombination and Spatial Proximity in the Etiology of the Recurrent t(11;22). In *The American Journal of Human Genetics* (Vol. 79). www.ajhg.org
6. Ayob, A. Z., & Ramasamy, T. S. (2018). Cancer stem cells as key drivers of tumour progression. In *Journal of Biomedical Science* (Vol. 25, Issue 1). BioMed Central Ltd. https://doi.org/10.1186/s12929-018-0426-4
7. Bandele, O. J., & Osheroff, N. (2007). Bioflavonoids as poisons of human topoisomerase IIα and IIβ. *Biochemistry*, *46*(20), 6097–6108. https://doi.org/10.1021/bi7000664
8. Bantikassegn, A., Song, X., & Politi, K. (2015). Isolation of epithelial, endothelial, and immune cells from lungs of transgenic mice with oncogene-induced lung adenocarcinomas. *American Journal of Respiratory Cell and Molecular Biology*, *52*(4), 409–417. https://doi.org/10.1165/rcmb.2014-0312MA
9. Bariar, B., Greer Vestal, C., & Richardson, C. (2013). Long-term effects of chromatin remodeling and DNA damage in stem cells induced by environmental and dietary agents. *Journal of Environmental Pathology, Toxicology and Oncology*, *32*(4), 307–327. https://doi.org/10.1615/JEnvironPatholToxicolOncol.2013007980
10. Bariar, B., Vestal, C. G., Deem, B., Goodenow, D., Engledove, R. W., Sahyouni, M., & Richardson, C. (2018). Bioflavonoids promote stable translocations between MLL - AF9 breakpoint cluster regions independent of normal chromosomal context : Model system to screen environmental risks. *Environmental and Molecular Mutagenesis*. https://doi.org/10.0.3.234/em.22245
11. Barker, J. E., Keenan, M. A., & Raphals, L. (1969). Development of the mouse hematopoietic system. II. Estimation of spleen and liver “stem” cell number. *Journal of Cellular Physiology*, *74*(1), 51–55. https://doi.org/10.1002/jcp.1040740107
12. Beerman, I., Seita, J., Inlay, M. A., Weissman, I. L., & Rossi, D. J. (2014). Quiescent hematopoietic stem cells accumulate DNA damage during aging that is repaired upon entry into cell cycle. *Cell Stem Cell*, *15*(1), 37–50. https://doi.org/10.1016/j.stem.2014.04.016
13. Belson, M., Kingsley, B., & Holmes, A. (2007). Risk factors for acute leukemia in children: A review. In *Environmental Health Perspectives* (Vol. 115, Issue 1, pp. 138–145). https://doi.org/10.1289/ehp.9023

14. Bishop, A. J. R. (2000). Homologous recombination as a mechanism for genome rearrangements: environmental and genetic effects. *Human Molecular Genetics*, *9*(16), 2427–2334. https://doi.org/10.1093/hmg/9.16.2427
15. Blackford, A. N., & Jackson, S. P. (2017). ATM, ATR, and DNA-PK: The Trinity at the Heart of the DNA Damage Response. In *Molecular Cell* (Vol. 66, Issue 6, pp. 801–817). Cell Press. https://doi.org/10.1016/j.molcel.2017.05.015
16. Blanc, G., Barakat, A., Guyot, R., Cooke, R., & Delseny, M. (2000). Extensive Duplication and Reshuffling in the Arabidopsis Genome. In *www.plantcell.org The Plant Cell* (Vol. 12). www.plantcell.org
17. Blanpain, C., Mohrin, M., Sotiropoulou, P. A., & Passegué, E. (2011). DNA-damage response in tissue-specific and cancer stem cells. In *Cell Stem Cell* (Vol. 8, Issue 1, pp. 16–29). https://doi.org/10.1016/j.stem.2010.12.012
18. Blokzijl, F., De Ligt, J., Jager, M., Sasselli, V., Roerink, S., Sasaki, N., Huch, M., Boymans, S., Kuijk, E., Prins, P., Nijman, I. J., Martincorena, I., Mokry, M., Wiegerinck, C. L., Middendorp, S., Sato, T., Schwank, G., Nieuwenhuis, E. E. S., Verstegen, M. M. A., … Van Boxtel, R. (2016). Tissue-specific mutation accumulation in human adult stem cells during life. *Nature*, *538*(7624), 260–264. https://doi.org/10.1038/nature19768
19. Brosens, I., Pijnenborg, R., Vercruysse, L., & Romero, R. (2011). The "great Obstetrical Syndromes" are associated with disorders of deep placentation. *American Journal of Obstetrics and Gynecology*, *204*(3), 193–201. https://doi.org/10.1016/j.ajog.2010.08.009
20. Burke, Z. D., Thowfeequ, S., Peran, M., & Tosh, D. (2007). Stem cells in the adult pancreas and liver. In *Biochemical Journal* (Vol. 404, Issue 2, pp. 169–178). https://doi.org/10.1042/BJ20070167
21. Chen, Y., Cui, Z., Chen, Z., Jiang, Y., & Mao, Z. (2023). IDDoR: a novel reporter mouse system for simultaneous and quantitative in vivo analysis of both DNA double-strand break repair pathways. *Protein & Cell*, *14*(5), 369–375. https://doi.org/10.1093/procel/pwac001
22. Chiruvella, K. K., Liang, Z., & Wilson, T. E. (2013). Repair of double-strand breaks by end joining. *Cold Spring Harbor Perspectives in Biology*, *5*(5). https://doi.org/10.1101/cshperspect.a012757
23. Choi, Y., Ta, M., Atouf, F., & Lumelsky, N. (2004). Adult Pancreas Generates Multipotent Stem Cells and Pancreatic and Nonpancreatic Progeny. *STEM CELLS*, *22*(6), 1070–1084. https://doi.org/10.1634/stemcells.22-6-1070
24. Choma, D., Daurès, J. P., Quantin, X., & Pujol, J. L. (2001). Aneuploidy and prognosis of non-small-cell lung cancer: A meta-analysis of published data. *British Journal of Cancer*, *85*(1), 14–22. https://doi.org/10.1054/bjoc.2001.1892
25. Chun, J., Buechelmaier, E. S., & Powell, S. N. (2013). Rad51 Paralog Complexes BCDX2 and CX3 Act at Different Stages in the BRCA1-BRCA2-Dependent Homologous Recombination Pathway. *Molecular and Cellular Biology*, *33*(2), 387–395. https://doi.org/10.1128/mcb.00465-12
26. Ciccia, A., & Elledge, S. J. (2010). The DNA Damage Response: Making It Safe to Play with Knives. In *Molecular Cell* (Vol. 40, Issue 2, pp. 179–204). https://doi.org/10.1016/j.molcel.2010.09.019
27. Clairambault, J., & Shen, S. (2020). Cell plasticity in cancer cell populations. In *F1000Research* (Vol. 9). F1000 Research Ltd. https://doi.org/10.12688/f1000research.24803.1
28. Clarke, M. F., & Fuller, M. (2006). Stem Cells and Cancer: Two Faces of Eve. In *Cell* (Vol. 124, Issue 6, pp. 1111–1115). Elsevier B.V. https://doi.org/10.1016/j.cell.2006.03.011

29. Coïc, E., Feldman, T., Landman, A. S., & Haber, J. E. (2008). Mechanisms of Rad52-independent spontaneous and UV-induced mitotic recombination in Saccharomyces cerevisiae. *Genetics*, *179*(1), 199–211. https://doi.org/10.1534/genetics.108.087189
30. Coopera, T. J., Garcia, V., & Neale, M. J. (2016). Meiotic DSB patterning: A multifaceted process. *Cell Cycle*, *15*(1), 13–21. https://doi.org/10.1080/15384101.2015.1093709
31. Corbin, K. L., West, H. L., Brodsky, S., Whitticar, N. B., Koch, W. J., & Nunemaker, C. S. (2021). A Practical Guide to Rodent Islet Isolation and Assessment Revisited. In *Biological Procedures Online* (Vol. 23, Issue 1). BioMed Central Ltd. https://doi.org/10.1186/s12575-021-00143-x
32. Coster, G., & Goldberg, M. (2010). The cellular response to DNA damage: A focus on MDC1 and its interacting proteins. *Nucleus*, *1*(2), 166–178.
33. Criscimanna, A., Speicher, J. A., Houshmand, G., Shiota, C., Prasadan, K., Ji, B., Logsdon, C. D., Gittes, G. K., & Esni, F. (2011). Duct cells contribute to regeneration of endocrine and acinar cells following pancreatic damage in adult mice. *Gastroenterology*, *141*(4). https://doi.org/10.1053/j.gastro.2011.07.003
34. Daley, J. M., & Sung, P. (2014). 53BP1, BRCA1, and the Choice between Recombination and End Joining at DNA Double-Strand Breaks. *Molecular and Cellular Biology*, *34*(8), 1380–1388. https://doi.org/10.1128/mcb.01639-13
35. Davis, A. J., Chen, B. P. C., & Chen, D. J. (2014). DNA-PK: A dynamic enzyme in a versatile DSB repair pathway. *DNA Repair*, *17*, 21–29. https://doi.org/10.1016/j.dnarep.2014.02.020
36. Decottignies, A. (2013). Alternative end-joining mechanisms: A historical perspective. In *Frontiers in Genetics* (Vol. 4, Issue APR). https://doi.org/10.3389/fgene.2013.00048
37. Derijck, A., Van der heijden, G., Giele, M., Philippens, M., & De boer, P. (2008). DNA double-strand break repair in parental chromatin of mouse zygotes, the first cell cycle as an origin of de novo mutation. *Human Molecular Genetics*, *17*(13), 1922–1937. https://doi.org/10.1093/hmg/ddn090
38. Dickey, J. S., Baird, B. J., Redon, C. E., Sokolov, M. V., Sedelnikova, O. A., & Bonner, W. M. (2009). Intercellular communication of cellular stress monitored by γ-H2AX induction. *Carcinogenesis*, *30*(10), 1686–1695. https://doi.org/10.1093/carcin/bgp192
39. Diossy, M., Sztupinszki, Z., Borcsok, J., Krzystanek, M., Tisza, V., Spisak, S., Rusz, O., Timar, J., Csabai, I., Fillinger, J., Moldvay, J., Pedersen, A. G., Szuts, D., & Szallasi, Z. (2021). A subset of lung cancer cases shows robust signs of homologous recombination deficiency associated genomic mutational signatures. *Npj Precision Oncology*, *5*(1). https://doi.org/10.1038/s41698-021-00199-8
40. Dor, Y., Brown, J., Martinez, O. I., & Melton, D. A. (2004). *Adult pancreatic b-cells are formed by self-duplication rather than stem-cell differentiation*. www.nature.com/nature
41. El-Gohary, Y., Wiersch, J., Tulachan, S., Xiao, X., Guo, P., Rymer, C., Fischbach, S., Prasadan, K., Shiota, C., Gaffar, I., Song, Z., Galambos, C., Esni, F., & Gittes, G. K. (2016). Intraislet pancreatic ducts can give rise to insulin-positive cells. *Endocrinology*, *157*(1), 166–175. https://doi.org/10.1210/en.2015-1175
42. Elliott, B., & Jasin, M. (2002). Human genome and diseases: Review double-strand breaks and translocations in cancer. *Cellular and Molecular Life Sciences*, *59*(2), 373–385. https://doi.org/10.1007/s00018-002-8429-3
43. Ema, H., & Nakauchi, H. (2000). Expansion of hematopoietic stem cells in the developing liver of a mouse embryo. *Blood*, *95*(7), 2284–2288. https://doi.org/10.1182/blood.V95.7.2284

44. Fernandez, J., Bloomer, H., Kellam, N., & LaRocque, J. R. (2019). Chromosome preference during homologous recombination repair of DNA double-strand breaks in Drosophila melanogaster. *G3: Genes, Genomes, Genetics*, *9*(11), 3773–3780. https://doi.org/10.1534/g3.119.400607
45. Ferone, G., Lee, M. C., Sage, J., & Berns, A. (2020). *Cells of origin of lung cancers: lessons from mouse studies*. https://doi.org/10.1101/gad.338228
46. Ferreira da Silva, J., Meyenberg, M., & Loizou, J. I. (2021). Tissue specificity of DNA repair: the CRISPR compass. In *Trends in Genetics* (Vol. 37, Issue 11, pp. 958–962). Elsevier Ltd. https://doi.org/10.1016/j.tig.2021.07.010
47. Ferreira, R. M. M., Sancho, R., Messal, H. A., Nye, E., Spencer-Dene, B., Stone, R. K., Stamp, G., Rosewell, I., Quaglia, A., & Behrens, A. (2017). Duct- and Acinar-Derived Pancreatic Ductal Adenocarcinomas Show Distinct Tumor Progression and Marker Expression. *Cell Reports*, *21*(4), 966–978. https://doi.org/10.1016/j.celrep.2017.09.093
48. Francis, D. B., Kozlov, M., Chavez, J., Chu, J., Malu, S., Hanna, M., & Cortes, P. (2014). DNA Ligase IV regulates XRCC4 nuclear localization. *DNA Repair*, *21*, 36–42. https://doi.org/10.1016/j.dnarep.2014.05.010
49. Francis, R., & Richardson, C. (2007a). Multipotent hematopoietic cells susceptible to alternative double-strand break repair pathways that promote genome rearrangements. *Genes and Development*, *21*(9), 1064–1074. https://doi.org/10.1101/gad.1522807
50. Francis, R., & Richardson, C. (2007b). Multipotent hematopoietic cells susceptible to alternative double-strand break repair pathways that promote genome rearrangements. *Genes and Development*, *21*(9), 1064–1074. https://doi.org/10.1101/gad.1522807
51. Gao, Y., Guan, W., & Bai, C. (2022). Pancreatic Duct Cells Isolated From Canines Differentiate Into Beta-Like Pancreatic Islet Cells. *Frontiers in Veterinary Science*, *8*. https://doi.org/10.3389/fvets.2021.771196
52. Georgieva, D. (2019). *BRCA1 and 53BP1 Mediate Reprogramming Through DNA Repair Pathway Choice*.
53. Goodarzi, A. A., Yu, Y., Riballo, E., Douglas, P., Walker, S. A., Ye, R., Härer, C., Marchetti, C., Morrice, N., Jeggo, P. A., & Lees-Miller, S. P. (2006). DNA-PK autophosphorylation facilitates Artemis endonuclease activity. *EMBO Journal*, *25*(16), 3880–3889. https://doi.org/10.1038/sj.emboj.7601255
54. Goodenow, D., Emmanuel, F., Berman, C., Sahyouni, M., & Richardson, C. (2020). Bioflavonoids cause DNA double-strand breaks and chromosomal translocations through topoisomerase II-dependent and -independent mechanisms. *Mutation Research - Genetic Toxicology and Environmental Mutagenesis*, *849*. https://doi.org/10.1016/j.mrgentox.2020.503144
55. Goodenow, D., Lalwani, K., & Richardson, C. (2021a). *DNA Damage and Repair Mechanisms Triggered by Exposure to Bioflavonoids and Natural Compounds*. https://doi.org/DOI: http://dx.doi.org/10.5772/intechopen.95453
56. Goodenow, D., Lalwani, K., & Richardson, C. (2021b). DNA Damage and Repair Mechanisms Triggered by Exposure to Bioflavonoids and Natural Compounds. In *IntechOpen* (Vol. 32, pp. 137–144). https://doi.org/http://dx.doi.org/10.5772/intechopen.95453
57. Grippo, P. J., Nowlin, P. S., Demeure, M. J., Longnecker, D. S., & Sandgren, E. P. (2003). Preinvasive pancreatic neoplasia of ductal phenotype induced by acinar cell targeting of mutant Kras in transgenic mice. *Cancer Research*, *63*(9), 2016–2019.
58. Guerra, C., Schuhmacher, A. J., Cañamero, M., Grippo, P. J., Verdaguer, L., Pérez-Gallego, L., Dubus, P., Sandgren, E. P., & Barbacid, M. (2007). Chronic Pancreatitis Is

Essential for Induction of Pancreatic Ductal Adenocarcinoma by K-Ras Oncogenes in Adult Mice. *Cancer Cell*, *11*(3), 291–302. https://doi.org/10.1016/j.ccr.2007.01.012
59. Gu, J., Lu, H., Tsai, A. G., Schwarz, K., & Lieber, M. R. (2007). Single-stranded DNA ligation and XLF-stimulated incompatible DNA end ligation by the XRCC4-DNA ligase IV complex: Influence of terminal DNA sequence. *Nucleic Acids Research*, *35*(17), 5755–5762. https://doi.org/10.1093/nar/gkm579
60. Haber, J. E. (2018). DNA Repair: The Search for Homology. *BioEssays*, *40*(5), 1–24. https://doi.org/10.1002/bies.201700229
61. Hamasaki, K., Matsumoto, T., Cologne, J., Mukai, M., Kodama, Y., Noda, A., & Nakamura, N. (2023). Translocations are induced in hematopoietic stem cells after irradiation of fetal mice. *Journal of Radiation Research*, *64*(1), 99–104. https://doi.org/10.1093/jrr/rrac078
62. Har-Vardi, I., Mali, R., Breietman, M., Sonin, Y., Albotiano, S., Levitas, E., Potashnik, G., & Priel, E. (2007). DNA topoisomerases I and II in human mature sperm cells: Characterization and unique properties. *Human Reproduction*, *22*(8), 2183–2189. https://doi.org/10.1093/humrep/dem170
63. Helmink, B. A., & Sleckman, B. P. (2012). The response to and repair of RAG-mediated DNA double-strand breaks. In *Annual Review of Immunology* (Vol. 30, pp. 175–202). https://doi.org/10.1146/annurev-immunol-030409-101320
64. Herrera, P. L., Nepote, V., & Delacour, A. (2002). Pancreatic cell lineage analyses in mice. *Endocrine*, *19*(3), 267–277. https://doi.org/10.1385/ENDO:19:3:267
65. Heyer, B. S., Macauley, A., Behrendtsen, O., & Werb, Z. (2000a). *Hypersensitivity to DNA damage leads to increased apoptosis during early mouse development*. www.genesdev.org
66. Heyer, B. S., Macauley, A., Behrendtsen, O., & Werb, Z. (2000b). *Hypersensitivity to DNA damage leads to increased apoptosis during early mouse development*. www.genesdev.org
67. Hoeijmakers, J. H. J. (2009). DNA Damage, Aging, and Cancer. *New England Journal of Medicine*, *361*(15), 1475–1485. https://doi.org/10.1056/nejmra0804615
68. Hogan, B. L. M., Barkauskas, C. E., Chapman, H. A., Epstein, J. A., Jain, R., Hsia, C. C. W., Niklason, L., Calle, E., Le, A., Randell, S. H., Rock, J., Snitow, M., Krummel, M., Stripp, B. R., Vu, T., White, E. S., Whitsett, J. A., & Morrisey, E. E. (2014). Repair and regeneration of the respiratory system: Complexity, plasticity, and mechanisms of lung stem cell function. In *Cell Stem Cell* (Vol. 15, Issue 2, pp. 123–138). Cell Press. https://doi.org/10.1016/j.stem.2014.07.012
69. Hustedt, N., & Durocher, D. (2017). The control of DNA repair by the cell cycle. In *Nature Cell Biology* (Vol. 19, Issue 1, pp. 1–9). Nature Publishing Group. https://doi.org/10.1038/ncb3452
70. Hwu, H. R., Roberts, J. W., Davidson, E. H., & Britten, R. J. (1986). *Insertion and/or deletion of many repeated DNA sequences in human and higher ape evolution (molecular evolution/higher primates/mobile genetic elements/Alu family/Kpn I Li family)* (Vol. 83).
71. Jackson, S. P., & Bartek, J. (2009). The DNA-damage response in human biology and disease. In *Nature* (Vol. 461, Issue 7267, pp. 1071–1078). https://doi.org/10.1038/nature08467
72. Jasin, M. (1996). Genetic manipulation of genomes with rare-cutting endonucleases. *Copyright© LCfl~,El~vivrScicm't'Ltd. Alltlght. Tt~r'.'¢d. Olf~8-EJq25/O6/SIq.~;~) 224 PII: ~)16V-9"525(96)] C 919-6*, *12*, 224–228.
73. Jasin, M., & Rothstein, R. (2013). Repair of strand breaks by homologous recombination. *Cold Spring Harbor Perspectives in Biology*, *5*(11), 1–18. https://doi.org/10.1101/cshperspect.a012740

74. Kantidze, O. L., & Razin, S. V. (2009). Chromatin loops, illegitimate recombination, and genome evolution. In *BioEssays* (Vol. 31, Issue 3, pp. 278–286). https://doi.org/10.1002/bies.200800165
75. Kass, E. M., Lim, P. X., Helgadottir, H. R., Moynahan, M. E., & Jasin, M. (2016). Robust homology-directed repair within mouse mammary tissue is not specifically affected by Brca2 mutation. *Nature Communications*, *7*, 1–10. https://doi.org/10.1038/ncomms13241
76. Kathiriya, J. J., Brumwell, A. N., Jackson, J. R., Tang, X., & Chapman, H. A. (2020). Distinct Airway Epithelial Stem Cells Hide among Club Cells but Mobilize to Promote Alveolar Regeneration. *Cell Stem Cell*, *26*(3), 346-358.e4. https://doi.org/10.1016/j.stem.2019.12.014
77. Keeney, S., Giroux, C. N., & Kleckner, N. (1997). *Department of Molecular and Cellular Biology. In *Cell* (Vol. 88). Kleckner.
78. Khanna, K. K., & Jackson, S. P. (2001). *DNA double-strand breaks: signaling, repair and the cancer connection*. http://genetics.nature.com
79. Khil, P. P., Smagulova, F., Brick, K. M., Camerini-Otero, R. D., & Petukhova, G. V. (2012). Sensitive mapping of recombination hotspots using sequencing-based detection of ssDNA. *Genome Research*, *22*(5), 957–965. https://doi.org/10.1101/gr.130583.111
80. Kimoto, T., Kay, J. E., Li, N., & Engelward, B. P. (2017). Recombinant cells in the lung increase with age via de novo recombination events and clonal expansion. *Environmental and Molecular Mutagenesis*, *58*(3), 135–145. https://doi.org/10.1002/em.22082
81. Kolas, N. K., Chapman, J. R., Nakada, S., Ylanko, J., Chahwan, R., Sweeney, F. D., Panier, S., Mendez, M., Wildenhain, J., Thomson, T. M., Pelletier, L., Jackson, S. P., & Durocher, D. (2007). Orchestration of the DNA-damage response by the RNF8 ubiquitin ligase. *Science*, *318*(5856), 1637–1640. https://doi.org/10.1126/science.1150034
82. Konopka, A., & Atkin, J. D. (2022). The Role of DNA Damage in Neural Plasticity in Physiology and Neurodegeneration. In *Frontiers in Cellular Neuroscience* (Vol. 16). Frontiers Media S.A. https://doi.org/10.3389/fncel.2022.836885
83. Kopinke, D., & Murtaugh, L. C. (2010). Exocrine-to-endocrine differentiation is detectable only prior to birth in the uninjured mouse pancreas. *BMC Developmental Biology*, *10*. https://doi.org/10.1186/1471-213X-10-38
84. Kopp, J. L., von Figura, G., Mayes, E., Liu, F. F., Dubois, C. L., Morris, J. P., Pan, F. C., Akiyama, H., Wright, C. V. E., Jensen, K., Hebrok, M., & Sander, M. (2012). Identification of Sox9-Dependent Acinar-to-Ductal Reprogramming as the Principal Mechanism for Initiation of Pancreatic Ductal Adenocarcinoma. *Cancer Cell*, *22*(6), 737–750. https://doi.org/10.1016/j.ccr.2012.10.025
85. Kosmider, B., Lin, C. R., Vlasenko, L., Marchetti, N., Bolla, S., Criner, G. J., Messier, E., Reisdorph, N., Powell, R. L., Madesh, M., Kelsen, S., Xander, N., Correll, K. A., Mason, R. J., & Bahmed, K. (2019). Impaired non-homologous end joining in human primary alveolar type II cells in emphysema. *Scientific Reports*, *9*(1). https://doi.org/10.1038/s41598-018-37000-z
86. Kuzminov, A. (2011). Homologous Recombination—Experimental Systems, Analysis, and Significance. *EcoSal Plus*, *4*(2). https://doi.org/10.1128/ecosalplus.7.2.6
87. Lalwani, K., French, C., & Richardson, C. (2022). *Mouse Models to Understand Mutagenic Outcomes and Illegitimate Repair of DNA Damage*. https://doi.org/DOI: 10.5772/intechopen.103929
88. Lalwani, K., Goodenow, D., & Richardson, C. (2020). Eukaryotic Recombination: Initiation by Double-Strand Breaks. In *eLS* (pp. 69–76). Wiley. https://doi.org/10.1002/9780470015902.a0029148

89. Lam, I., & Keeney, S. (2015). Mechanism and regulation of meiotic recombination initiation. *Cold Spring Harbor Perspectives in Biology*, *7*(1). https://doi.org/10.1101/cshperspect.a016634
90. Lardon, J., Huyens, N., Rooman, I., & Bouwens, L. (2004). Exocrine cell transdifferentiation in dexamethasone-treated rat pancreas. *Virchows Archiv*, *444*(1), 61–65. https://doi.org/10.1007/s00428-003-0930-z
91. Lavin, M. F., Delia, D., & Chessa, L. (2006). ATM and the DNA damage response. *EMBO Reports*, *7*(2), 154–160. https://doi.org/10.1038/sj.embor.7400629
92. Lee, J., Reddy, R., Barsky, L., Weinberg, K., & Driscoll, B. (2006). Contribution of proliferation and DNA damage repair to alveolar epithelial type 2 cell recovery from hyperoxia. *Am J Physiol Lung Cell Mol Physiol*, *290*, 685–694. https://doi.org/10.1152/ajplung.00020.2005.-In
93. Lee, L. K., Ueno, M., Van Handel, B., & Mikkola, H. K. A. (2010). Placenta as a newly identified source of hematopoietic stem cells. In *Current Opinion in Hematology* (Vol. 17, Issue 4, pp. 313–318). Lippincott Williams and Wilkins. https://doi.org/10.1097/MOH.0b013e328339f295
94. Lei, T., Du, S., Peng, Z., & Chen, L. (2022). Multifaceted regulation and functions of 53BP1 in NHEJ-mediated DSB repair (Review). In *International Journal of Molecular Medicine* (Vol. 50, Issue 1). Spandidos Publications. https://doi.org/10.3892/IJMM.2022.5145
95. Levine, A. J. (1997). p53, the Cellular Gatekeeper Review for Growth and Division. In *Cell* (Vol. 88).
96. Levitsky, K. L., Toledo-Aral, J. J., López-Barneo, J., & Villadiego, J. (2013). Direct confocal acquisition of fluorescence from X-gal staining on thick tissue sections. *Scientific Reports*, *3*. https://doi.org/10.1038/srep02937
97. Lindahl, T., & Barnes, D. E. (2000). Repair of endogenous DNA damage. *Cold Spring Harbor Symposia on Quantitative Biology*, *65*, 127–133. https://doi.org/10.1101/sqb.2000.65.127
98. Li, T., Zhou, Z. W., Ju, Z., & Wang, Z. Q. (2016). DNA Damage Response in Hematopoietic Stem Cell Ageing. In *Genomics, Proteomics and Bioinformatics* (Vol. 14, Issue 3, pp. 147–154). Beijing Genomics Institute. https://doi.org/10.1016/j.gpb.2016.04.002
99. Liu, J. C., Lerou, P. H., & Lahav, G. (2014a). Stem cells: Balancing resistance and sensitivity to DNA damage. In *Trends in Cell Biology* (Vol. 24, Issue 5, pp. 268–274). Elsevier Ltd. https://doi.org/10.1016/j.tcb.2014.03.002
100. Liu, J. C., Lerou, P. H., & Lahav, G. (2014b). Stem cells: Balancing resistance and sensitivity to DNA damage. In *Trends in Cell Biology* (Vol. 24, Issue 5, pp. 268–274). Elsevier Ltd. https://doi.org/10.1016/j.tcb.2014.03.002
101. Lübbert, M., Mirro, J., Kitchingman, G., McCormick, F., Mertelsmann, R., Herrmann, F., & Koeffler, H. P. (1992). Prevalence of N-ras mutations in children with myelodysplastic syndromes and acute myeloid leukemia. *Oncogene*, *7*(2), 263–268. http://europepmc.org/abstract/MED/1549347
102. Lukaszewicz, A., Lange, J., Keeney, S., & Jasin, M. (2018). Control of meiotic double-strand-break formation by ATM: local and global views. In *Cell Cycle* (Vol. 17, Issue 10, pp. 1155–1172). Taylor and Francis Inc. https://doi.org/10.1080/15384101.2018.1464847
103. Mahaney, B. L., Meek, K., & Lees-Miller, S. P. (2009). Repair of ionizing radiation-induced DNA double-strand breaks by non-homologous end-joining. In

Biochemical Journal (Vol. 417, Issue 3, pp. 639–650). https://doi.org/10.1042/BJ20080413

104. Mailand, N., Bekker-Jensen, S., Faustrup, H., Melander, F., Bartek, J., Lukas, C., & Lukas, J. (2007). RNF8 Ubiquitylates Histones at DNA Double-Strand Breaks and Promotes Assembly of Repair Proteins. *Cell*, *131*(5), 887–900. https://doi.org/10.1016/j.cell.2007.09.040
105. Malinova, A., Veghini, L., Real, F. X., & Corbo, V. (2021). Cell Lineage Infidelity in PDAC Progression and Therapy Resistance. *Frontiers in Cell and Developmental Biology*, *9*(December), 1–19. https://doi.org/10.3389/fcell.2021.795251
106. Malkova, A. (2018). Break-Induced Replication: The Where, The Why, and The How. In *Trends in Genetics* (Vol. 34, Issue 7, pp. 518–531). Elsevier Ltd. https://doi.org/10.1016/j.tig.2018.04.002
107. Manesia, J. K., Xu, Z., Broekaert, D., Boon, R., van Vliet, A., Eelen, G., Vanwelden, T., Stegen, S., Van Gastel, N., Pascual-Montano, A., Maria-Fendt, S., Carmeliet, G., Carmeliet, P., Khurana, S., & Verfaillie, C. M. (2015). Highly proliferative primitive fetal liver hematopoietic stem cells are fueled by oxidative metabolic pathways. *Stem Cell Research*, *15*(3), 715–721. https://doi.org/10.1016/j.scr.2015.11.001
108. Mani, C., Reddy, P. H., & Palle, K. (2020). DNA repair fidelity in stem cell maintenance, health, and disease. In *Biochimica et Biophysica Acta - Molecular Basis of Disease* (Vol. 1866, Issue 4). Elsevier B.V. https://doi.org/10.1016/j.bbadis.2019.03.017
109. Mansell, E., Zareian, N., Malouf, C., Kapeni, C., Brown, N., Badie, C., Baird, D., Lane, J., Ottersbach, K., Blair, A., & Case, C. P. (2019). DNA damage signalling from the placenta to foetal blood as a potential mechanism for childhood leukaemia initiation. *Scientific Reports*, *9*(1). https://doi.org/10.1038/s41598-019-39552-0
110. Maréchal, A., & Zou, L. (2013). DNA damage sensing by the ATM and ATR kinases. *Cold Spring Harbor Perspectives in Biology*, *5*(9). https://doi.org/10.1101/cshperspect.a012716
111. Marié, I. J., Brambilla, L., & Levy, D. E. (2022). Assessing the Presence of Hematopoietic Stem and Progenitor Cells in Mouse Spleen. *Bio-Protocol*, *12*(11). https://doi.org/10.21769/BioProtoc.4438
112. Marx, J. (2002). Debate surges over the origins of genomic defects in cancer. In *Science* (Vol. 297, Issue 5581, pp. 544–546). https://doi.org/10.1126/science.297.5581.544
113. Matos-Rodrigues, G., Martini, E., & Lopez, B. S. (2021). Mouse models for deciphering the impact of homologous recombination on tumorigenesis. In *Cancers* (Vol. 13, Issue 9). MDPI AG. https://doi.org/10.3390/cancers13092083
114. Mehta, A., & Haber, J. E. (2014). Sources of DNA double-strand breaks and models of recombinational DNA repair. *Cold Spring Harbor Perspectives in Biology*, *6*(9). https://doi.org/10.1101/cshperspect.a016428
115. Mori, R., Matsuya, Y., Yoshii, Y., & Date, H. (2018). Estimation of the radiation-induced DNA double-strand breaks number by considering cell cycle and absorbed dose per cell nucleus. *Journal of Radiation Research*, *59*(3), 253–260. https://doi.org/10.1093/jrr/rrx097
116. Moutier, R., Tchang, F., Caucheteux, S. M., & Kanellopoulos-Langevin, C. (2003). Placental anomalies and fetal loss in mice, after administration of doxycycline in food for Tet-system activation. In *Transgenic Research* (Vol. 12).
117. Mujoo, K., Pandita, R. K., Tiwari, A., Charaka, V., Chakraborty, S., Singh, D. K., Hambarde, S., Hittelman, W. N., Horikoshi, N., Hunt, C. R., Khanna, K. K., Kots, A. Y., Butler, E. B., Murad, F., & Pandita, T. K. (2017). Differentiation of Human Induced

Pluripotent or Embryonic Stem Cells Decreases the DNA Damage Repair by Homologous Recombination. *Stem Cell Reports*, *9*(5), 1660–1674. https://doi.org/10.1016/j.stemcr.2017.10.002

118. Murtaugh, L. C., & Keefe, M. D. (2015). Regeneration and repair of the exocrine pancreas. *Annual Review of Physiology*, *77*, 229–249. https://doi.org/10.1146/annurev-physiol-021014-071727

119. Nickoloff, J. A., Sharma, N., Taylor, L., Allen, S. J., & Hromas, R. (2021). The Safe Path at the Fork: Ensuring Replication-Associated DNA Double-Strand Breaks are Repaired by Homologous Recombination. In *Frontiers in Genetics* (Vol. 12). Frontiers Media S.A. https://doi.org/10.3389/fgene.2021.748033

120. Nimrat Chatterjee* and Graham C. Walker. (2017). 乳鼠心肌提取 HHS Public Access. *Physiology & Behavior*, *176*(3), 139–148. https://doi.org/10.1016/j.physbeh.2017.03.040

121. Pachkowski, B. F., Guyton, K. Z., & Sonawane, B. (2011). DNA repair during in utero development: A review of the current state of knowledge, research needs, and potential application in risk assessment. In *Mutation Research - Reviews in Mutation Research* (Vol. 728, Issues 1–2, pp. 35–46). https://doi.org/10.1016/j.mrrev.2011.05.003

122. Palacio, S., McMurry, H. S., Ali, R., Donenberg, T., Silva-Smith, R., Wideroff, G., Sussman, D. A., Lima, C. M. S. R., & Hosein, P. J. (2019). DNA damage repair deficiency as a predictive biomarker for FOLFIRINOX efficacy in metastatic pancreatic cancer. *Journal of Gastrointestinal Oncology*, *10*(6), 1133–1139. https://doi.org/10.21037/jgo.2019.09.12

123. Perkhofer, L., Gout, J., Roger, E., Kude De Almeida, F., Baptista Simões, C., Wiesmüller, L., Seufferlein, T., & Kleger, A. (2021). DNA damage repair as a target in pancreatic cancer: State-of-the-art and future perspectives. In *Gut* (Vol. 70, Issue 3, pp. 606–617). BMJ Publishing Group. https://doi.org/10.1136/gutjnl-2019-319984

124. Pietras, E. M., Warr, M. R., & Passegué, E. (2011). Cell cycle regulation in hematopoietic stem cells. In *Journal of Cell Biology* (Vol. 195, Issue 5, pp. 709–720). https://doi.org/10.1083/jcb.201102131

125. Pour, P. M., Pandey, K. K., & Batra, S. K. (2003). What is the origin of pancreatic adenocarcinoma? *Molecular Cancer*, *2*, 1–10. https://doi.org/10.1186/1476-4598-2-13

126. Quek, L., Otto, G. W., Garnett, C., Lhermitte, L., Karamitros, D., Stoilova, B., Lau, I. J., Doondeea, J., Doondeea, B., Kennedy, A., Metzner, M., Goardon, N., Ivey, A., Allen, C., Gale, R., Davies, B., Sternberg, A., Killick, S., Hunter, H., … Vyas, P. (2016). Genetically distinct leukemic stem cells in human CD34-acute myeloid leukemia are arrested at a hemopoietic precursor-like stage. *Journal of Experimental Medicine*, *213*(8), 1513–1535. https://doi.org/10.1084/jem.20151775

127. Ramaiah, L., Bounous, D. I., & Elmore, S. A. (2013). Hematopoietic System. In *Haschek and Rousseaux's Handbook of Toxicologic Pathology, Third Edition: Volume 1-3* (Vols. 1–3, pp. 1863–1933). Elsevier. https://doi.org/10.1016/B978-0-12-415759-0.00050-9

128. Reichert, M., & Rustgi, A. K. (2011a). Pancreatic ductal cells in development, regeneration, and neoplasia. In *Journal of Clinical Investigation* (Vol. 121, Issue 12, pp. 4572–4578). https://doi.org/10.1172/JCI57131

129. Reichert, M., & Rustgi, A. K. (2011b). Pancreatic ductal cells in development, regeneration, and neoplasia. *Journal of Clinical Investigation*, *121*(12), 4572–4578. https://doi.org/10.1172/JCI57131

130. Reliene, R., & Schiestl, R. H. (2003). Mouse models for induced genetic instability at endogenous loci. *Oncogene*, *22*(45 REV. ISS. 5), 7000–7010. https://doi.org/10.1038/sj.onc.1206904
131. Remon, J., Besse, B., Leary, A., Bièche, I., Job, B., Lacroix, L., Auguste, A., Mauduit, M., Audigier-Valette, C., Raimbourg, J., Madroszyk, A., Michels, S., Bayar, M. A., Jimenez, M., Soria, J. C., Rouleau, E., & Barlesi, F. (2020). Somatic and Germline BRCA 1 and 2 Mutations in Advanced NSCLC From the SAFIR02-Lung Trial. *JTO Clinical and Research Reports*, *1*(3). https://doi.org/10.1016/j.jtocrr.2020.100068
132. Richardson, C., & Jasin, M. (2000). *Frequent chromosomal translocations induced by DNA double-strand breaks*. www.nature.com
133. Rinaldi, C., Pizzul, P., Longhese, M. P., & Bonetti, D. (2021). Sensing R-Loop-Associated DNA Damage to Safeguard Genome Stability. In *Frontiers in Cell and Developmental Biology* (Vol. 8). Frontiers Media S.A. https://doi.org/10.3389/fcell.2020.618157
134. Romer, A. I., & Sussel, L. (2015). Pancreatic islet cell development and regeneration. *Current Opinion in Endocrinology, Diabetes and Obesity*, *22*(4). https://journals.lww.com/co-endocrinology/Fulltext/2015/08000/Pancreatic_islet_cell_development_and_regeneration.2.aspx
135. Rossi, D. J., Jamieson, C. H. M., & Weissman, I. L. (2008). Stems Cells and the Pathways to Aging and Cancer. In *Cell* (Vol. 132, Issue 4, pp. 681–696). Elsevier B.V. https://doi.org/10.1016/j.cell.2008.01.036
136. Rossi, L., Challen, G., Sirin, O., Lin, K., & Goodel, M. (2011). HSC Characterisation and Isolation. *Bone*, *23*(1), 1–7. https://doi.org/10.1007/978-1-61779-145-1
137. Roth, D. B. (2014). V(D)J Recombination: Mechanism, Errors, and Fidelity. *Microbiology Spectrum*, *2*(6). https://doi.org/10.1128/microbiolspec.mdna3-0041-2014
138. Rothkamm, K., Krüger, I., Thompson, L. H., & Löbrich, M. (2003). Pathways of DNA Double-Strand Break Repair during the Mammalian Cell Cycle. *Molecular and Cellular Biology*, *23*(16), 5706–5715. https://doi.org/10.1128/mcb.23.16.5706-5715.2003
139. Rudiger, N. S., Gregersen1, N., & Kielland-Brandt2, M. C. (1995). homology with prokaryotic chi. In *Nucleic Acids Research* (Vol. 23, Issue 2).
140. Sakofsky, C. J., & Malkova, A. (2017). Break induced replication in eukaryotes: mechanisms, functions, and consequences. In *Critical Reviews in Biochemistry and Molecular Biology* (Vol. 52, Issue 4, pp. 395–413). Taylor and Francis Ltd. https://doi.org/10.1080/10409238.2017.1314444
141. Sallmyr, A., & Tomkinson, A. E. (2018). Repair of DNA double-strand breaks by mammalian alternative end-joining pathways. In *Journal of Biological Chemistry* (Vol. 293, Issue 27, pp. 10536–10549). American Society for Biochemistry and Molecular Biology Inc. https://doi.org/10.1074/jbc.TM117.000375
142. Schatz, D. G., & Ji, Y. (2011). Recombination centres and the orchestration of V(D)J recombination. In *Nature Reviews Immunology* (Vol. 11, Issue 4, pp. 251–263). https://doi.org/10.1038/nri2941
143. Schmitt, C. E., Lizama, C. O., & Zovein, A. C. (2014). From transplantation to transgenics: Mouse models of developmental hematopoiesis. In *Experimental Hematology* (Vol. 42, Issue 8, pp. 707–716). Elsevier Inc. https://doi.org/10.1016/j.exphem.2014.06.008

144. Seita, J., & Weissman, I. L. (2010). Hematopoietic stem cell: Self-renewal versus differentiation. In *Wiley Interdisciplinary Reviews: Systems Biology and Medicine* (Vol. 2, Issue 6, pp. 640–653). https://doi.org/10.1002/wsbm.86
145. Seol, J. H., Shim, E. Y., & Lee, S. E. (2018). Microhomology-mediated end joining: Good, bad and ugly. In *Mutation Research - Fundamental and Molecular Mechanisms of Mutagenesis* (Vol. 809, pp. 81–87). Elsevier B.V. https://doi.org/10.1016/j.mrfmmm.2017.07.002
146. Sjakste, N., & Riekstiņa, U. (2021). DNA damage and repair in the differentiation of stem cells and cells of connective cell lineages: A trigger or a complication? In *European Journal of Histochemistry* (Vol. 65).
147. Small, K., Iber, J., & Warren, S. T. (1997). Emerin deletion reveals a common X-chromosome inversion mediated by inverted repeats. *Nature Genetics*, *16*(1), 96–99. https://doi.org/10.1038/ng0597-96
148. Small, K., Wagener, M., & Warren, S. T. (1997). Isolation and characterization of the complete mouse emerin gene. *Mammalian Genome*, *8*(5), 337–341. https://doi.org/10.1007/s003359900435
149. Spella, M., Lilis, I., Pepe, M. A., Chen, Y., Armaka, M., Lamort, A.-S., Zazara, D. E., Roumelioti, F., Vreka, M., Kanellakis, N. I., Wagner, D. E., Giannou, A. D., Armenis, V., Arendt, K. A., Klotz, L. V, Toumpanakis, D., Karavana, V., Zakynthinos, S. G., Giopanou, I., … Stathopoulos, G. T. (2019). *Club cells form lung adenocarcinomas and maintain the alveoli of adult mice*. https://doi.org/10.7554/eLife.45571.001
150. Stanger, B. Z., & Hebrok, M. (2013). Control of cell identity in pancreas development and regeneration. *Gastroenterology*, *144*(6), 1170–1179. https://doi.org/10.1053/j.gastro.2013.01.074
151. Stoof, J., Harrold, E., Mariottino, S., Lowery, M. A., & Walsh, N. (2021). DNA Damage Repair Deficiency in Pancreatic Ductal Adenocarcinoma: Preclinical Models and Clinical Perspectives. *Frontiers in Cell and Developmental Biology*, *9*(October), 1–15. https://doi.org/10.3389/fcell.2021.749490
152. Stracker, T. H., & Petrini, J. H. J. (2011). The MRE11 complex: Starting from the ends. In *Nature Reviews Molecular Cell Biology* (Vol. 12, Issue 2, pp. 90–103). https://doi.org/10.1038/nrm3047
153. Strick, R., Strissel, P. L., Borgers, S., Smith, S. L., & Rowley, J. D. (2000). Dietary bioflavonoids induce cleavage in the MLL gene and may contribute to infant leukemia. *Proceedings of the National Academy of Sciences*, *97*(9), 4790–4795. https://doi.org/10.1073/pnas.070061297
154. Sukup-Jackson, M. R., Kiraly, O., Kay, J. E., Na, L., Rowland, E. A., Winther, K. E., Chow, D. N., Kimoto, T., Matsuguchi, T., Jonnalagadda, V. S., Maklakova, V. I., Singh, V. R., Wadduwage, D. N., Rajapakse, J., So, P. T. C., Collier, L. S., & Engelward, B. P. (2014). Rosa26-GFP Direct Repeat (RaDR-GFP) Mice Reveal Tissue- and Age-Dependence of Homologous Recombination in Mammals In Vivo. *PLoS Genetics*, *10*(6). https://doi.org/10.1371/journal.pgen.1004299
155. Sun, S., Osterman, M. D., & Li, M. (2019). Tissue specificity of DNA damage response and tumorigenesis. *Cancer Biology and Medicine*, *16*(3), 396–414. https://doi.org/10.20892/j.issn.2095-3941.2019.0097
156. Szostak, J. W., Orr-Weaver, T. L., Rothstein, R. J., & Stahl, F. W. (1983). The double-strand-break repair model for recombination. *Cell*, *33*(1), 25–35. https://doi.org/10.1016/0092-8674(83)90331-8

157. Teo, M. Y., & O'Reilly, E. M. (2016). Is it time to split strategies to treat homologous recombinant deficiency in pancreas cancer? In *Journal of Gastrointestinal Oncology* (Vol. 7, Issue 5, pp. 738–749). AME Publishing Company. https://doi.org/10.21037/jgo.2016.05.04
158. Thompson, L. H. (2012). Recognition, signaling, and repair of DNA double-strand breaks produced by ionizing radiation in mammalian cells: The molecular choreography. In *Mutation Research - Reviews in Mutation Research* (Vol. 751, Issue 2, pp. 158–246). https://doi.org/10.1016/j.mrrev.2012.06.002
159. Tichy, E. D., & Stambrook, P. J. (2008). DNA repair in murine embryonic stem cells and differentiated cells. In *Experimental Cell Research* (Vol. 314, Issue 9, pp. 1929–1936). Academic Press Inc. https://doi.org/10.1016/j.yexcr.2008.02.007
160. Tubbs, A., & Nussenzweig, A. (2017). Endogenous DNA Damage as a Source of Genomic Instability in Cancer. In *Cell* (Vol. 168, Issue 4, pp. 644–656). Cell Press. https://doi.org/10.1016/j.cell.2017.01.002
161. Udall, J. A., Quijada, P. A., & Osborn, T. C. (2005). Detection of chromosomal rearrangements derived from homeologous recombination in four mapping populations of Brassica napus L. *Genetics*, *169*(2), 967–979. https://doi.org/10.1534/genetics.104.033209
162. Uziel, T., Lerenthal, Y., Lilach, M., Andergeko, Y., Mittelman, L., & Shiloh, Y. (2003). Requirement of the MRN complex for ATM activation by DNA damage. *The EMBO Journal*, *22*, 5612–5621.
163. Vanhees, K., de Bock, L., Godschalk, R. W. L., van Schooten, F. J., & van Waalwijk van Doorn-Khosrovani, S. B. (2011). Prenatal exposure to flavonoids: Implication for cancer risk. *Toxicological Sciences*, *120*(1), 59–67. https://doi.org/10.1093/toxsci/kfq388
164. Vignard, J., Mirey, G., & Salles, B. (2013). Ionizing-radiation induced DNA double-strand breaks: A direct and indirect lighting up. In *Radiotherapy and Oncology* (Vol. 108, Issue 3, pp. 362–369). https://doi.org/10.1016/j.radonc.2013.06.013
165. Vilenchik, M. M., & Knudson, A. G. (2003). *Endogenous DNA double-strand breaks: Production, fidelity of repair, and induction of cancer*. www.pnas.orgcgidoi10.1073pnas.2135498100
166. Vogelstein, B., Civin, C. I., Preisinger, A. C., Krischer, J. P., Steuber, P., Ravindranath, Y., Weinstein, H., Ellferich, P., & Bos, J. (1990). RAS gene mutations in childhood acute myeloid leukemia: A pediatric oncology group study. *Genes, Chromosomes and Cancer*, *2*(2), 159–162. https://doi.org/https://doi.org/10.1002/gcc.2870020212
167. Waddell, N., Pajic, M., Patch, A. M., Chang, D. K., Kassahn, K. S., Bailey, P., Johns, A. L., Miller, D., Nones, K., Quek, K., Quinn, M. C. J., Robertson, A. J., Fadlullah, M. Z. H., Bruxner, T. J. C., Christ, A. N., Harliwong, I., Idrisoglu, S., Manning, S., Nourse, C., … Grimmond, S. M. (2015). Whole genomes redefine the mutational landscape of pancreatic cancer. *Nature*, *518*(7540), 495–501. https://doi.org/10.1038/nature14169
168. Walker, J. R., Corpina, R. A., & Goldberg, J. (2001). Structure of the Ku heterodimer bound to DNA and its implications for double-strand break repair. In *NATURE* (Vol. 412). www.nature.com
169. Weeden, C. E., Chen, Y., Ma, S. B., Hu, Y., Ramm, G., Sutherland, K. D., Smyth, G. K., & Asselin-Labat, M. L. (2017). Lung Basal Stem Cells Rapidly Repair DNA Damage Using the Error-Prone Nonhomologous End-Joining Pathway. *PLoS Biology*, *15*(1). https://doi.org/10.1371/journal.pbio.2000731

170. Weinfeld, M., Mani, R. S., Abdou, I., Aceytuno, R. D., & Glover, J. N. M. (2011). Tidying up loose ends: The role of polynucleotide kinase/phosphatase in DNA strand break repair. In *Trends in Biochemical Sciences* (Vol. 36, Issue 5, pp. 262–271). https://doi.org/10.1016/j.tibs.2011.01.006
171. Welty, S., Teng, Y., Liang, Z., Zhao, W., Sanders, L. H., Greenamyre, J. T., Rubio, M. E., Thathiah, A., Kodali, R., Wetzel, R., Levine, A. S., & Lan, L. (2018). RAD52 is required for RNA-templated recombination repair in post-mitotic neurons. *Journal of Biological Chemistry*, *293*(4), 1353–1362. https://doi.org/10.1074/jbc.M117.808402
172. White, R. R., Sung, P., Vestal, C. G., Benedetto, G., Cornelio, N., & Richardson, C. (2013). Double-Strand Break Repair by Inter-chromosomal Recombination: An In Vivo Repair Mechanism Utilized by Multiple Somatic Tissues in Mammals. *PLOS ONE*, *8*(12), e84379. https://doi.org/10.1371/journal.pone.0084379
173. Wiktor-Brown, D. M., Hendricks, C. A., Olipitz, W., & Engelward, B. P. (2006). Age-dependent accumulation of recombinant cells in the mouse pancreas revealed by in situ fluorescence imaging. *Proceedings of the National Academy of Sciences of the United States of America*, *103*(32), 11862–11867. https://doi.org/10.1073/pnas.0604943103
174. Witherspoon, D. J., Watkins, W. S., Zhang, Y., Xing, J., Tolpinrud, W. L., Hedges, D. J., Batzer, M. A., & Jorde, L. B. (2009). Alu repeats increase local recombination rates. *BMC Genomics*, *10*. https://doi.org/10.1186/1471-2164-10-530
175. Wogan, G. N., Hecht, S. S., Felton, J. S., Conney, A. H., & Loeb, L. A. (2004). Environmental and chemical carcinogenesis. *Seminars in Cancer Biology*, *14*(6), 473–486. https://doi.org/10.1016/j.semcancer.2004.06.010
176. Wright, W. D., Shah, S. S., & Heyer, W. D. (2018). Homologous recombination and the repair of DNA double-strand breaks. *Journal of Biological Chemistry*, *293*(27), 10524–10535. https://doi.org/10.1074/jbc.TM118.000372
177. Yang, Y. G., Saidi, A., Frappart, P. O., Min, W., Barrucand, C., Dumon-Jones, V., Michelon, J., Herceg, Z., & Wang, Z. Q. (2006). Conditional deletion of Nbs1 in murine cells reveals its role in branching repair pathways of DNA double-strand breaks. *EMBO Journal*, *25*(23), 5527–5538. https://doi.org/10.1038/sj.emboj.7601411
178. Yoo, S., & Dynan, W. S. (1999). Geometry of a complex formed by double strand break repair proteins at a single DNA end: recruitment of DNA-PKcs induces inward translocation of Ku protein. In *Nucleic Acids Research* (Vol. 27, Issue 24).
179. Zeman, M. K., & Cimprich, K. A. (2014). *R E V I E W Causes and consequences of replication stress*.
180. Zhang, Y., Houchen, C. W., & Li, M. (2022). *Attenuating DNA damage response and immunosuppression radiosensitizes pancreatic cancer*. https://doi.org/10.1016/j
181. Zheng, D., Limmon, G. V, Yin, L., Leung, N. H. N., Yu, H., Chow, V. T. K., & Chen, J. (2013). A cellular pathway involved in Clara cell to alveolar type II cell differentiation after severe lung injury. *PloS One*, *8*(8), e71028. https://doi.org/10.1371/journal.pone.0071028
182. حممد, فروخ, & Furrukh, M. (2013). ئة الر وسرطان التبغ تدخني احلقائق تغري اك إدر *Tobacco Smoking and Lung Cancer Perception-changing facts* (Vol. 13, Issue 3).